ELECTRODICS OF SULFIDE MINERALS

(Implications for Induced Polarization)

by

Frank Dale Oliver Morgan

B.Sc (1970): University of the West Indies

M.Sc (1972): University of the West Indies

SUBMITTED IN PARTIAL FULFILLMENT OF THE REQUIREMENTS

FOR THE DEGREE OF

DOCTOR OF PHILOSOPHY

at the

MASSACHUSETTS INSTITUTE OF TECHNOLOGY

January 1981

Signature of Author Signature redacted
Department of Earth & Planetary Sciences

Certified by Signature redacted
Thesis Supervisor

Accepted by Signature redacted
Chairman, Departmental Committee on Graduate Students

Undgren
MASSACHUSETTS INSTITUTE OF TECHNOLOGY
AUG 3 1981
LIBRARIES

ELECTRODICS OF SULFIDE MINERALS

(IMPLICATIONS FOR INDUCED POLARIZATION)

by

Frank Dale Oliver Morgan

Submitted to the Department of Earth and Planetary Sciences
on January 30, 1981 in partial fulfillment
of the requirements for the Degreee of Doctor of Philosophy in Geophysics

ABSTRACT

This thesis reports the results of investigations into the electrochemical causes of the Induced Polarization phenomena. The experimental measurements were carried out on plane parallel electrodes immersed in various aqueous media.

Past studies in this laboratory had shown that the impedance spectra of metallic minerals was quite insensitive to variations in solution chemistry.

We investigated this problem in detail. In doing so, we considered several new equivalent circuit models for the processes occuring at the electrode. Arguments will be presented in favour of an equivalent circuit model which incorporates the solution resistance in series with three parallel paths. The non-faradaic path is represented by the triple layer capacitance. The faradiac branch is modelled as a diffusion impedance in series with a reaction resistance. The third path is due to adsorption phenomena, associated with the supporting electrolyte. The latter path is necessary in order to explain the large phase angles often observed at low frequencies. We suggest that the faradiac path is controlled by surface reactions among adsorbed intermediate species.

We also addressed the question of mineral discrimination by Induced Polarization measurements. From data presented on pyrite and chalcocite, mineral discrimination certainly seems possible; especially using the phase data at low frequencies. We feel we now have a better understanding of the processes controlling electrode impedances and this opens many interesting avenues for further studies into IP behavior of rocks.

Thesis Supervisor: Dr. Theodore R. Madden

Title: Professor of Geophysics

Dedicated

to

Alison

and

our families

ACKNOWLEDGEMENT

TO

PROFESSOR T.R. MADDEN

Professor T.R. Madden has been more than a thesis advisor, he has been a friend.

He tried over these years to teach me the meaning of good scientific research. To search for fundamentals rather than details and to substantiate our findings by mathematical and experimental arguments. I hope that some of this methodology and a little of his intuitive genius has rubbed-off on me. I have come to believe that the only reward he seeks is to see his students continue research with the same rigour they have experienced while working with him. I hope, in the future, to reward him in this way.

His family Halima, Salim, Ishamel, Nadia, Jennifer, and "Baba" showed my wife and I tremendous warmth. His wife Halima, was always willing to lend an ear to our petty moans and groans.

Professor Madden to you and your family, I would like to say on behalf of my wife and I ____ thanks!.

ACKNOWLEDGMENTS

I would like to thank Professors Aki, Brace, Molnar, Simmons and Toksöz for their contributions to my education in Geophysics.

I cannot measure how much I have learned from my office mates: Gerry LaTorraca, Earle Williams, Steve Park, Adolfo Figueroa-Vinas, Olu Agunloye, John Williams, Ru-shan Wu, Frances Bagenal, Gerardo Suarez, and Ranga Ranganayaki. Thanks!

Many other colleagues have been helpful in various ways, in particular: Joe Walsh, Steve Roecker, Bill Ellsworth, Howard Patton, Shamita Das, Bob Collier, Bernard Chouet, Michel Bouchon, Brian Evans and Karl Coyner.

The technical advice and assistance of Dave Smith, Howard Berman, Tibor Lukac, George Keough, Frank Miller and Jock Hirst was greatly appreciated.

My wife and I found it extremely gratifying to have known the following groups of people. Gerry LaTorraca's family has always offered open arms and hearts to us. Mrs. Cameron, her family and crew at Mt. Ida College have been as close to us as our families. We will always treasure their caring.

Professors Newberne and Rogers, in the Department of Nutrition, where my wife worked for many years, have been of great assistance to us. I would also like to say thanks to the many friends we made throughout that department.

Judy Roos' assistance can only be described as superlative. Without her help the production of this thesis would have been painful.

The assistance of Tansy Mattingly and Debby Gillett was greatly appreciated. I would like to thank Danielle Chouet for typing most of this thesis.

Thanks are addressed to the members of my thesis committee: Professors Aki, Edmond, Lataneson, Madden and Morel. Anthony Guissipe was also of much assistance in the preparation of this thesis.

I would like to acknowledge, with great appreciation, my fellowship from the OAS/Trinidad and Tobago Government and the funding of the project by the National Science Foundation under Grant 77-02488EAR. Without these fundings this project would not have been possible.

Finally, I would like to thank my wife, Alison, to whom I have dedicated this thesis, for her unending support. I could not have made it without her.

TABLE OF CONTENTS

ABSTRACT		i
ACKNOWLEDGEMENT TO PROFESSOR T.R. MADDEN		ii
ACKNOWLEDGEMENTS		iii
CONTENTS		v
CHAPTER I:	INTRODUCTION	1
1.1	HISTORICAL REVIEW	1
1.2	OBJECTIVES OF THE PRESENT STUDY	2
1.3	OUTLINE OF THESIS	6
CHAPTER II:	EQUIVALENT CIRCUIT MODELS	
	INTRODUCTION	7
2.1	THE NON-FARADAIC BRANCH	8
2.2	THE FARADAIC BRANCH	12
	2.2.1 Effects of a Finite Diffusion Layer on the Warburg Impedance	18
	2.2.2 Effects of the Dissociation of Water on the Warburg Impedance	23
	2.2.3 Effects of Surface Processes on the Faradaic Branch	26
2.3	THE ADSORPTION BRANCH	28
2.4	ESTIMATION OF THE IMPEDANCE PARAMETERS	34
	SUMMARY	35
CHAPTER III:	EXPERIMENTAL METHODS	
	INTRODUCTION	37
3.1	POURBAIX (Eh-pH) DIAGRAMS	37
	3.1.1 The Electrochemical Stability of H_2O	38
	3.1.2 Cu-H_2O System	39
	3.1.3.Eh Measurements	41
	3.1.4 Pourbaix (E_M-pH) Diagrams-Concluding Remarks	45

3.2 THE EXPERIMENT -- APPARATUS, METHODOLOGY AND ACCURACY

3.2.1 Cell Design 46

3.2.2 Solution Preparation 49

3.2.3 Electrode Preparation 49

3.2.4 Data Acquisition 50

3.2.5 Experimental Accuracy and Reproducibility 52

3.3 AN EXPERIMENT WITH KNOWN IMPEDANCES 53

3.4 I.P. EXPERIMENTS ON THE Cu /$CuSO_4$ SYSTEM 55

3.5 EFFECTS OF STIRRING THE SOLUTION 64

SUMMARY 66

CHAPTER IV: INDUCED POLARIZATION RESPONSE OF SULFIDE MINERALS

INTRODUCTION 67

4.1 ELECTROCHEMICAL STABILITY OF SULFIDE MINERALS 69

4.1.1 The Acid Oxidizing Region (AO) 71

4.1.2 The Neutral Oxidizing Region (NO) 72

4.1.3 The Neutral Reducing Region (NR) 72

4.2 EXPERIMENTAL RESULTS 77

4.2.1 Potentiometric (d.c.) Data 77

4.2.2 I.P. Impedance Spectra 85

4.3 INTERPRETATION OF I.P. RESPONSE 85

4.4 INDUCED POLARIZATION RESPONSE OF CHALCOCITE 97

4.4.1 Chalcocite in the AO Region 97

4.4.2 Chalcocite in the NO Region 97

4.4.3 Chalcocite in the NR Region 100

4.5	INDUCED POLARIZATION RESPONSE OF PYRITE	100
	4.5.1 Pyrite in the AO and NO Region	100
	4.5.2 Pyrite in the NR Regions	104
4.6	INDUCED POLARIZATION RESPONSE OF COPPER	104
4.7	INDUCED POLARIZATION RESPONSE OF OTHER COPPER AND IRON SULFIDES	106
	SUMMARY	106
CHAPTER V:	SPECTRAL I.P.	
	INTRODUCTION	107
5.1	CONTRIBUTION OF ELECTRODICS TO SPECTRAL I.P.	107
	5.1.1 Mineral Discrimination in the AO Region	108
	5.1.2 Mineral Discrimination in the NO Region	110
	5.1.3 Mineral Discrimination in the NR Region	110
	SUMMARY	110
CHAPTER VI:	SUMMARY	
	INTRODUCTION	114
6.1	SUGGESTIONS FOR FURTHER RESEARCH - Electrochemical Studies	114
6.2	SUGGESTIONS FOR FURTHER RESEARCH - General Studies	114
6.3	CONCLUSIONS	115
APPENDIX A:	Parameter estimation	118
APPENDIX B:	Electronic Instrumentation	123
REFERENCES		133
BIOGRAPHICAL NOTE		137

I

INTRODUCTION

Metallic mineralized zones often exhibit a frequency dependent impedance. Such behavior is termed "Induced Polarization" (I.P.). As the name implies, the polarization exists only when an applied current is present. It is now generally accepted that this polarization impedance is associated with electrochemical phenomena occurring at the interface between the mineral and the pore liquid. However, the details of the electrochemical mechanisms are not well understood. Accordingly, this study is an attempt to further our understanding of the chemical nature of Induced Polarization.

"Electrodics" is a word apparently coined by J. O'M Bockris, one of the pioneers of modern electrochemistry (Bockris and Reddy, 1970). It aptly describes the field of study involving electrodes and ions.

I.P. is by far the most widely used electrical prospecting method for locating metallic mineralized bodies. It is claimed that it is possible to discern disseminated sulfides having a volume percent of less than one.

A brief review of I.P. studies is given in this section, after which the general objectives of the present investigation are described. Finally, an outline of the thesis is given.

1.1 HISTORICAL REVIEW

The I.P. phenomenon was discovered by Conrad Schlumberger in 1912. Unfortunately, the discovery occurred as an artifact during his classical studies of resistivity and self potential. For this reason, active

research in this area remained at a minimum until the late 1940's and 1950's.

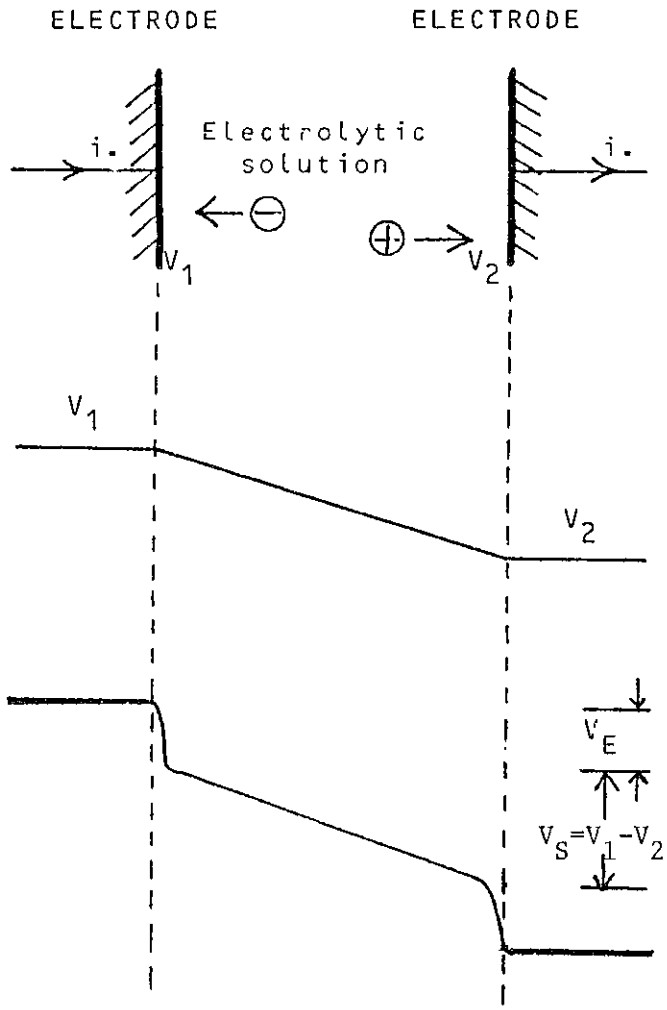
The monograph by Wait (1959), describes the work carried out at Newmont Exploration Ltd. The research there was largely initiated (1946) by A.A. Brant. About the same time Bleil was completing his Ph.D. thesis (1948) on I.P., which unfortunately was not published until 1953 (Bleil, 1953). At the New Mexico Institute of Mining and Technology, Vacquier (1957) attempted to utilize I.P. for the location of groundwater reservoirs. This latter type of I.P. is referred to as membrane polarization. At M.I.T., T.R. Madden directed a group which looked both at fundamental I.P. mechanisms and at interpretation methods (Hallof, 1975, Marshall, 1959, and Madden, 1961).

In recent years much effort has been directed at field interpretation methods, particularly to the problem of electromagnetic coupling (Wynn and Zonge, 1975, Pelton et. al., 1978). At present, an exciting area of research concerns the possible discrimination of metallic minerals (Hallof et. al. 1979, Halverson et. al., 1979, Wong, 1979). Klein and Shuey (1978) and also Agunloye (1977) investigated nonlinear properties of I.P. Angoran (1975) extended Madden's earlier work on the electrochemical causes of I.P.

1.2 OBJECTIVES OF THE PRESENT STUDY

The present study relies heavily on the concept of electrode impedances. Accordingly, we will describe in a qualitative way what is meant by an electrode impedance.

Figure 1.1 shows diagramatically in (a) a pair of electrodes between which there is an electrolytic solution. A constant current i is used to excite the system. If the potential distance plot looks like that in (b)



(a) Electrolytic Solution between Metallic Electrodes

(b) NO POLARIZATION

$$\text{Impedance} = R_S = \frac{V_1 - V_2}{i} = \frac{V_S}{i}$$

(c) INDUCED POLARIZATION

$$\text{Impedance} = Z = \frac{V_S + 2V_E}{i} = R_S + 2Z_E$$

Figure 1.1: Pictorial Representation of Induced Polarization

R_S = Solution resistance

V_e = Overpotential

then the total impedance of the system behaves resistively. As shown in (b) there is a linear change in potential between the electrodes. Conversely, in (c) we have a situation in which there is an "overpotential". It is this overpotential which gives rise to the additional electrode impedance. The electrode impedance is associated with phenomena occurring at or near the electrode surface. The electrode impedance can be caused by one or more of the following:

a. A resistance due to an electron transfer reaction at the electrode surface.

b. An impedance due to diffusion in solution.

c. The interfacial (double layer) capacitance.

d. Surface impedances.

e. Adsorption phenomena.

The electrode impedance therefore represents a rather complex physical and chemical system. In Chapter II expressions are derived for the electrode impedance incorporating the mechanisms (a) to (e).

Another issue germane to the present study is the question of the electrochemical stability fields of the sulfide minerals and their pore liquids. Figure 1.2 is a composite of many Eh measurements for naturally occurring waters. Eh is a measure of the oxidizing or reducing ablility of the solution.

We are now in a position to state the general objectives of the present investigation. A major problem in past studies of this nature (Madden, 1961, and Angoran, 1975) was that the impedance spectra was virtually invariant for many different environmental conditions. The major objectives of the present study are therefore,

1. Investigate the properties of the impedance spectra in an attempt to

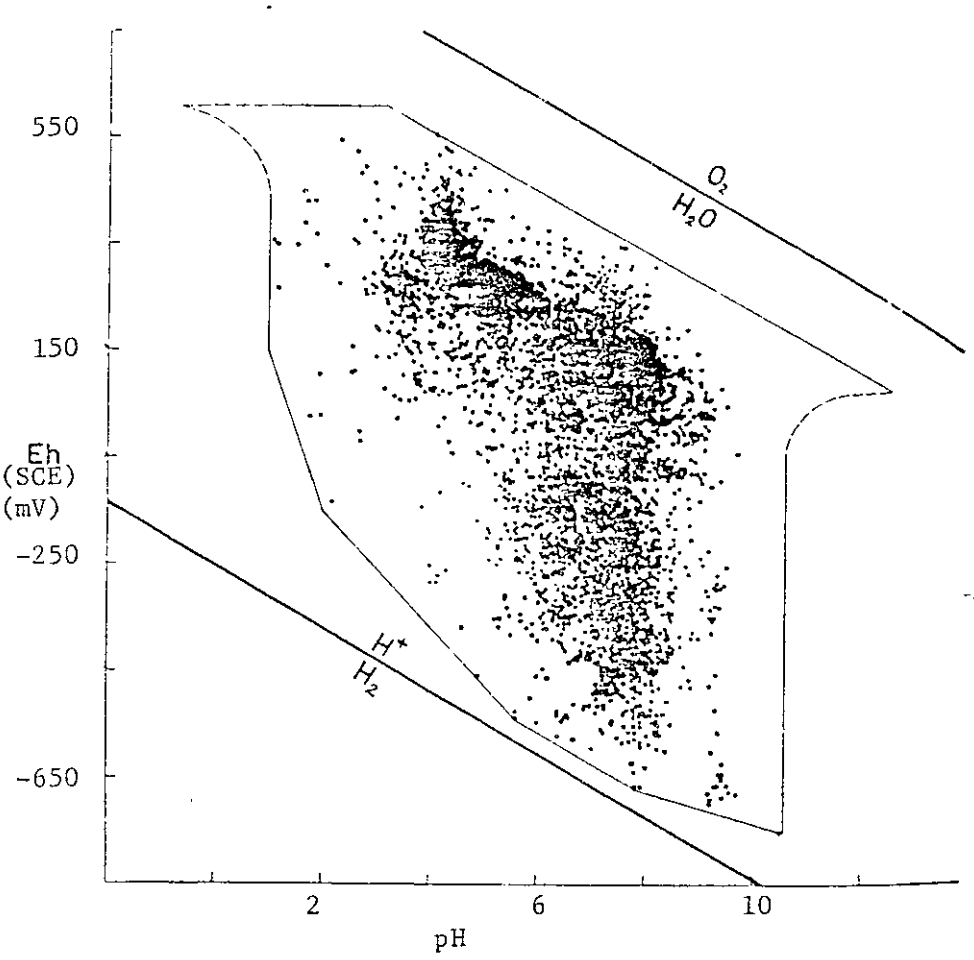


Figure 1.2: Eh-pH measurements of Natural Waters.
Adapted from Baas Becking et al (1960)

understand why it is approximately constant in many different environments. In attempting this we seek correlations between the electrode and impedance the associated Eh-pH environ mental conditions.

2. Look for systematic differences in Z among various mineral types, in an attempt to discriminate between minerals using I.P.

Our method will be to study the simple case of planar electrodes separated by various electrolytic solutions. We will not investigate the I.P. response of actual mineralized rocks.

1.3 OUTLINE OF THESIS

Chapter II describes various models of the electrode impedance. Expressions which model the electrode impedance as an electrical circuit will be presented.

Chapter III describes the experimental methods. The procedures for obtaining reliable and accurate I.P. data are discussed there.

In Chapter IV, much I.P. data, particularly on pyrite and chalcocite are presented and interpreted. Some of the problems associated with the interpretations are considered. An equivalent circuit incorporating an adsorption path will be used to interpret most of the data.

Chapter (V) discusses the applications of the results of this study to geophysics. In particular, the issue of mineral discrimination will be considered. We will present evidence to show that mineral discrimination may indeed be possible. Future work and extensions of the methods presented are also briefly mentioned in chapter VI.

Appendix A is a short summary of the Parameter Estimation methods used in this study. Appendix B is a tabulation of some of the electronic circuits used in the instrumentation.

II

EQUIVALENT CIRCUIT MODELS

INTRODUCTION

A variety of electrochemical reaction mechanisms will be treated in this Chapter. In particular, expressions for the electrode impedance associated with different electrical circuit models are discussed.

Previous work in this laboratory had considered an impedance model consisting of a solution resistance in series with two parallel branches, namely, the non-faradaic and faradaic paths (Madden, 1961, and Angoran, 1975). In the present study, modifications to the faradaic branch are discussed and a third parallel path, due to adsorption phenomena is introduced.

To be completely general in the derivation of electrode impedances, one needs to solve the appropriate kinetic equations (Madden, 1961). One result that emerges from such a proper mathematical treatment is that the non-faradaic and faradaic paths may be treated as being approximately independent. This decoupling holds if the indifferent electrolyte is much in excess of the species which is active in the faradaic branch. Decoupling between the non-faradaic and adsorption process can also be approximately assumed. We will discuss this later case in the section on adsorption.

In this chapter we will therefore assume that the three paths are independent. Such an approach, although approximate, allows us to focus on the physical and chemical aspects of the impedance, one path at a time. Finally, for completeness, a note on the method of parameter estimation is given. Particular attention is addressed to the concepts of resolution and

non-uniqueness. The reader unfamiliar with inverse methods should consult Appendix A.

2.1 THE NON-FARADAIC BRANCH

By definition, the non-faradaic path does not obey Faraday's law, which states that the applied current is proportional to the number of ions discharged. The branch is modelled as being purely capacative, thereby passing only displacement current.

This interfacial capacitance C has been the subject of extensive study. For details, the reader may refer to Bockris and Reddy (1970), Delahay (1965) and Overbeek (1952). In its most general form, the capacitance may be modelled as a triple layer. The triple layer consists of a 'fixed' layer close to the electrode surface and a diffuse zone extending out into solution. The fixed, or Stern layer, may be broken into two regions (Grahame, 1947). The innermost layer consists of H_2O molecules, plus any ions adsorbed onto the electrode surface. The outer part of the fixed layer consists mainly of hydrated ions. The total capacitance can be written as (Bockris and Reddy, 1970),

$$\frac{1}{C} = \frac{1}{C_{OHP}} - \frac{1}{C_{IHP \to OHP}} \left(\frac{dq_{SA}}{dq_M} \right) + \frac{1}{C_d} \qquad (2.1)$$

where C_{OHP} and $C_{IHP \to OHP}$ are the capacitances from the outer Helmoltz plane to the electrode surface and from the IHP to the OHP respectively. C_d is the normal diffuse zone (Gouy-Chapman) capacitance, extending from the OHP, away from the electrode, and encompassing the entire diffuse layer charge.

The term dq_{SA}/dq_M refers to changes in the charge density (q) due to

specifically (contact) adsorbed ions relative to changes in the total charge density of the metal or mineral. When $dq_{SA}/dq_M = 0$, there is no contact adsorption and the interface behaves as a classical 'double layer'. C_{OHP} may be expressed as:

$$\frac{1}{C_{OHP}} = \frac{1}{C_{IHP}} + \frac{1}{C_{IHP \rightarrow OHP}} \qquad (2.2)$$

In the IHP the dielectric constant is reduced to ~6, because of the high electric fields present ($\sim 10^7$ V/m). A rough calculation (see Bockris and Reddy, 1970) shows that $C_{IHP} \sim 20\mu F$. $C_{IHP \rightarrow OHP}$, which represents a broader region with a dielectric constant of 35 to 40, does not contribute significantly C_{OHP} since its value is ~80μF. Order of magnitude values of C_{OHP} and $C_{IHP \rightarrow OHP}$ therefore give a fixed layer capacitance,

$$\frac{1}{C_F} = \frac{1}{16} - \frac{1}{80}\left(\frac{dq_{SA}}{dq_M}\right) \qquad (2.3)$$

When contact adsorption is absent C_F ~16μF and this is usually referred to as the constant capacity region. The inclusion of adsorption forces causes C_F to increase because $dq_{SA}/dq_M > 0$. The change of q_{SA} with q_M is such that a 'hump' is produced in the curve of C relative to the electrode potential. Cations are generally not strongly adsorbed. The adsorption of anions depends mainly on the degree to which they are hydrated. Hydration is a function of the ionic radius such that smaller ions are more strongly hydrated. The larger, weakly hydrated ions can thus find their way to the electrode surface, thereby becoming contact adsorbed. Experimentally, it has been found that the degree of adsorption, from the most strongly adsorbed to the least adsorbed is approximately:

$I^- > NO_3^{2-} > Br^- > Cl^- > SO_4^{2-} > OH^- > F^-$ (Grahame, 1947)

Figure 2.2 shows some of these effects.

Let us turn our attention to the third part of the triple layer capacitance, namely C_d. This capacitance is given by $C_d = (Ze\kappa\Sigma C/kT)\times \cosh(Ze\Psi^o/2kT)$, wherein $\kappa^2 = k\leq\epsilon kT/2\pi$, C = concentration and ϵ the dielectric constant of water. Ψ^o is the potential of the OHP, which is approximately equal to the zeta-potential. In the Table below we show computed values of C_d as a function of concentration and zeta-potential.

C	$\pm \Psi^o$ (V)						
moles/l	0.00	0.02	0.04	0.06	0.08	0.10	0.20
0.1	73	79	97	132	187	274	1986
0.01	23	25	31	42	59	87	68
0.001	7.3	7.9	9.7	13	19	27	199

Table 2.1 Diffuse zone capacitance C_d as a function of concentration and zeta-potential (Z=1).

We are now in a position to discuss, quantitatively, the expected values of the total triple layer capacitance. Note that because the total capacitance is made-up of three capacitors in series, the smallest valued capacitor tends to control the capacitance. Figure 2.1 shows that at very negative potentials (relative to the point of zero charge pZC), C ~16μF and constant. This is the region in which C_{OHP} dominates and adsorption is absent. When the electrode is positive, relative to the pZC, adsorption

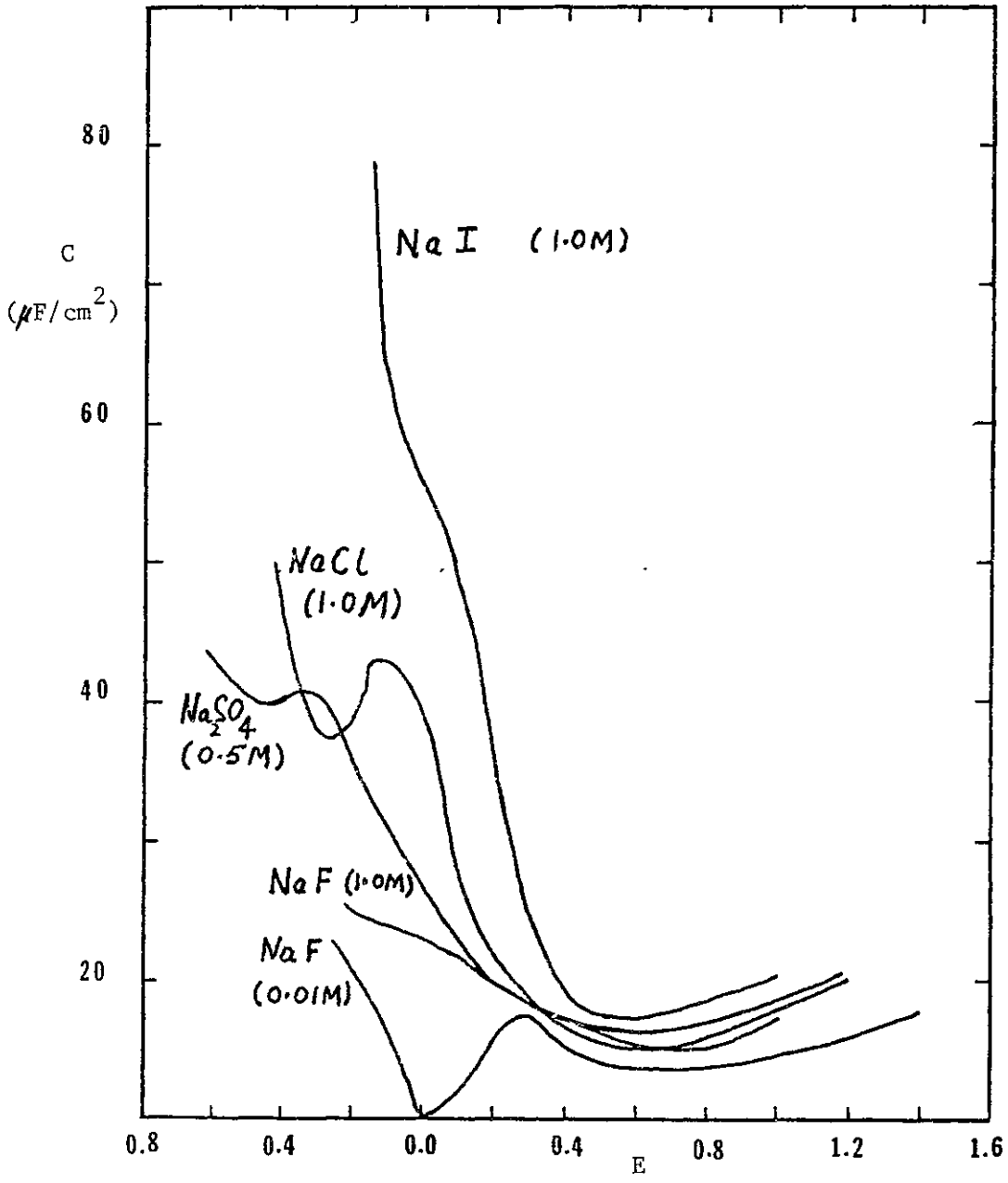


Figure 2.1: Adsorption Effects on the Interfacial Capacitance (After Grahame, 1947)

increases the capacitance. The degree of adsorption depends mainly on the ionic type and less on the concentration of the electrolyte. Our experiments are usually performed with supporting electrolytes of concentration of 10^{-2} or 10^{-3}M. C_d could dominate C if $C_d \ll C_F$. Table 2.1 shows that for zero and moderate zeta-potentials, C_d can indeed be less than C_F. The parabolic shape, with low C, around the pZC is thus attributed to C_d. In summary, C lies somewhere between 10 and 100 μF, depending mainly upon the type of electrode, the electrode potential and on the ionic type.

2.2 THE FARADAIC BRANCH

Consider now the electrochemical kinetics controlling the Faradaic path of the electrode impedance. Under an applied electric potential ϕ, the rate of the forward (+) and backward (-) reactions of a simple redox couple like,

$$O + n\,e \underset{v_-}{\overset{v_+}{\rightleftharpoons}} R \tag{2.4}$$

is given by,

$$v_{+,-} = \frac{kT}{h} A_{O,R}\, e^{-(\Delta G_{+,-}/RT)} \tag{2.5}$$

where ΔG is the total Gibbs energy. ΔG may be decomposed into a chemical free energy of activation ΔG_o and an electrical free energy associated with the potential across the interface ϕ. k and h are Boltzman's and Planck's constant respectively. A_O and A_R are the activities of the oxidized and reduced species. Expanding ΔG as,

$$\Delta G_+ = \Delta G_+^o + \alpha nF\phi \quad \text{and} \quad \Delta G_- = \Delta G_-^o - (1-\alpha)nF\phi \tag{2.6}$$

where α is the fraction of the applied potential in the forward direction, gives,

$$v_+ = \frac{KT}{h} e^{-\Delta G^o_+/RT} A_O \, e^{-\alpha nF\phi/RT} \tag{2.7}$$

$$v_- = \frac{kT}{h} e^{-\Delta G^o_-/RT} A_R \, e^{(1-\alpha)nF\phi/RT} \tag{2.8}$$

Figure 2.2 depicts some of these ideas. As seen in that Figure ΔG represents the energy barrier that must be surpassed before a reaction occurs at the electrode. We can simplify (2.7) and (2.8) by defining rate constants k_+ and k_- such that

$$v_+ = k_+ A_O \, e^{\alpha nF\phi/RT} \tag{2.9}$$

$$v_- = k_- A_R \, e^{(1-\alpha)nF\phi/RT} \tag{2.10}$$

Furthermore the current densities associated with these reaction rates can be obtained since $i = nFv$, where F is the Faraday's constant. Thus,

$$i_+ = nFk_+ A_O \, e^{-\alpha\gamma(E+\eta)} \tag{2.11}$$

and

$$i_- = nFk_- A_R \, e^{(1-\alpha)\gamma(E+\eta)} \tag{2.12}$$

where we have separated the total potential ϕ into an equilibrium potential E and an overpotential η. We have also defined $\gamma = nF/RT$.

At equilibrium, $\eta = 0$ and,

$$i_+ = i_- \equiv i_O = nFk_+ A_O \, e^{-\alpha\gamma E} = nFk_- A_R e^{(1-\alpha)\gamma E} \tag{2.13}$$

The equilibrium current i_o defined by (2.13) is called the exchange

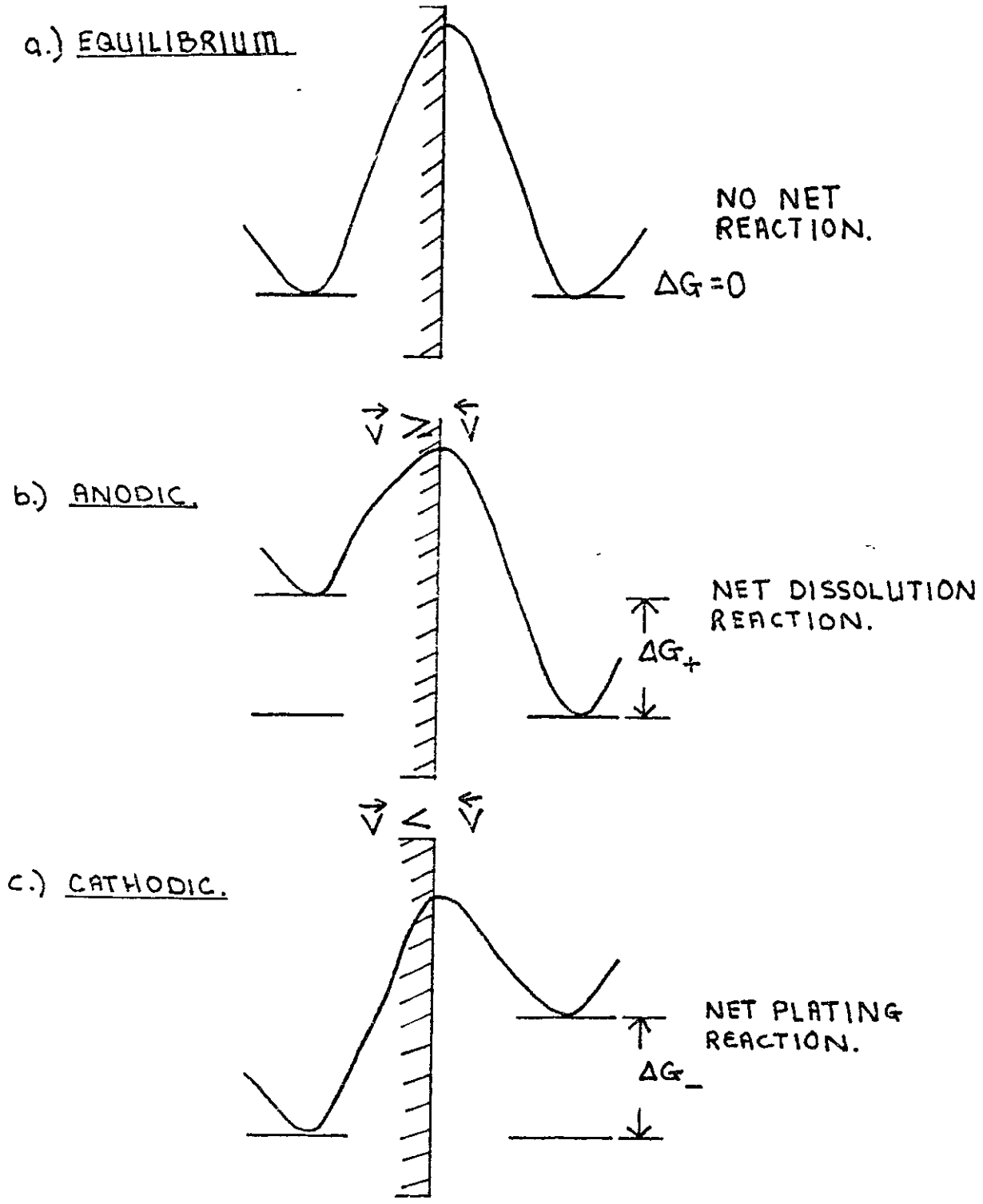


Figure 2.2: Energetics of the Activation Process

current density. Since the Nernst equation, which can be derived from (2.13) also holds at equilibrium,

$$E = E^{o} + \frac{RT}{nF} \ln\left(\frac{A_O}{A_R}\right) \tag{2.14}$$

Substituting (2.14) into (2.13) leads to an expression relating i_o to the activities, namely,

$$i_O = nFk_S A_O^{1-\alpha} A_R^{\alpha} \tag{2.15}$$

k_s is the heterogeneous rate constant of the reaction and it is defined by:

$$k_S \equiv k_+ e^{-\alpha\gamma E^{o}} = k_- e^{(1-\alpha)\gamma E^{o}} \tag{2.16}$$

We can now write the total faradaic current as (Butler-Volmer equation):

$$i_f \equiv i_+ - i_- = i_o\left(e^{-\alpha\gamma\eta} - e^{(1-\alpha)\gamma\eta}\right) \tag{2.17}$$

If we expand (2.17), about equilibrium, using Taylor's expansion to first order we get,

$$\Delta i_f = i_0\left(\gamma\Delta\eta + \frac{\Delta A_O}{A_O} - \frac{\Delta A_R}{A_R}\right) \tag{2.18}$$

or the faradaic impedance,

$$\frac{\Delta\eta}{\Delta i_f} = Z_f = \frac{RT}{nFi_0} + \frac{RT}{nF}\left(\frac{\Delta A_O}{A_O} - \frac{\Delta A_R}{A_R}\right)\frac{1}{i_f} \tag{2.19}$$

In a solution with a large concentration of indifferent (supporting) electrolyte, transport to the electrode will be mainly by diffusion, since electrical migration (conduction) will be reduced by the high conductivity

of the solution. In order to obtain expressions from the change in activities ($\Delta A_O, \Delta A_R$) at the electrode surface, we must solve the diffusion equation with the appropriate boundary conditions. The diffusion equation,

$$\frac{\partial A}{\partial t} = D\left(\frac{\partial^2 A}{\partial x^2}\right) \tag{2.20}$$

has a solution (see for example, Carslaw and Jaeger, 1947),

$$A(x,t) = A + \Delta A\, e^{-x\sqrt{j\omega/D} + j\omega t} \tag{2.21}$$

where we have assumed a sinusoidal time dependence. D is the diffusion constant and A is the activity of the species in the bulk solution. At the electrode surface we must satisfy,

$$i_f = -nFD\left(\frac{\partial A}{\partial x}\right)_{x=0} \tag{2.22}$$

From (2.21) and (2.22),

$$\Delta A = \left(i_f/nF \quad j\omega D\right) e^{-j\omega t} \tag{2.23}$$

Substituting into (2.19) gives,

$$\underline{Z}_f = \frac{RT}{nFi_O} + \frac{RT}{n^2F^2\sqrt{j\omega}}\left(\frac{1}{A_R\sqrt{D_R}} + \frac{1}{A_O\sqrt{D_O}}\right) \tag{2.24}$$

It is common practice to define a reaction resistance and a Warburg impedance by,

$$\text{Reaction (Activation) Resistance} \equiv R_1 \equiv \Theta \equiv \frac{RT}{nFi_O} \tag{2.25}$$

$$\text{Warburg Impedance} \equiv \underline{W} \equiv \frac{RT(1-j)}{n^2F^2\sqrt{2\omega}}\left(\frac{1}{A_R\sqrt{D_R}} + \frac{1}{A_O\sqrt{D_O}}\right) =$$

$$(\sigma_R+\sigma_O)\omega^{-1/2}(i-j) = \sigma\omega^{-1/2}(i-j) \qquad (2.26)$$

Note that W has a phase shift of -45° for all frequencies and also depends inversely on the square root of the frequency. Accordingly, W cannot be represented in any simple way by a combination of standard circuit elements. The name and symbol of the Warburg impedance was suggested by Grahame (1952), in view of the fact that Warburg (1899) was the first to derive an expression for this diffusion impedance.

Let us compute some values for the Warburg impedance. Substituting R = 8.31 J/deg. mole, F = 96500 coul/mole and T = 298°K into equation (2.26), with ω = 1 rad/sec results in,

$$W = \frac{2.66\times10^{-5}}{n^2}\left(\frac{1}{A_O\sqrt{D_O}} + \frac{1}{A_R\sqrt{D_R}}\right) \quad \Omega\text{-cm}^2 \qquad (2.27)$$

Table 2.2 shows values of W for A = 10^{-3}M. We have also assumed, for simplicity, that only one of the species A_O or A_R dominates the impedance.

Table 2.2 Computed values of W for A = 10^{-3}M. ω = 1 rad/s.

ION	H_+	OH^-	Cu^{2+}	Cu^+	Cl^-	SO_4^{2-}	I^-	Br^-	ClO_4^-
D(cm^2/s)	9.3	5.2	0.75	1.35	2.0	1.1	2.0	2.1	1.8
W(Ω-cm^2)	28	37	24	72	59	20	59	58	63

Warburg impedances at activities different from 10^{-3}M can easily be extrapolated from Table 2.2. The remarkable feature of Table 2.2 is that the values of W do not differ by much more than a factor of two.

The magnitude of the reaction resistance R_1 can vary widely, depending on the value of the exchange current i_0 ($R_1 = RT/nFi_0$). Since i_0 can be any value from 10^{-1} to 10^{-16} A/cm^2 (Bockris and Reddy, 1970), R_1 can range from less than 1 to 10^{12} Ω.

If we include the solution resistance R_S and the triple layer capacitance C, the total electrode impedance can be written as

$$\underline{Z} = R_s + j\omega C + \left(\frac{1}{R_1+\omega^{-1/2}\sigma(1-j)}\right)^{1/2} \qquad (2.28)$$

The equivalent circuit representing this impedance is shown in Figure 2.3. This is the classical Randles equivalent circuit (Randles, 1947). It is also the circuit that both Madden (1961) and Angoran (1975) found appropriate for explaining most of their I.P. data. Some modifications to the faradaic branch are now considered.

2.2.1 Effects of a Finite Diffusion Layer on the Warburg-Impedance

The expression (equation 2.26), derived for the Warburg impedance, shows that W is inversely proportional to the square root of frequency. The implication is that $W\to\infty$, as $\omega\to 0$. Concomitant with this, is the idea that the diffusion layer grows unbounded. In practice, the diffusion layer has a finite thickness δ of approximately 0.025 to 0.05 cm. The applied current produces concentration changes close to the electrode causing natural convection to limit the diffusion layer zone. In our experiments, which utilize plane parallel electrodes, δ is probably closer to 0.025 cm

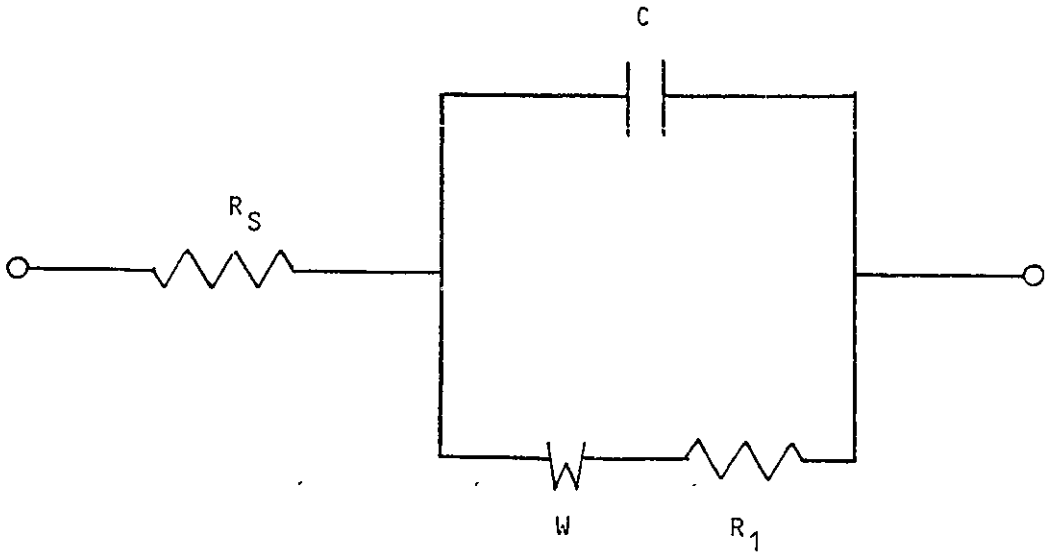


Figure 2.3: Randles Equivalent Circuit Model

R_S = Solution resistance

C = Triple layer capacitance

W = Warburg impedance

R_1 = Reaction resistance

(Levich, 1962). δ depends inversely on the relative speed between the solution and the electrode, but reaches a limiting value of ~0.001 cm for extreme stirring or agitation. There is also a weak inverse relationship between δ and the concentration, $\delta \sim C^{-1/4}$ (Levich, 1962). Our a.c. experiments are normally performed with the electrode at its d.c. rest potential. If we altered this d.c. potential by applying current to the electrodes, via a third electrode, then δ would also be lowered (Barada and Trumpler, 1954).

When solving the diffusion equation, we assumed that $A(x \to \infty, t) = A$. That is, the activity very far from the electrodes is equal to the activity in the bulk solution. This condition allows the diffusion layer to extend in theory, to infinity. To correct this situation it is necessary to modify the above condition to $A(x \geq \delta, t) = A$.

The appropriate mathematical modifications were carried out by Llopis and Colon (1956), and somewhat modified by Sluyters-Rehbach and Sluyters (1970). Recently, Dawson and John (1980) also discussed this problem, and the form of their result is perhaps the most useful. The modified diffusion impedance $\underline{W}_M$ is given by:

$$W_R = \frac{\sigma}{\omega^{1/2}} \left(\frac{\text{Sinh } K\omega^{1/2} + \text{Sin } K\omega^{1/2}}{\text{Cosh } K\omega^{1/2} + \text{Cos } K\omega^{1/2}} \right) \tag{2.29}$$

$$W_I = \frac{\sigma}{\omega^{1/2}} \left(\frac{\text{Sinh } K\omega^{1/2} - \text{Sin } K\omega^{1/2}}{\text{Cosh } K\omega^{1/2} + \text{Cos } K\omega^{1/2}} \right) \tag{2.30}$$

where we have taken $\underline{W}_M = W_R - jW_I$. The diffusion factor K is defined by:

$$K = \delta(2/D)^{1/2} \tag{2.31}$$

where D ($D_O = D_R = D$) is the diffusion constant of the active ion and δ the maximum value of the diffusion length, for the given experimental conditions. Note that as $\omega \to 0$, the magnitude $|W_M| \to \sigma K$, while the phase angle $\to 0^\circ$.

In Table 2.3 we display some values of K computed by equation (2.31). Note that we have taken δ(stagnant) ~0.02 cm. We choose this value instead of a larger one, because we usually stirr our solution prior to taking impedance measurements and some residual motion is probably still present.

Ion	Stagnant δ ~ 0.02 cm	Stirred δ ~ 0.01 cm	Max. Stirring δ ~ 0.001 cm
H^+	2.9	1.5	0.15
OH^-	3.9	2.0	0.20
Cu^{2+}	10	5.2	0.52

Table 2.3 Diffusion factors K for H^+,OH^- and Cu^{2+}

Stirring, in our system is accomplished by a magnetic stirrer, and the velocity of the solution at the electrode is not very great. We certainly do not get close to the maximum stirring regime, when δ reduces to the limiting value of ~0.001 cm. Such small diffusion layer thicknesses are usually obtained with a rotating disc electrode. Figure 2.4 shows the effects of the finite diffusion layer on the Warburg impedance for four representative values of K. Note that the classical Warburg impedance is modified only for K<5 at a frequency of 0.1 HZ, the lowest frequency in many of our experiments. The actual choice of K is very difficult and

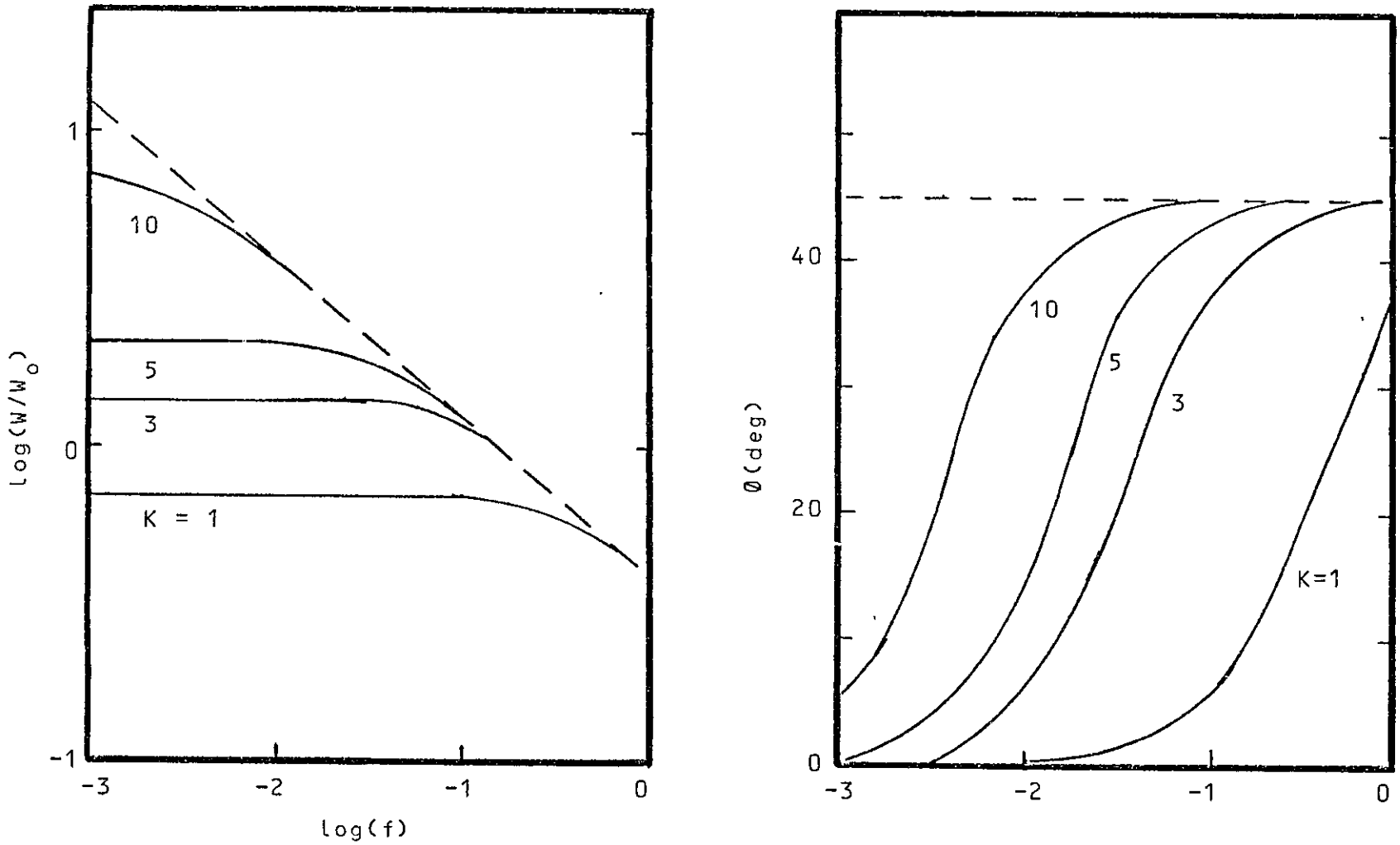


Figure 2.4: Warburg magnitude and phase as modified by the finite diffusion layer

W_o = W at w = 1 rad/s $K = \delta(2/D)^{1/2}$

estimates are probably good only to a factor of 2 or 3. Nevertheless, the above modification should be incorporated into any interpretation of data obtained at low frequency (0.1 HZ) and/or with stirring. Note also that the effects are more pronounced for the H^+ and OH^- ions.

2.2.2 Effects of the Dissociation of Water on the Warburg Impedance.

A special situation arises when the active ion in the electro-chemical reaction involves H^+ or OH^-. Changes in the concentration of H^+ or OH^- are buffered by the dissociation of water according to,

$$H_2O \underset{k_r}{\overset{k_f}{\rightleftharpoons}} H^+ + OH^- \tag{2.32}$$

we follow the approach of Madden (1961) in deriving an expression for the Warburg impedance under these conditions. The diffusion of components to and from the electrode is constrained by (2.32.) This modifies Fick's Law to read

$$\frac{\partial X}{\partial t} = D\left(\frac{\partial^2 X}{\partial x^2}\right) - k_r XY + k_f \tag{2.33}$$

$$\frac{\partial Y}{\partial t} = D\left(\frac{\partial^2 Y}{\partial x^2}\right) - k_r XY + k_f \tag{2.34}$$

where we have assumed for algebraic simplicity that $(H^+) = X$ and $(OH^-) = Y$ and also that the diffusion coefficients of H^+ and OH^- are equal. The product XY may be expanded as: $XY = (X_o + \Delta X)(Y_o + \Delta Y) \approx X_o Y_o + \Delta X\, Y_o + \Delta Y\, X_o$ to first order. $X_o\, Y_o = 10^{-14}$ the equilibrium value for the dissociation constant of water. Assuming a solution of the form $\exp\{j(\omega t + kx)\}$

(2.33) and (2.34) lead to:

$$j\omega X = -Dk^2X - k_rX\Delta Y - k_rY\Delta X + k_f - k_rX_oY_o \tag{3.35}$$

$$j\omega Y = -Dk^2Y - k_rX\Delta Y - k_rY\Delta X + k_f - k_rX_oY_o \tag{3.36}$$

Because of the equilibrium condition that $k_f/k_r = 10^{-14}$, the last two terms in (2.35) and (2.36) cancel. In order to have a solution to the coupled equations (2.35) and (2.36), the following determinant must be zero.

$$\begin{vmatrix} Dk^2 + j\omega + k_rY & k_rX \\ k_rY & Dk^2 + j\omega + k_rY \end{vmatrix} = 0 \tag{2.37}$$

This leads to two roots,

$$k_1 = -j\omega/D \tag{2.38}$$

$$k_2 = -\{j\omega + k_r(Y_o + X_o)\}/D \tag{2.39}$$

The solutions are now constrained by four constants such that,

$$\Delta H^+ = \Delta X = B_1 e^{jk_1x} + B_2 e^{jk_2x} \tag{2.40}$$

$$\Delta OH^- = \Delta Y = A_1 e^{jk_1x} + A_2 e^{jk_2x} \tag{2.41}$$

If we consider alkaline solutions where OH^- is the active ion then the boundary conditions are,

$$\left(\frac{\partial X}{\partial x}\right)_{x=0} = 0 \tag{2.42}$$

and

$$\left(\frac{\partial Y}{\partial x}\right)_{x = 0} = -i_b / jnFD \tag{2.43}$$

which gives, upon substitution, into (2.40) and (2.41)

$$A_1 = \frac{k_1}{k_2}\ \frac{X_o}{Y_o} = A_2 = B_2 = \frac{-k_1}{k_2} B_1 \tag{2.44}$$

In alkaline environments $Y_o >> X_o$, thus $|B_1| << |A_1|$ and $|A_2| >> |A_1|$, hence

$$i_b = -jnFD\left(k_1 A_1 + k_2\ \frac{k_1}{k_2}\ \frac{X_o}{Y_o} A_1\right) \tag{2.45}$$

therefore

$$A_1 = \frac{-i_b}{nF\sqrt{j\omega D}\ (1+ X/Y)} \tag{2.46}$$

and

$$A_2 = \frac{-k_1 X i_b}{nFk_2\ Y\sqrt{j\omega D}\ (1+ X/Y)} \tag{2.47}$$

Defining $k_1/k_2 = K$, the total concentration change can be written as,

$$A_1 + A_2 = \frac{i_b}{nF\sqrt{j\omega D}}\ \frac{(1+KX/Y)}{(1 + X/Y)} \tag{2.48}$$

leading to a diffusion impedance, defined by (2.19), given by

$$W_b = \frac{RT}{n^2F^2(OH^-)\sqrt{j\omega D}}\left(\frac{1 + K\ (H^+)/(OH^-)}{1 + (H^+)/(OH^-)}\right) \tag{2.49}$$

Castellan (1971) gives $k_r = 1.4 \times 10^9\ M^{-1}\ s^{-1}$ and $k_f = 2.5 \times 10^{-5}\ s^{-1}$. Substituting these values gives $K << 1$ for all concentrations of H^+ and OH^-. Accordingly, the maximum buffering effect occurs when $(H^+) = (OH^-)$,

at pH = 7. This causes a factor of two reduction in the Warburg impedance. At higher OH^- concentrations there is essentially no buffering. In acid environments, H^+ is likely to be the active ion. The boundary conditions (2.42) and (2.43) are therefore interchanged. This results in the same expression for W_b, but with H^+ and OH^- interchanged.

Generally, the buffering action of the dissociation of H_2O amounts to no more than a factor of two and this occurs at pH = 7.

2.2.3 Effects of Surface Processes on the Faradaic Branch

The incorporation of surface processes into the electrode impedance model was considered in great detail by Fleichmann et. al. (1967). We give only their results here. Figure 2.5 shows the general reaction mechanisms and the associated equivalent circuit. An ion M^+ diffuses through solution (W) to the electrode surface, where it is discharged (R_1). The adatom then diffuses along the surface to some preferred adsorption site ($\underline{Z}_S$). The adsorbed ion may then be incorporated into the crystallographic lattice of the electrode material (R_L). The possible accumulation of adatoms gives rise to the capacitance C_S, which is normally called the pseudo-capacitance. The expressions for W and R_1 are obviously unchanged, whereas,

$$\underline{Z} = LR_1\left(\frac{k_1}{D_s}\right)^{1/2}\left(\frac{1}{1+j\omega/k}\right)^{1/2} \tag{2.50}$$

$$R_L = LR_1\left(\frac{k_1}{k_2}\right) \tag{2.51}$$

$$C_s = \frac{1}{k_1 R_1} \tag{2.52}$$

M^+ $\xrightarrow[\text{in Solution}]{\text{Diffuses}}$ M^+ (Surface)

M^+ (Surface) $\xrightarrow[\text{transfer}]{\text{electron}}$ $M_{adsorbed}$

M_{ads} $\xrightarrow[\text{on Surface}]{\text{Diffusion}}$ M_{edge}

M_{edge} $\longrightarrow$ $M_{lattice}$

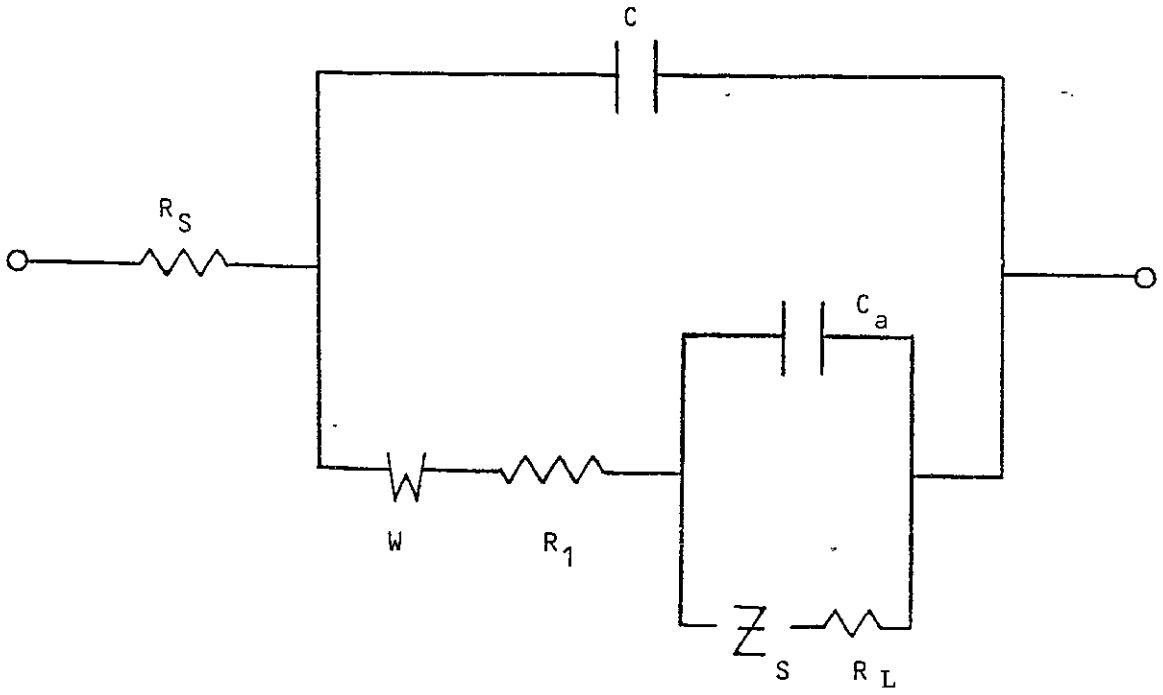


Figure 2.5: Reaction Paths and Equivalent Circuit Incorporating Surface Phenomena

C_a → Pseudocapacitance

Z_S → Surface Diffusion Impedance

R_L → Crystallization Resistance

where k_1, and k_2 are reaction rate constants, L the average distance between active sites and D_S the diffusion coefficient along the surface. $\underline{Z}_S$ behaves like a classical Warburg impedance at 'high' frequencies and becomes resistive at 'low' frequencies. Under many circumstances ω is small enough to make Z_S resistive and the surface processes can then be represented by a parallel combination of C_S and a resistor R. Note also that it is possible to obtain phase angles larger in magnitude than 45^o with the equivalent circuit of Figure 2.4.

In the next section we discuss the effects of adsorption on the electrode impedance.

2.3 THE ADSORPTION BRANCH

Many measured impedance spectra show phase angles with magnitudes greater than 45^o, at low frequencies (10^{-1} to 10^{-2} HZ). This can only be accounted for by making C, in the equivalent circuit extremely large. In practice, C must be made so large that it cannot be interpreted as a normal triple layer capacitance.

Numerous attempts at solving this problem were made by various electrochemists (Laitinen and Randles, 1955; Llopis et. al., 1959, 1961; Senda and Delahay, 1961; and Timmer et. al. 1968a, 1968b). The common denominator in these studies was adsorption, although the resulting equivalent circuits differed greatly depending upon the postulated boundary conditions. A few excellent reviews on this subject are available (Sluyters-Rehbach and Sluyters, 1970; Parsons, 1970; Bauer et. al. 1972, Gileadi and Conway, 1964).

Three types of adsorption effects may be considered:

1. Electroinactive species: these are usually ions of the supporting electrolyte that do not take part in an actual electrode reaction (i.e. electron transfer).

2. Electroactive species; for example, in a metal/metal ion reaction, the ion in addition to obeying the normal electrochemical laws, as discussed previously, may itself be chemically adsorbed.

3. Reaction Intermediates: this category refers to the adsorption of species formed during the electrochemical reaction. Such species are assumed to be transformed further, hence the terminology - intermediates.

For the purpose of deriving an expression for the impedance of an electrode reaction with adsorption present, the differentiation between electroactive and electroinactive species is immaterial. The differentiation is only important when considering the details of the impedance elements. We will not consider reaction intermediates in any detail here, although the pseudocapacitance C_S of the last section belongs to this category.

At the present time, the most widely accepted solution to the adsorption problem is that of Delahay (1966). The results of Sluyters Rehbach et. al. (1967) and Timmer et. al. (1967) are similar, but more readable. Below we derive an expression for the adsorption impedance assuming that the process is independent of the normal faradaic and non-faradaic branches of the total impedance. The resulting adsorption impedance therefore acts in parallel with C, and the series combination of R_1 and W.

Adsorption is usually related to a quantity Γ, which is defined as the surface excess of the adsorbed ion (for more details on Γ, see for example, Gileadi, 1967). We seek a relationship between the potential E, the activity of the adsorbed ion in the bulk solution A, and the surface excess Γ, when the electrode is subjected to a sinusoidal current. In general, we should consider both oxidized and reduced species, namely (Γ_O,Γ_R) and (AO, A_R), but to simplify the discussion we treat only one specie. Expanding

E, we can write

$$dE = \left(\frac{\partial E}{\partial A}\right)_{\Gamma} dA + \left(\frac{\partial E}{\partial \Gamma}\right)_{A} d\Gamma \tag{2.53}$$

expanding further,

$$dE = \left(\frac{\partial E}{\partial A}\right)_{\Gamma} dA + \left(\frac{\partial E}{\partial \Gamma}\right)_{A} \left(\frac{\partial \Gamma}{\partial q_M}\right) dq_M \tag{2.54}$$

where q_M is the surface charge density of the electrode, such that, the adsorption current is,

$$i_a = dq_M/dt \tag{2.55}$$

The apparent depletion or accumulation of ions at the electrode surface, due to the time dependence of the adsorption process, must be neutralized by diffusional transport in solution. A solution to the diffusion equation (2.20), is given by (2.21),

$$A(x,t) = A + \Delta A e^{-x\sqrt{j\omega/D}} + j\omega t \tag{2.56}$$

The equality of fluxes at the electrode surface also requires that,

$$i_a = -nFD \left(\frac{\partial A}{\partial x}\right)_{x=0} \tag{2.57}$$

Using (2.42) this gives,

$$\Delta A = i_a / nF\sqrt{j\omega D} \tag{2.58}$$

Writing (2.56) as,

$$i_a = \frac{dq_m}{dt} = \frac{dq_M}{dA}\left(\frac{dA}{dt}\right)_{x=0} \tag{2.59}$$

results in,

$$dq_M = (i_a / j\omega)\, e^{-j\omega t} \tag{2.60}$$

Substituting (2.58) and (2.60) into (2.54) leads to an expression $\underline{Z}a$ given by:

$$\underline{Z}_a = \frac{1}{j\omega C_a} + \frac{W_a}{\sqrt{j\omega}} \tag{2.61}$$

where

$$C_a \equiv \frac{dq_M}{d\Gamma}\left(\frac{\partial \Gamma}{\partial E}\right)_A \tag{2.62}$$

and

$$W_a = \left(\frac{\partial E}{\partial A}\right)_\Gamma / nF\sqrt{D} \tag{2.63}$$

If we define, by analogy with equation (2.26), a Warburg impedance for a specie in solution by,

$$W_{sol} = W = \frac{RT}{n^2F^2A\sqrt{D}} \tag{2.64}$$

then W_a becomes,

$$W_a = W_{sol}\left(\frac{nF}{RT}\right)\left(\frac{\partial E}{\partial \ln A}\right)_\Gamma \tag{2.65}$$

It is also possible to write (2.35) in a different form, since $f(\Gamma, A, E) = 0$ then

$$\left(\frac{\partial E}{\partial \Gamma}\right)_A \left(\frac{\partial \Gamma}{\partial A}\right)_E = -\left(\frac{\partial E}{\partial A}\right)_\Gamma \tag{2.66}$$

thereby giving,

$$W_a = -\frac{\left(\frac{\partial E}{\partial \Gamma}\right)_A \left(\frac{\partial \Gamma}{\partial A}\right)_E}{nF\sqrt{D}} \tag{2.67}$$

Equation (2.67) is the form normally encountered in the literature, but as we will discuss below, (2.65) is more meaningful in practice.

For electroinactive species E is not directly dependent on the activity A, at least, not by any Nernestian equation. In other words, the species belonging to A are not potential determining and it is in this sense that they are electroinactive. For example, suppose E is pH dependent and A refers to the activity of Cl^-. In a linear experiment $|\Delta E| \sim 6mV$. This change in E produces a corresponding change in pH but the change in (Cl^-) is probably close to zero. From (2.65) we therefore see that $W_a >> W_{sol}$. This result could also be obtained directly from energy arguments. Species belonging to this class are exactly those discussed in Section 2.1, when adsorption in the triple layer was being considered. Accordingly, the adsorption of anions produce not only an increase in C_1, the capacitance of the triple layer, but also a Warburg impedance and a capacitor, both in parallel with C. The resulting equivalent circuit is shown in Figure 2.6. An interesting feature of this equivalent circuit is that the faradaic branch $(W\text{-}R_1)$ probably controls the impedance and potential at d.c. equilibrium, but under a.c. conditions it is possible that the adsorption process $(W_a - C_a)$ dominates the impedance. This feature will be discussed further in Chapter IV.

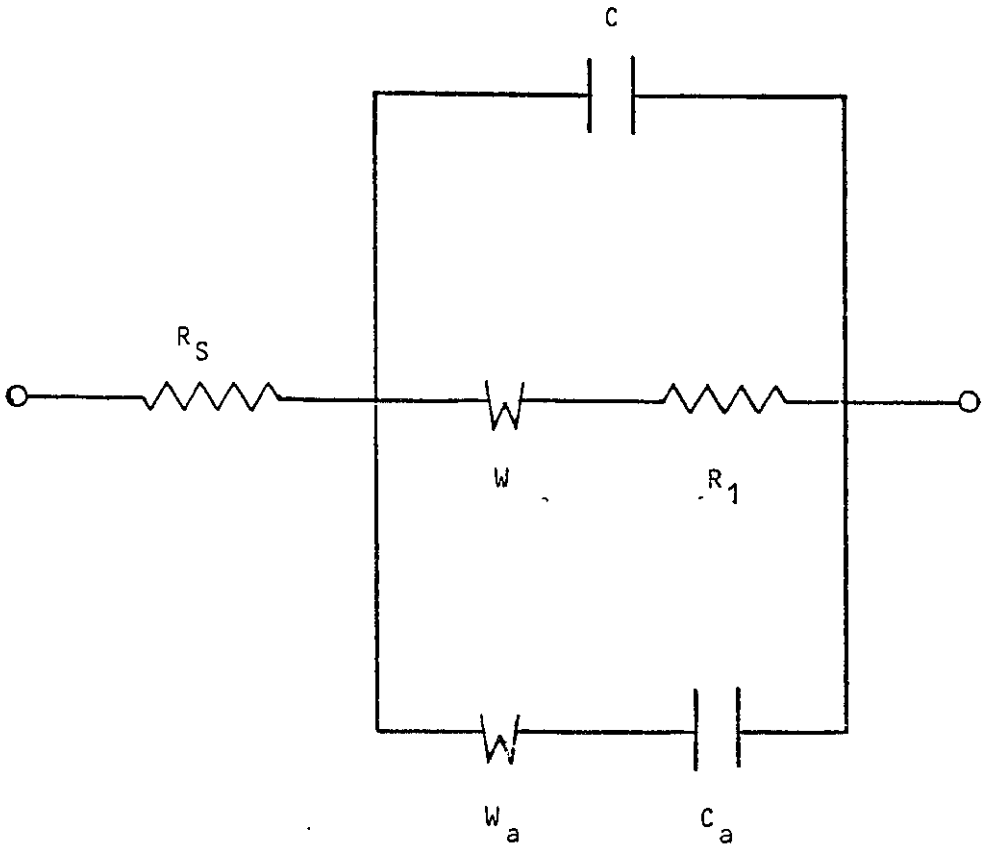


Figure 2.6: Equivalent circuit including effects of adsorption

W_a → Adsorption Warburg

C_a → Adsorption Capacitance

The other circuit elements have their usual wearing.

Electroactiveactive species are by definition, potential determining, hence E is related to the activity A by a Nernstian equation, such that, by (2.65) $W_a = W_{sol}$. The equivalent circuit remains the same as that in Figure 2.6, only the interpretation is different.

Consider again the problem of decoupling between the non-faradaic and adsorption paths. The change in concentration associated with the adsorption path is much larger than that of the non-faradaic path. This is so because of the presence of the diffusion component W_a, in the adsorption branch. Moreover, C (the double layer capacitance) is normally much less than C_a. The current in the non-faradaic path is therefore much less than in the adsorption branch. Our approximate solution, assuming decoupling, is therefore adequate in practice.

We have now completed the review of the electrode models we wish to use at various points in this study. In the next section we briefly outline our methods of interpretation.

2.4 ESTIMATION OF THE IMPEDANCE PARAMETERS

As described in the next chapter, most of our impedance measurements consisted of magnitude and phase data taken at frequencies in the range 10^{-2} to 10^{+3}HZ. We used an iterative damped least squares method to estimate the parameters of a given equivalent circuit model. The mathematical details of this inverse method can be found in Appendix A. Generally, the parameter estimation was reliable and accurate. We discuss now, in a qualitative way, the concepts of parameter resolution and non-uniqueness.

Resolution essentially refers to the sensitivity of the inverse scheme to a particular parameter. A well resolved parameter is one that we would normally assume to have been accurately determined. The solution

resistance was usually the best resolved parameter for all the models considered. The remaining parameters showed varying degrees of resolution.

Non-uniqueness arises in two ways. For a given model, different initial guesses of the parameters may produce dissimilar final results. Nonuniqueness also exists between different equivalent circuit models. Experience has shown that for the models considered, the former type of non-uniqueness very rarely existed and the iterations usually converged to a unique set of parameters. Obviously, only highly resolved parameters showed this uniqueness. The latter type of non-uniqueness was a more serious problem. Many impedance spectra were such, that more than one equivalent circuit model produced similar errors of misfit between the model and data. Examples of this type of non-uniqueness will be encountered later in this study.

Nevertheless, our method of interpretation normally led to very reliable parameter estimates and the technique is certainly much superior to the graphical methods used by most electrochemists.

SUMMARY

In this chapter we discussed a number of equivalent circuits used for modelling the electrode impedance. Our approach tended to separate different effects, but in practice, the impedance may have many mechanisms operating simultaneously. For example, adsorption, a finite diffuse layer, buffering by H_2O and surface phenomena may all be important at a given electrode at the same time. The resultant equivalent circuit then becomes too complicated for interpretational purposes. In order to obtain reasonable resolution and uniqueness in our estimates of parameters, we hope that one of the above mechanisms is clearly rate determining, thereby domi-

nating the impedance and simplifying the equivalent circuit model. Fortunately, this is normally the situation.

III

EXPERIMENTAL METHODS

INTRODUCTION

The experimental techniques used in this study are now discussed. The purpose of this chapter is to consider the framework within which accurate and reliable I.P. experiments may be performed.

We review the important features of Pourbaix diagrams as they pertain to our experimental method. Particular attention is paid to the interpretation of Eh measurements. The experimental apparatus and methods are then described. Finally, we discuss some experiments to illustrate the accuracy of the methods. The experiments described also provide us with confidence that the impedance spectrum in Induced Polarization measurements can indeed be related to electrochemical properties.

3.1 POURBAIX (Eh-pH) DIAGRAMS

The objective of our laboratory experiments is to correlate the induced polarization behaviour of a particular mineral electrode, with its Eh/pH environment. The electrochemical stability fields of various solid and aqueous species are conveniently described graphically, on an Eh-pH diagram. The systematics of such diagrams have been described by Pourbaix and co-workers (Pourbaix 1949, 1966, 1973, and also Christ and Garrels, 1965). Because Pourbaix diagrams are germane to the present study, an understanding of their construction and limitations is therefore of critical importance. Accordingly, we describe how the Pourbaix diagram for copper, in H_2O, is realized. We describe the Cu/H_2O system because it is simple, and at the same time contains all the features of more complicated

Pourbaix diagrams. Copper was chosen because of its relationship to the copper sulfides and also because its electrochemical properties are quite well known. Prior to discussing the Cu/H_2O system we turn our attention to the stability of H_2O, which forms the basis of all Eh-pH diagrams in aqueous media.

3.1.1 The Electrochemical Stability of H_2O

The limits of stability of H_2O are constrained by two redox couples. In terms of Eh the upper limit of stability is given by:

$$O_2(g) + 4H^+ + 4e = 2H_2O$$

therefore:

$$Eh(mV) = 1230 + \frac{RT}{4F} \ln (P_{O_2}) + \frac{RT}{F} \ln (H^+)$$

relative to a standard hydrogen electrode (SHE). Because our Eh measurements are taken relative to a saturated calomel electrode (SCE), we have:

$$Eh(SCE) \approx Eh(SHE) - 245(mV)$$

For $T = 25^{\circ}C$ and Eh values in mV, we therefore get,

$$Eh(SCE) = 985 + \frac{59.2}{4} \log P_{O_2} - 59.2pH \qquad (a)$$

Henceforth, all Eh measurements will be referenced to the SCE and given in mV. Equation (a) is usually plotted for $P_{O_2} = 1$.

Similarly, the lower limit of stability of H_2O is given by:

$$2H^+ + 2\,e = H_2(g)$$

whereby,

$$Eh = -245 - \frac{59.2}{2} \log P_{H_2} - 59.2pH \qquad (b)$$

Again this is usually plotted for $P_{H_2} = 1$. Lines (a) and (b) are fundamental to all Pourbaix diagrams in aqueous media. They are shown in Figure 3.1. Water is only stable between these lines, decomposing into $O_2(g)$ above (b) and into $H_2(g)$ below (a).

Of considerable importance in practical electrochemistry is the stability of hydrogen peroxide. Sato (1960) showed that most Eh measurements in oxidizing environments are indeed controlled by the H_2O_2 stability field. The reaction is,

$$O_2(g) + 2H^+ + 2\,e = H_2O_2$$

therefore:

$$Eh = 435 - 59.2pH + 29.6 \log (P_{O_2}/(H_2O_2))$$

Because the ratio of P_{O_2} to H_2O_2 controls the Eh, the Eh is usually expressed as,

$$Eh = 435 - 59.2\ pH + 29.6 \log(q) \qquad (c)$$

where $q = P_{O_2}/(H_2O_2)$. The shaded region of Figure 3.1 is constrained by (c), with $q = 1$ to 10^{-6}.

3.1.2 Cu-H_2O System

We have just described how the stability of H_2O and H_2O_2 can be expressed on an Eh-pH diagram. To complete a Pourbaix diagram it is necessary to write down all possible electrochemical and chemical reactions possible among the species under consideration. For the Cu/H_2O system we consider the following species: Cu, Cu^+, Cu^{2+}, CuO, Cu_2O, $HCuO_2^-$, H^+ and OH^-. The other oxides and hydroxides of Cu are less stable than CuO and

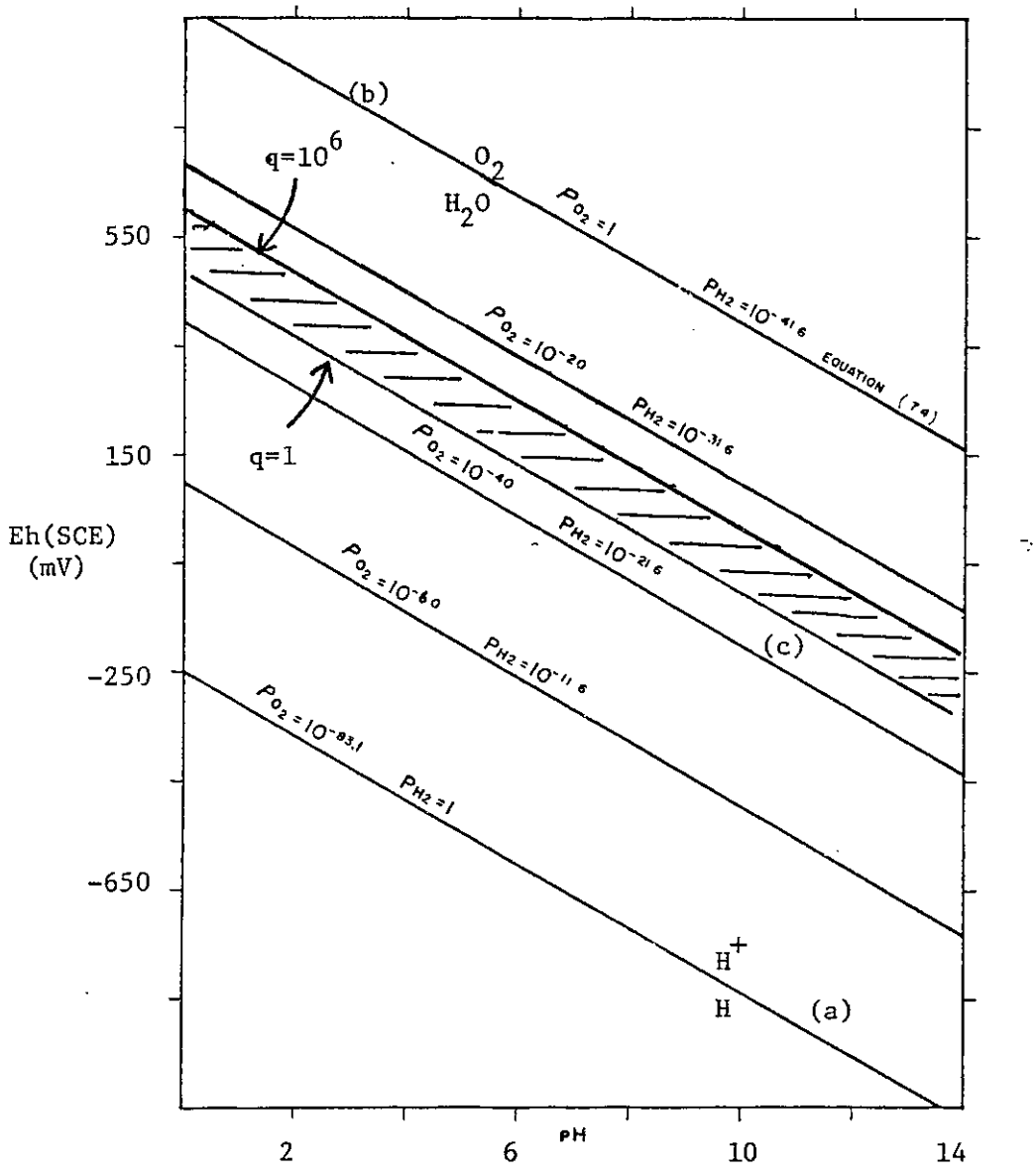


Figure 3.1: Stability limits of water and hydrogen peroxide. Adapted from Garrels and Christ (1965).

Cu_2O, hence they will not be considered. The possible reactions are displayed in Table 3.1 and plotted in Figure 3.2. The lower limit of concentration of aqueous species is ARBITRARILY set at 10^{-6}M. A point on this diagram is described by a single (Eh,pH) value. Under suitable conditions, as described below, the (Eh,pH) value can thus be correlated with the species that are stable at this point. Accordingly, I.P. responses can be catalogued in terms of the Eh and pH at which the measurements are taken.

3.1.3 Eh Measurements

Reactions (a), (b) and (c) are always present in aqueous media. Additionally, many other redox couples may be operative, and they may be represented quite generally as,

$$O^x + ne \rightarrow R^y \qquad (d)$$

therefore:

$$Eh = E_o + \frac{RT}{nF} \ln \frac{(O)^x}{(R)^y}$$

If we define the Eh of reactions (a), (b), (c) and (d) as Eh_a, Eh_b, Eh_c and Eh_d, respectively, then at EQUILIBRIUM,

$$Eh_a \equiv Eh_b \equiv Eh_c \equiv Eh_d \equiv Eh$$

The problems associated with Eh measurements are twofold: (1) how do we measure the Eh accurately and (2) what meaning, if any, can we attach to the measurement when the system is not at equilibrium.

Let us consider firstly what is involved in an Eh measurement. One way of attempting to measure the Eh (i.e. the electron activity) of a solution is by means of an inert electrode (platinum is the most popular). The electrode is inert in the sense that it does not take part in any anion/cation exchange, but acts simply as an electron donor/acceptor. If

TABLE 3.1

Electrochemical Reactions for the $Cu-H_2O$ system

Chemical Reactions (vertical lines)

(1) $2\,Cu^{+} + H_2O = Cu_2O + 2H^{+}$	$pH = -0.84 \log(Cu^{+})$
(2) $Cu^{2+} + H_2O = CuO + 2H^{+}$	$pH = 3.94 - 1/2\log(Cu^{2+})$
(3) $Cu^{2+} + 2H_2O = HCuO_2^{-} + 3H^{+}$	$pH = 8.91 + 1/3\log(HCuO_2^{-})(Cu^{2+})$

Redox Reactions - pH Dependent (variable slopes)

(4) $Cu_2O + 2H^{+} + 2e = 2Cu + H_2O$	$E_h = 229 - 59.2\ pH$
(5) $2Cu^{2+} + H_2O + 2e = Cu_2O + 2H^{+}$	$E_h = -39 + 59.2\ pH + 59.2\log(Cu^{2+})$
(6) $2CuO + H^{+} + 2e = Cu_2O + H_2O$	$E_h = (427 \text{ to } 505) - 59.2\ pH$
(7) $CuO + 2H^{+} + e = Cu^{+} + H_2O$	$E_h = (378 - 118.4\ pH - 59.2\log(Cu^{+})$
(8) $HCuO_2^{-} + 3H^{+} + e = Cu^{+} + 2H_2O$	$E_h = 1491 - 177.3\ pH$

Redox Reactions - pH Independent (horizontal lines)

(9) $Cu^{+} + e = Cu$	$E_h = 278 + 59.2 \log (Cu^{+})$
(10) $Cu^{2+} + 2e = Cu$	$E_h = 95 + 29.6 \log(Cu^{2+})$
(11) $Cu^{2+} + e = Cu^{+}$	$E_h = -84 + 59.2 \log(Cu^{2+})(Cu^{+})$

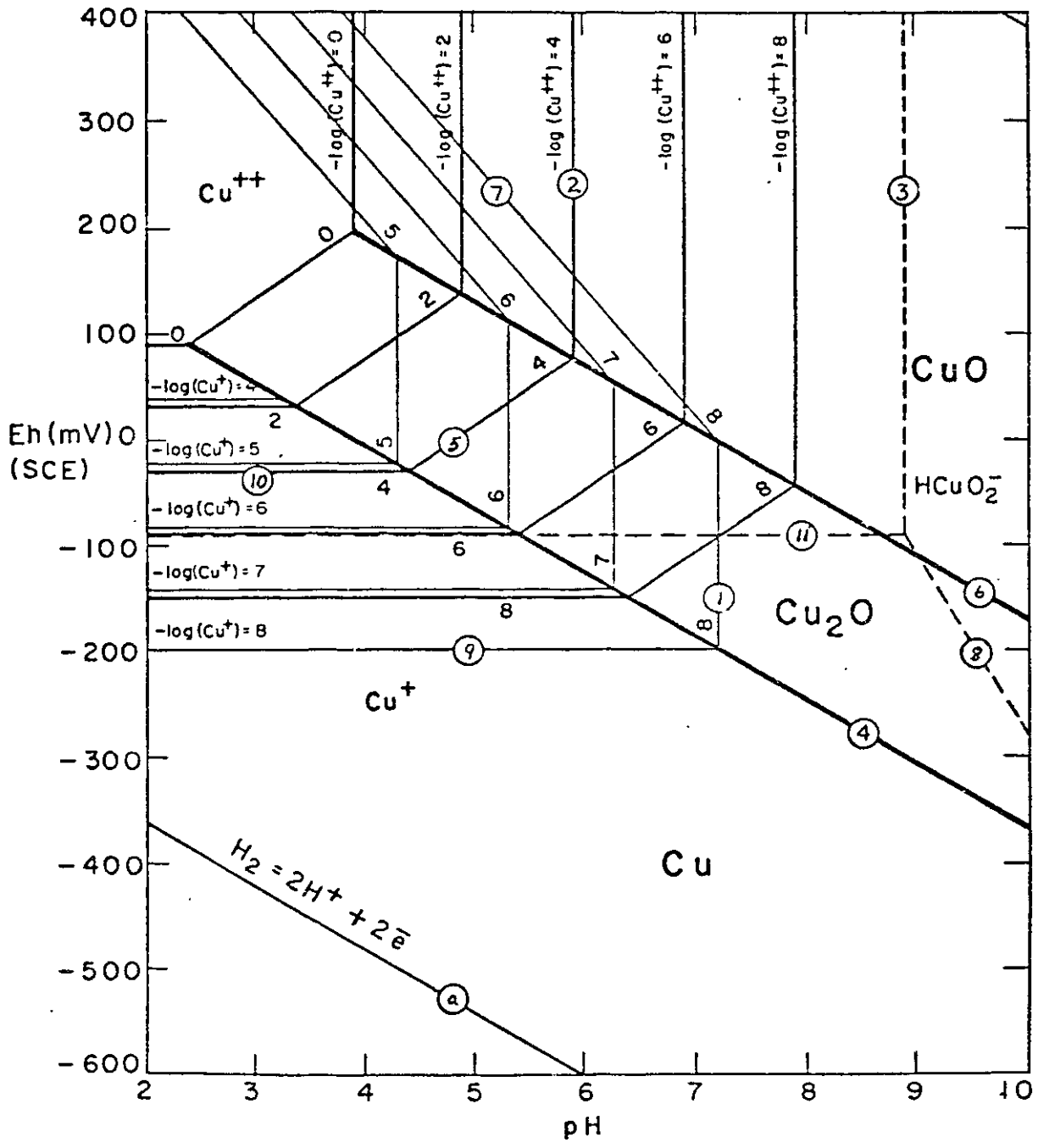


Figure 3.2 Eh-pH Diagram of Copper in Water (adapted from Pourbaix, 1966)

a deposit forms on the Pt electrode it ceases to behave as an inert electrode. For this reason the Pt electrode must always be kept clean. The other important point is that the measuring instrument should ideally draw zero current. Our Eh meter has an imput resistance of about 10^{13} ohms. Since the normal values of Eh are approximately $\pm$1V, the current through the meter is on the order of 10^{-13}A. Providing the exchange current i_o is much greater than this value, then our system approximately fulfills the ideal condition of zero current. This condition is indeed met for many redox couples.

Consider now the question of equilibrium, in relation to Eh measurements. As mentioned above, at equilibrium all the redox systems in solution adjust themselves to the same potential. In practice, equilibrium is hardly ever attained before an Eh reading is taken. It is therefore very important to understand the meaning of Eh measurements taken under non-equilibrium conditions.

Generally, as described in Chapter II, the impedance at an electrode normally consists of a surface impedance, an impedance due to mass transport in solution and an activation resistance. At equilibrium, each reaction gives the same potential E, even though their impedances may be very different. Because the impedances of different reactions act in parallel with each other the reaction with the smallest impedance controls the electrode impedance.

In non-equilibrium situations the electrode impedance is also controlled by the reaction with the lowest impedance. Accordingly, the measured potential is associated with this reaction and it may be very different from the potentials of the other redox couples. Moreover, the

quasi-equilibrium that exists at the Pt electrode and at the electrode under study may be very different. Since the electrode impedance we measure, is associated with the quasi-equilibrium in the vicinity of the electrode that we are studying, we should correlate the I.P. response with the electrode potential and not with Eh.

3.1.4 Pourbaix (E_M-pH) Diagrams - Concluding Remarks

Since our objective is to correlate the I.P. behaviour of various electrodes with their equilibrium positions on a Pourbaix diagram, we should therefore plot the values of the electrode potentials instead of the Eh. Henceforth, we plot Pourbaix diagrams as E_M-pH diagrams, where E_M refers to the potential of the metallic or mineral electrode under study. We retain the term Eh, for the potential at the platinum electrode.

We caution that the use of Pourbaix diagrams as E_M-pH plots does not completely solve all of the problems associated with the Pourbaix diagram. We have simply reduced the uncertainty, in non-equilibrium cases by one-half. E_M is a fairly precise measure of the redox reactions occurring at the electrode, but the other variable needed, namely the pH, must still be measured in the bulk of the solution. In non-equilibrium cases there is no reason why the bulk pH should be the same as that close to the electrode.

3.2 THE EXPERIMENT -- APPARATUS, METHODOLOGY AND ACCURACY

Electrode impedances may be measured in either the linear or non-linear regimes. At signal voltages greater than 25 mV (kT at room temperature), the current/voltage relationship becomes non-linear. Whereas

for signals much less than 25mV, there is an approximate linearity between voltage and current. For our linear experiments we keep the applied a.c. voltage at the electrodes at approximately 6mV peak-to-peak.

When acquiring data on the linear electrode impedance, we measure the complex impedance as a function of frequency. The magnitude and phase of the impedance are recorded at 5 or 6 frequencies, in decade steps, from 1KHZ down to 0.1 or 0.01 HZ. We record Eh, pH, E_M and sometimes E_{Cu_2S}, the latter being used as a monitor of the Cu^{2+} concentration. The non-linear measurements are done at a single low frequency, usually 0.03 or 0.01 HZ.

3.2.1 Cell Design

The electrochemical cell is essentially the same as that used by Angoran (1975). Figure 3.3 with some modifications, is taken from his thesis. The cell is made of plexiglass and has a volume of approximately 2 liters. It can also be made airtight, which is a necessity when studying electrode phenomena in reducing environments.

A critical aspect of the cell design is the actual electrode configuration. Our electrodes are usually about 1 cm^2, set in epoxy and contacted via watertight, spring loaded screw contacts in the rear.

In order to obtain the greatest measurement sensitivity, we wish to reduce the contribution of the solution resistance to a minimum, so that the total impedance is dominated by the actual interphasial impedance. The reduction or removal of the solution resistance R_S can be accomplished in three ways:

1. Increase the concentration of the supporting electrolyte.
2. Reduce the spacing between the electrodes.
3. Reduce or remove R_S electronically.

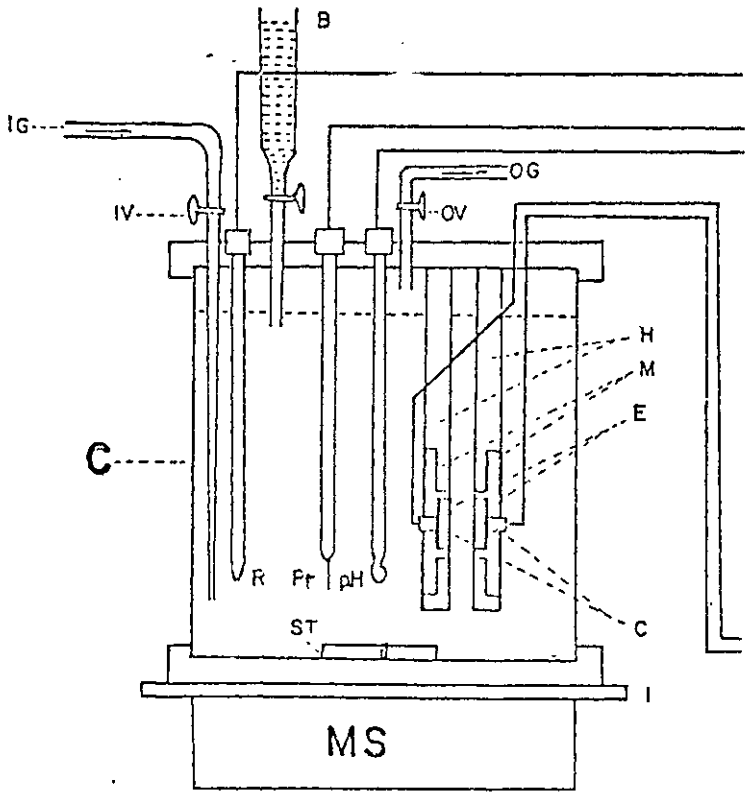


Figure 3.3: Schematic of experimental cell.

LC = line converter

M = molds in which electrodes are imbeded

C = spring loaded contacts

OG = outlet gas

IV = inlet valve

B = burette

Pt = platinum probe Eh electrode

ST = magnetic bar

MS = magnetic stirrer

H = electrode holders

E = working electrodes

IG = inlet gas

IV = inlet valve

OV = outlet valve

R = calomel reference electrode

pH = pH glass electrode

C = cell

We discuss these approaches below.

The supporting electrolytic solution should be inert, but under certain circumstances a very concentrated solution may become reactive. Accordingly, we set the concentration of supporting electrolyte to be one or two orders of magnitude greater than the expected concentration of the species which is active at the electrodes.

The lower limit of electrode separation is set by the diffusion length under the given experimental conditions. The theory presented in Chapter II assumed that the diffusion layers at the electrodes are independent, that is, they do not overlap with each other. The diffusion length in the frequency domain is given by $\delta \sim (D/\pi f)^{1/2}$, where D is the diffusion constant and f the frequency. Since the lowest frequency normally used is 0.01 HZ, the maximum diffusion length is ~0.1 mm. The spacing of our electrodes was made 10 times larger (~1 mm). Note that in the limit of very low frequency (d.c.), the diffusion layer actually reaches a limiting value of ~0.25 to 0.5 mm. Our spacing of 1 mm is therefore a practical optimum.

The third method, namely the reduction or removal of R_S by electronic means is very popular among electrochemists (Greef, 1978). The method normally incorporates positive feedback to compensate for the solution resistance. Positive feedback circuits are inherently unstable. In Appendix B we propose a method of compensation that does not utilise positive feedback. The experiments discussed in this and the next chapter were performed without any type of solution resistance compensation.

In summary, we note that R_S usually accounts for 10 to 20% of the magnitude of the impedance at the lower frequencies. At the higher frequencies, the phase angle would increase, and its measurement accuracy

somewhat improved, if R_S could be reduced. The solution resistance is normally the best resolved parameter of the equivalent circuit and it can therefore be accounted for quite accurately. Nevertheless, a reduction of its value would improve the experimental data, particularly the phase measurement.

3.2.2 Solution Preparation

Most of our experiments were conducted with deionised water (ρ~10KΩ-m) as the solvent. No attempt was made to remove the $CO_2(g)$ from the deionised water (pH 5.5) for experiments in oxidizing environments. To study phenomena in reducing environments, the $O_2(g)$ must be removed from solution. This was accomplished by bubbling $N_2(g)$, while stirring. $CO_2(g)$ was also removed by this process. Such a reduced solution has a pH~7 and an Eh between -100 and -200 mV. The Eh can be further reduced (<-600 mV) by bubbling $H_2(g)$ until it saturates the solution. We have found, that with water which was deionised, then distilled, that the $N_2(g)$ bubbling alone, reduced the Eh below -200 mV. This result indicates that the deionised water posesses some specie or species that is difficult to reduce.

3.2.3 Electrode Preparation

The electrodes are minerals or metals mounted in epoxy. The surface area of each electrode is ~1cm^2. They are usually polished with #600 silicon carbide paper, then washed thoroughly with distilled water, before insertion in the electrochemical cell.

Angoran (1975), measured very large impedances with electrodes that were polished with 1μ diamond polish. He attributed the high impedances to the smoothness of the electrode. We repeated these experiments and found

that the increased impedance was caused by the polishing compound used with the diamond polish. Apparently, the polishing liquid leaves a film on the electrode surface. If this film was removed with acid or the electrode polished with 1μ alumina polish, the impedance returned to about its normal value.

We also investigated the effects of surface roughness on the electrode impedance by using polishing grit sizes from 1μm to 45μm. No substantial difference was noted, although there might be a small increase in the impedance with electrode smoothness.

3.2.4 Data Acquisition

Figure 3.4 is a block diagram depicting the experimental arrangement used for the induced polarization measurements. The signal from a low frequency sinusoidal generator was converted to a constant current, which then passed through the electrode. The V-to-I converter acted as an a.c. constant current source, with zero phase shift for all frequencies less than 1KHZ. An amplifier with a gain of 100, sensed the voltage across the electrodes. This amplifier can also apply a d.c. shift, prior to the application of the signal current, to buck out the potential difference between the electrodes. A Tetronik (5103N) storage oscilloscope, in its X-Y mode, was used as the recording instrument. Details of the electronic circuits can be found in Appendix B.

For the linear measurements, the input current was adjusted to keep the output voltage across the electrodes at 6 mV(p-p). The phase difference (ϕ) was computed from the displayed Lissajous pattern. The magnitude (Z) of the impedance was measured, by comparison with a standard decade resistor, as shown in Figure 3.4.

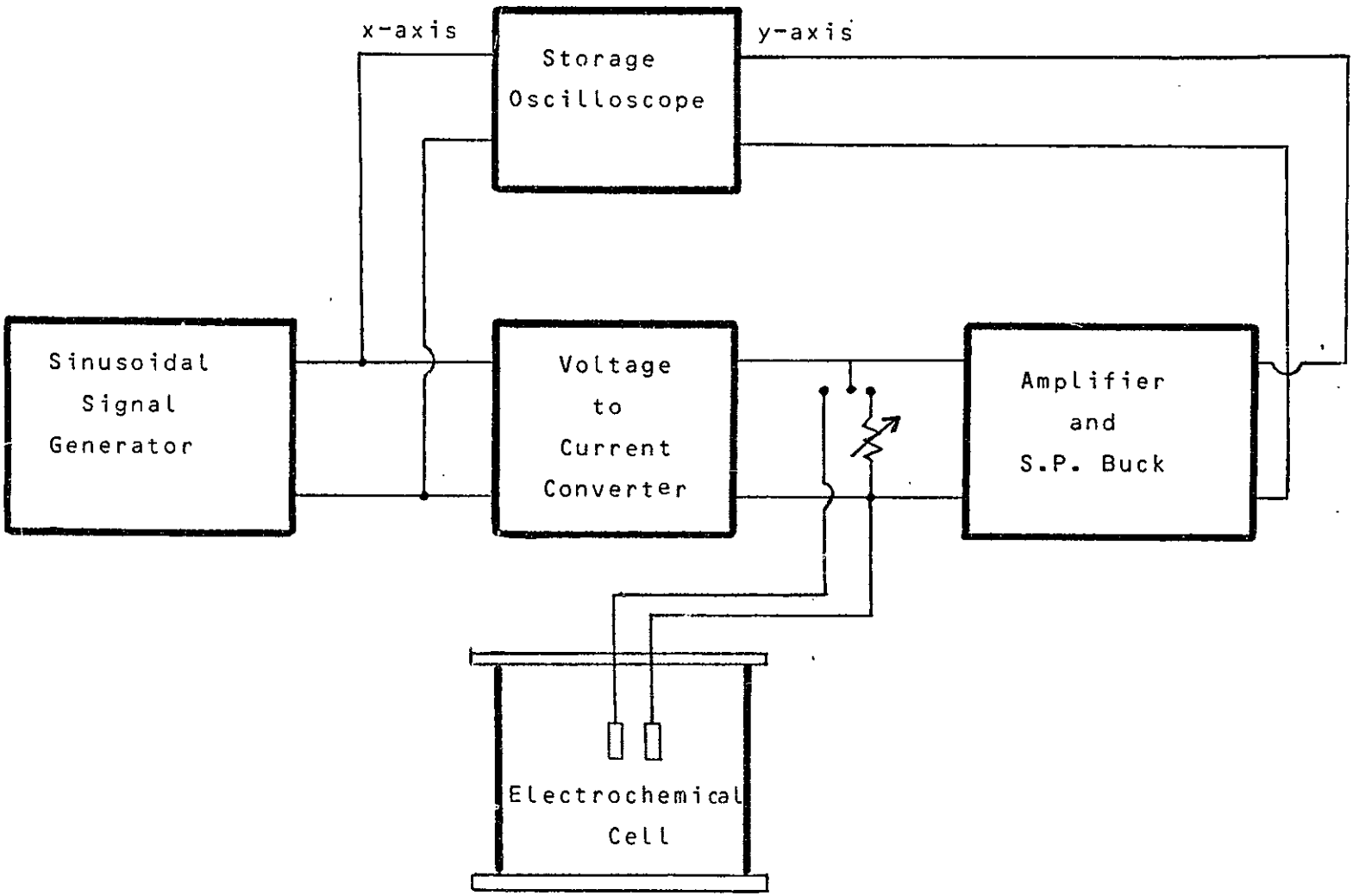


Figure 3.4: Experimental Configuration of Measurement System

The procedure for measuring the electrode impedance was as follows:

(1) the electrodes were cleaned, inserted in the electrode holders and then immersed in solution;

(2) we usually waited until E_M and/or Z(0.1 HZ) had stabilized;

(3) Eh, E_M, pH, T etc. were measured;

(4) Z and ϕ were measured, from the lowest to the highest frequency;

(5) Z and ϕ at the lowest frequency was measured again;

(6) we repeated (3).

The above method was tedious but worked quite well if there was no drift in the electrode impedance over the span of the measurements. Steps (3) to (5) normally took 15 to 20 minutes, when the lowest frequency used was 0.1 HZ. If 0.01 HZ was also used, it took up to one hour to obtain reliable results.

3.2.5 Experimental Accuracy and Reproducibility

In the final analysis, any experiment must be judged on its accuracy and reproducibility. To a lesser extent the ease and speed with which the measurements can be taken is also important. We estimate that the individual measurements of amplitude and phase have errors of approximately 2% and 2° respectively. However, when the impedance was changing during the measurement of the impedance spectrum, an effective error, as large as 10 or 30% may be produced.

Irreproducibility has remained one of the major problems in electrodics. The large differences among the results of different workers is certainly caused by dissimilar methods of solution and electrode preparation. We have found that we could obtain reproducible results (<10%

variation), when the solution and electrodes were prepared identically and the system was at equilibrium. It is imperative, when considering reproducibility, to ensure that the electrodes are at equilibrium. We assumed that the electrodes were at equilibrium when E_M and Z(0.1 HZ) were stable. In general, reproducibility to about a factor of 2 or 3 was usually possible for systems in quasi-equilibrium.

To improve the data acquisition time and the accuracy of the measurements we have embarked on a new measurement system. This digital recording method is described in Appendix B.

In the following section we discuss some basic experiments which highlight the accuracy and reproducibility of the experimental method.

3.3 AN EXPERIMENT WITH KNOWN IMPEDANCES

Before proceeding to electrochemical impedance measurements, we thought it advisable to test the experimental system and the interpretation methods on an accurately known impedance. The test load chosen was the simplest resistance-capacitance circuit we could use that would illustrate some of the important features of the method. The circuit is shown in Table 3.2.

The results of the experiment (Test I) and the inversion are also displayed in Table 3.2. It is obvious that the observed and model data agree quite well, which is evidenced by the low RMS error. Accordingly, the estimated parameters are in good agreement with the known values. The RMS% error referred to here is equal to $100\sigma_{RMS}$.

A parameter with a value one on the diagonal of the resolution matrix indicates that that unknown is very well resolved. This means that the inversion is very sensitive to this parameter. Diagonal elements with

Table 3.2 Data and results of experiment#: Test 1

OBSERVED and MODEL DATA

f (HZ)	$z_0(\Omega)$	ϕ_0 (deg)	z_N	ϕ_N
1000	1000	0.6	1000	0
100	1010	4.6	1009	4
10	1500	19.3	1502	19
1	1990	3.4	1989	4
.1	2000	0.0	2001	0

ESTIMATED PARAMETERS

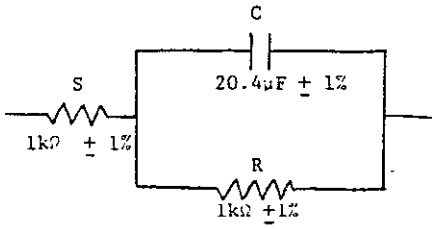
S= 1000 Ω

C= 20.2 μF RMS ERROR= 0.3%

R= 1000 Ω

RESOLUTION MATRIX

	S	C	R
S	1.00	.00	.00
C	-.01	.91	.01
R	.00	.01	.98



values smaller than one indicate reduced sensitivity or resolution. Large off-diagonal terms are produced by non-independence (correlation) between the two parameters involved. Accordingly, both R and C are less well resolved than S. R is better resolved than C.

This experiment and its interpretation illustrate that the methods used are capable of high accuracy, under favourable conditions. In this experiment the impedance obviously did not drift and all the parameters are well resolved. Clearly if we dropped S to say 10Ω, resolution of this parameter would become more difficult. Accordingly, each interpretation must be looked at critically. To this end, we rely heavily on the elements of the resolution matrix.

3.4 I.P. EXPERIMENTS ON THE $Cu/CuSO_4$ SYSTEM

We now test our methods on a real electrode/electrolyte system. As mentioned in the beginning of this Chapter, we used copper in these basic experiments because its properties are better understood than those of the metallic sulfides.

We describe two experiments with copper electrodes in 10^{-3}M $CuSO_4$. The solution also contained 10^{-2}M K_2SO_4 as the supporting electrolyte. One experiment was done in a reducing environment and the other under oxidizing conditions. We expected the copper ions to be active on copper and therefore the computed Warburg impedance should be directly related to the 10^{-3}M $CuSO_4$.

Consider firstly the experiment in the reducing environment. Nitrogen, and then hydrogen were bubbled to reduce the Eh to -350 mV. Note that this value of Eh was measured with a clean Pt electrode. A con-

centration of 10^{-3}M copper ions is not stable at such a low Eh. Accordingly, copper was seen to deposit on the Pt within about fifteen minutes. Thereafter, the Pt electrode obviously gave the same potential as the copper electrodes.

The measured impedances and the estimated parameters are shown in Table 3.3. We have fitted the data with both a four parameter (Type a) and a six parameter (Type b) equivalent circuit. The only parameters that are well resolved are the solution resistance S and the Warburg impedance W. The Warburg impedance is evaluated at 1 radian/sec. The large values of C_S and the zero value of R, together with their lack of resolution, clearly show that these parameters are not needed to interpret the data.

Table 3.4 displays the data and the estimated parameters for the experiment which was done in the oxidizing environment. These results indicate that the data is better interpreted when C_S and R are included in the model. This can be seen from the lower RMS error obtained with the type b equivalent circuit and also from the good resolution displayed by all of the parameters. The Warburg impedance (47Ω) obtained with the type b circuit is in close agreement with that obtained in experiment #42a, namely 46Ω.

The 4% error in experiment #42a is due mainly to a phase misfit at 0.01 HZ. A similar low frequency misfit is observed for experiment #41b. The 7% error obtained with experiment 41b is a little large when compared to the experimental accuracy. Moreover, C(=313μF) is much larger than that of a typical triple layer capacitance.

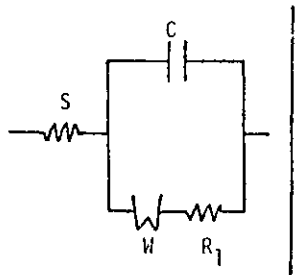
We tried other equivalent circuits utilizing the finite diffusion layer concept and adsorption phenomena in an attempt to reduce the RMS

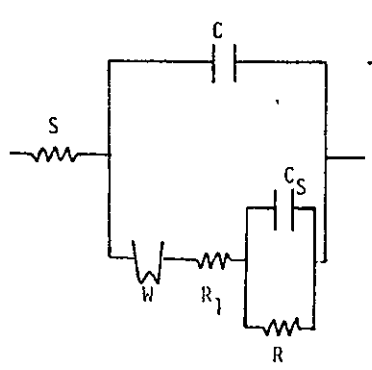
Reducing Environment			4 Parameter Inversion			6 Parameter Inversion		
f(HZ)	Z_o(Ω)	ϕ_o(deg)	Z_M	ϕ_M	Parameters	Z_M	ϕ_M	Parameters/cm^2
1000	21	3.2	21	3	S = 19	21	3	S = 18Ω
100	22	4.0	22	4	C = 42	22	4	C = 18μF
10	26	8.6	25	10	R_1 = 2	25	10	R_1 = 2Ω
1	34	21.1	36	21	W = 46	36	21	W = 46Ω
.1	75	35.5	73	33	RMS = 4%	73	33	C_S = 6800μF
.01	200	36.9	199	41		199	41	R = 0Ω
								RMS = 4%

Resolution Matrices (ϵ^2 = 0.01)

4 Parameters

	S	C	R_1	W
S	.99	-.03	.05	.00
C		.05	.09	.00
R_1			.24	.01
W				.99





6 Parameters

	S	C	R_1	W	C_S	R
S	.98	-.03	.09	.00	.00	.00
C		.07	.12	.00	.00	.01
R_1			.25	.00	-.01	.01
W				.99	.00	.00
C_S					.00	.00
R						.00

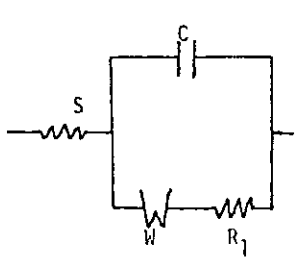
Table 3.3: Results of experiment #: Cu-Cu 42a
10^{-3}M $CuSO_4$ + 10^{-2}M K_2SO_4, pH = 7
E_h = -350 mV, E_{Cu} = -14 mV, E_{Cu_2S} = 136 mV

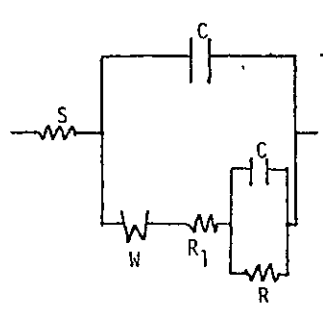
Oxidizing Environment			4 Parameter Inversion			6 Parameter Inversion		
f(HZ)	Z_o (Ω)	ϕ_o (deg)	Z_M	ϕ_M	Parameters	Z_M	ϕ_M	Parameters/cm^2
1000	23	5.2	23	5	S = 22	23	1	S = 23Ω
100	26	6.9	27	7	C = 78	25	9	C = 313μF
10	32	13.3	33	12	R_1 = 5	34	12	R_1 = 8Ω
1	52	26.1	49	23	W = 68	49	26	W = 47Ω
.1	117	32.0	104	35	RMS = 12%	124	31	C_S = 18380μF
.01	256	27.0	288	41		251	33	R = 49Ω
								RMS = 7%

Resolution Matrices (ε^2 = 0.01)

4 Parameters

	S	C	R_1	W
S	.99	-.04	.03	.00
C		.32	.03	.01
R_1			.72	.01
W				.99





6 Parameters

	S	C	R_1	W	C_S	R
S	.99	-.02	.01	.00	.00	.00
C		.59	-.06	.01	.00	-0.1
R_1			.81	.02	-.02	-.03
W				.97	-.02	.05
C_S					.82	-.03
R						.84

Table 3.4: Results of experiment #: Cu-Cu 41b.
10^{-3}M Cu SO_4 + 10^{-2}M K_2SO_4, pH = 5.5
E_h = 450mV, E_{Cu} = -11 mV, E_{Cu_2S} = 138 mV

error of experiment #42a. No improvement could be obtained.

Similar trials were performed on the data of experiment #41b.

The equivalent circuit, which included an adsorption path, produced a substantial drop in the RMS error to ~3%. Table 3.5 shows the result of this inversion. Note that we have lost all sensitivity to C and that W is now approximately $22\Omega\text{-cm}^2$. Associated with W is a marked decline in resolution compared with the results of Table 3.4. This drop of resolution is certainly associated with the strong correlations betwen W,R_1 and Ca.

There are three possibilities for the inclusion of W_a in the equivalent circuit model. Recall that the only differences between experiments #42a and #41b is that the Eh is vastly different. In experiment #41b $O_2(g)$ and $CO_2(g)$ are present in solution. Furthermore, the copper electrode certainly oxidized to some extent. We can eliminate any active contributions from the carbonate species because they are of the order of 10^{-5}M whereas the observed W_a is associated with a more concentrated species. The concentration of oxygen in an air saturated solution is $10^{-3.5}$M. This concentration is very close to that inferred from W_a(87Ω-cm2). The final possibility, and the more likely, is that SO_4^{2-} is being adsorbed on the partly oxidized copper surface.

We consider now, possible reaction mechanisms to see if we can justify the observed values of W. There are essentially three paths by which copper ions may be discharged at the electrode surface. As shown in Figure 3.5 either Cu^{2+} or Cu^{+} may be discharged directly to Cu. Alternatively, Cu^{2+} may gain only one electron at the electrode surface. The Cu^{+} which is now at the electrode surface gains another electron to become Cu. In the bulk solution an equilibrium exists between Cu^{2+} and Cu^{+} given by

Table 3.5: Results of Experiment #: Cu-Cu 41b
Equivalent circuit includes adsorption

f(HZ)	$Z_o(\Omega)$	$\emptyset_o$(deg)	Z_M	$\emptyset_M$
1000	23	5.2	24	2
100	26	6.9	25	6
10	32	13.3	32	14
1	52	26.1	53	26
.1	117	32.0	117	32
.01	256	27.0	256	27

RMS = 3%

Parameters (1 cm^2)

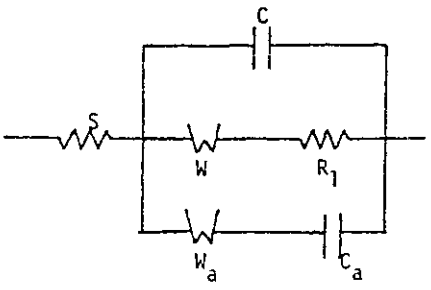
$S = 23\ \Omega$ $W = 22\ \Omega$

$C = 10\mu F$ $C_a = 54{,}063\ \mu F$

$R_1 = 263\ \Omega$ $W_a = 87\ \Omega$

Resolution Matrix ($\varepsilon^2 = 0.01$)

	S	C	W_a	C_a	W	R_1
S	1.0	0.0	0.0	0.0	0.0	0.0
C		0.0	0.0	0.0	0.0	0.0
W_a			1.0	0.0	0.0	0.0
C_a				0.9	-0.2	0.1
W					0.5	0.2
R_1						0.8



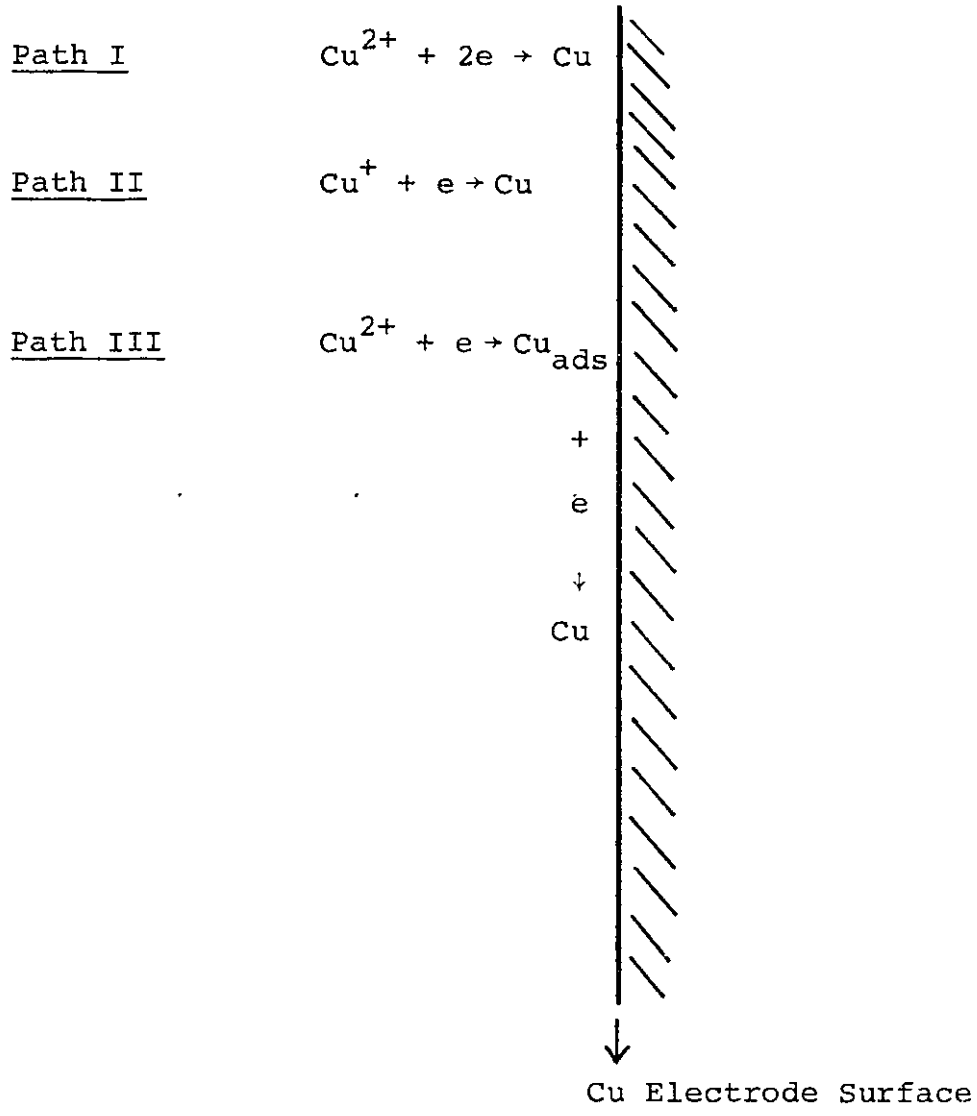


Figure 3.5: Possible discharge paths for Cu^{2+} and Cu^{+}

$(Cu^{2+})/(Cu^{+})^2 \sim 10^6$, hence in our experiments $(Cu^{+2}) \sim 10^{-3}$M and $(Cu^{+}) \sim 10^{-4.5}$M. Reaction path II can therefore be eliminated since the associated W (see Table 2.2) would be approximately 2kΩ-cm^2.

Note that we have written Cu^+ as Cu^+_{ads} in reaction path III. We consider this ion to be adsorbed, because it is generally believed that the reaction $Cu^+ + e \rightarrow Cu$ is very fast (i.e. low reaction resistance). Consequently, Cu^+ is not allowed to diffuse away into solution and the rate determining step becomes $Cu^{2+}\ e \rightarrow Cu^+_{ads}$ (Bockris and Enyo, 1962, Burrows et. al., 1975, Dermedts and Van Peteghem, 1978). Cu^+_{ads} thus behaves as if it had an activity of one, and reaction path III therefore looks like $Cu^{2+} + 2e \rightarrow Cu$, which is path I. In summary, we note therefore, that if $Cu^+_{ads} + e \rightarrow Cu$ is very fast then paths I and II give rise to the same Warburg impedance. Other electrochemical methods are necessary to distinguish between paths I and III.

We obtained the diffusion coefficient of Cu^{2+} by averaging two values from Peters and Cruser (1965) with one value from Kolthoff and Lingane (1946) to obtain D = 0.75 ($\pm$0.03) x 10^{-5} cm^2/s. Substituting into equation 2.22 leads to,

$$W = \frac{0.023}{(Cu^{2+})}\ \Omega\text{-cm}^2 \qquad (3.1)$$

where (Cu^{2+}) is the activity of Cu^{2+} ions. The activity is related to the concentration by $\gamma[Cu^{2+}] = (Cu^{2+})$.

To obtain an estimate of the activity coefficient γ, we use Davies equation (Stumm and Morgan, 1970). The equation is given by,

$$\log\gamma = -0.5Z^2\left(\frac{\sqrt{I}}{1+\sqrt{I}} - 0.3I\right) \qquad (3.2)$$

I is the ionic strength which is defined as $1/2\Sigma C_i \cdot Z_i^2$. C_i is the concentration of the ith ion with charge Z_i. For our experiments, we get $I = 10^{-1.49}M$, hence $\gamma = 0.51$. The Warburg impedance can now be expressed as $W = 0.023/(0.51[Cu^{2+}])$. Substituting $[Cu^{2+}] = 10^{-3}M$ gives $W = 46\Omega\text{-cm}^2$. This value is exactly the one obtained in experiment 42a. In experiment #41b the values are $47\Omega\text{-cm}^2$ for the type b equivalent circuit and $22\Omega\text{-cm}^2$ for the equivalent circuit with an independent adsorption path. The agreement between the predicted and measured diffusion impedances therefore seems very satisfactory, especially in the reducing environment where the interfering influences of oxidation are not present.

It is probably worthwhile at this point to discuss the experiment in terms of the Pourbaix diagram of copper. As we have previously mentioned, the Pourbaix diagram is useful only under equilibrium conditions. In both experiments we have deliberately taken the impedance measurements before equilibrium had been established. In the reducing environment, the copper ion would eventually precipitate out of solution. We estimate, in view of corrosion experiments, that this would take approximately one year. The process is very slow because there are only 2 cm^2 of copper surface onto which the ions can catalyze. Because we wanted to measure the impedance with $10^{-3}M$ $CuSO_4$ present, we clearly did not want much reduction to have taken place. Accordingly, our measurements were taken as soon after immersion as possible. In the second experiment, measurements were also taken soon after immersion, before the very rapid oxide formation became substantial.

We note also, that even though the Eh varied by nearly 600 mV between the two experiments, E_{Cu} changed by only 3mV. It is the latter potential,

as described in section 3.1, that should be correlated with the electrode impedance. The experiment substantiates this because the Warburg impedance had approximately the same value for both experiments.

The Nernst expression for the reaction $Cu^{2+} + 2e \rightarrow Cu$ gives,

$$E_{Cu} = 82 + 29.6 \log (Cu^{2+}) \qquad (3.3)$$

Since $(Cu^{2+}) \simeq 10^{-3.3}$ M in our experiments then (3.3) gives $E_{Cu} = -16$mV. This is in excellent agreement with the measured values of -11 and -14mV for experiments 42a and 41b respectively. Electrochemically, the Warburg impedances should therefore be interpreted as resulting essentially from the Cu^{2+}/Cu redox couple.

Experiments with varying Cu^{2+} concentrations have also rendered results that correlate well with the theoretical predictions. Figure 3.6 shows the analytical concentration of Cu^{2+} plotted against the concentration inferred from the estimated Warburg impedance. The agreement is quite satisfactory.

We have described in this section, very fundamental induced polarization experiments. The results have shown us that the methods are capable of reasonable accuracy and can lead to meaningful results.

3.5 Effects of Stirring the Solution

The Warburg impedance is a measure of the charge transport (by diffusion) across the diffusion layer. Normally, forced convection diminishes the diffusion layer and thereby lowers the impedance as discussed previously in Section 2.2. We use the effect of stirring simply to indicate whether or not the diffusion impedance is in solution or not. Surface

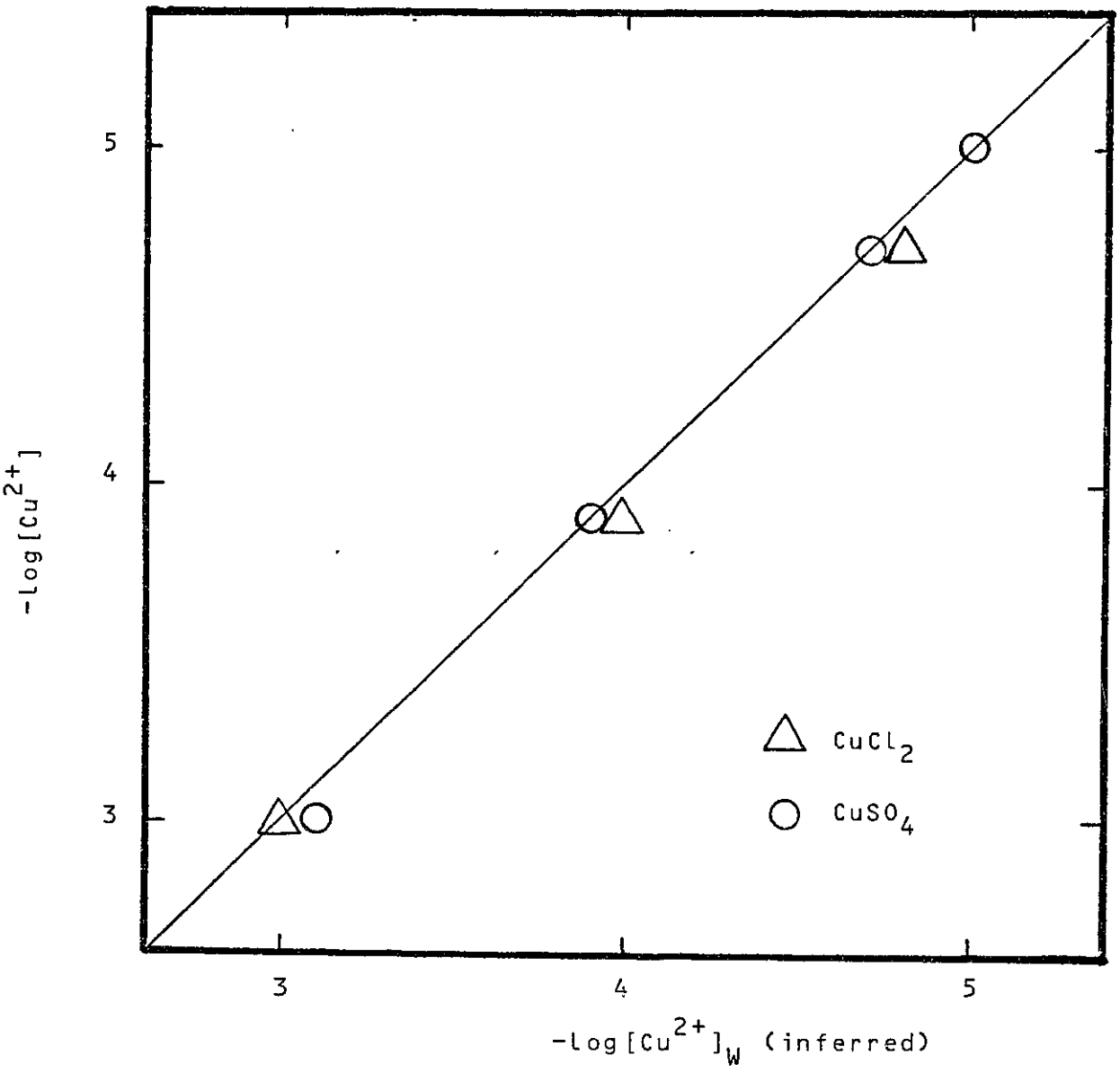


Figure 3.6: Comparison of Cu^{2+} concentration with that inferred from the magnitude of the Warburg impedance

diffusion should not be influenced by stirring. Both experiments 41b and 42a showed a drop in Warburg impedance with stirring, to 24Ω-cm^2 and 14Ω-cm^2 respectively. We take this as evidence that the Warburg impedance is indeed in the solution.

When an electrode is in a corrosive environment the concentration of active species in the vicinity of the electrode is greater than it is in the bulk of the solution. In this case stirring increases the Warburg impedance. We have experienced this on many occasions. Nevertheless, a Warburg impedance that is in solution will always be affected by stirring. Stirring is therefore a powerful tool for differentiating between solution and surface phenomena.

SUMMARY

We have shown that it is possible to correlate I.P. behaviour with the position of the electrode equilibrium on an E_M-pH diagram. Eh serves a more restricted purpose when the system is not in equilibrium. In non-equilibrium cases the Eh can sometimes indicate the direction (oxidizing or reducing) in which the system is being forced. Having shown that it is possible to obtain reasonable results from the methods, we proceed to study in the following Chapter the I.P. responses of sulfide minerals.

IV

INDUCED POLARIZATION RESPONSE OF SULFIDE MINERALS

INTRODUCTION

In previous chapters the groundwork for measuring and interpreting I.P. data was established. After a brief discussion of the electrochemical stability of sulfide minerals, the results of I.P. experiments, principally on pyrite and chalcocite, are discussed. Experiments in typical oxidizing and reducing environments are presented. With respect to interpretation, the basic problem centers around,

(1) the invariance of the impedance spectra to changes in solution chemistry, and

(2) the observation of phase angles larger than $|45°|$ at low frequencies.

As stated in Chapter I, resolution of these problems is one of the major objectives of this study. This "background" impedance effect was constantly observed by both Madden (1961) and Angoran (1975), but no satisfactory explanation was obtained.

Both of the above studies relied on the Randles equivalent circuit in their interpretations. We will demonstrate that inclusion of the third path discussed in Chapter II, namely, the adsorption branch, accounts satisfactorily for the large phase angles at low frequencies. To first order an adsorption dominated model consisting of R_s, C, W_a and C_a (see Fig. 4.11 , II) seems to offer an adequate explanation of the data. Such a four-parameter model results in RMS misfits of approximately 5%.

Inclusion of the faradaic path generally causes this RMS error to be reduced to 1 to 2%.

We will show when we present E_M-pH plots that many of the reactions giving approximately constant impedances are associated with pH dependent d.c. behavior involving metallic oxides and hydroxides. An attractive feature of the total equivalent circuit model (Fig. 4.11, VIII) is that non-faradaic and adsorption paths have infinite impedance at d.c. Consequently, the d.c. impedance must be controlled by the faradaic path and ought to show the expected pH dependence. It turns out that the latter is not true and that the faradaic path although quite well resolved is approximately pH independent. We will also show that the faradaic path is not very sensitive to the type of circuit element placed there. In an attempt to resolve this paradox we considered many possibilities, some of which are listed below. We investigated the possibility that any one or more of the following may give rise to a pH independent faradaic impedance approximatley constant in value:

(1) $H_2(g)$ reaching saturation levels close to the electrode

(2) Atomic hydrogen (H) diffusing into the metal/mineral

(3) Surface processes

(4) Electrochemical Intermediates

(5) $O_2(g)$ and/or $CO_2(g)$

(6) Impurities in solution

(7) The buffering action of the H_2O dissociation reaction.

Possibilities (1) to (4) are dependent on (7) since they can only control the impedance, and render pH independent impedances if (7) behaves in such

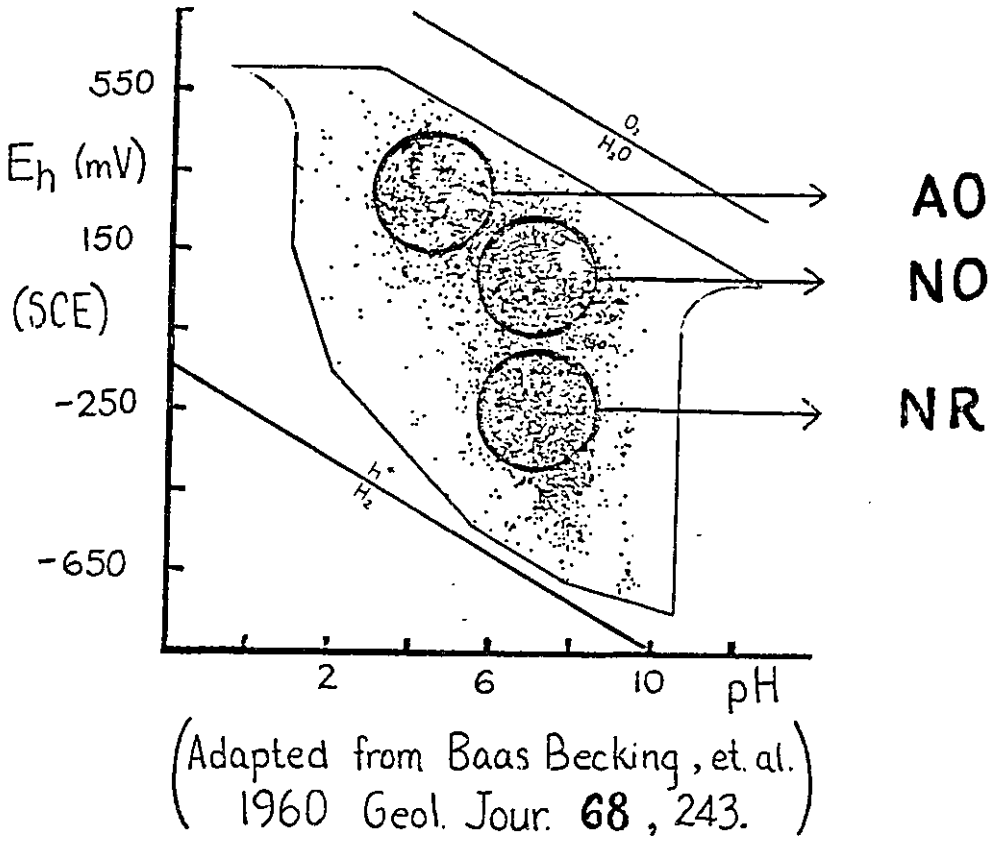
a manner that the effective concentration of H^+ or OH^- is comparatively large, thereby making their associated impedances negligible. Both (5) and (6) give rise to independent faradaic paths in parallel with the three existing ones. In this latter case, the normal faradaic branch must have a very large impedance such that it is always approximately an open circuit.

As shown in Chapter II, the maximum buffering effect of H_2O dissociation occurs at pH = 7, but it amounts to no more than a factor of two. At high and low pH values there is no buffering. This is the main reason for rejecting possibilities (1) to (4) and also (5), since the $O_2(g)$ and $CO_2(g)$ reactions are dependent on pH and can only become pH independent if there is substantial H_2O buffering. Although it is very possible that there are impurities (most likely organics) present whose concentrations are pH independent, it would be very fortuitous for an impurity-derived faradaic path to dominate the impedance under a.c. conditions only, becoming large compared to the normal faradaic path at d.c.

We hope to demonstrate in this chapter that a general mechanism involving adsorbed intermediates is quite plausible as an explanation of the observed results. We reiterate that the primary paths are the non-faradaic and adsorption branches, while the faradaic path represents phenomena of secondary importance in so far as the parameter estimation in an I.P. model is concerned.

4.1 ELECTROCHEMICAL STABILITY OF SULFIDE MINERALS

Natural waters possess a wide range of Eh-pH values as shown in Figure 4.1. For convenience, we categorize this data into three regions:



AO ⟶ Acid Oxidizing
NO ⟶ Neutral Oxidizing
NR ⟶ Neutral REDUCING

Figure 4.1: Eh-pH measurements of Natural Waters

Acid Oxidizing (AO): 150 mV<Eh<600 mV; 3<pH<5

Neutral Oxidizing (NO): -150 mV<Eh<150 mV; 6<pH<9

Neutral Reducing (NR): -650 mV<Eh<-150 mV; 6<pH<9

These three approximate regions, superimposed on Figure 1.2, are displayed in Figure 4.1. Below, we discuss briefly, the electrochemical factors that govern each region.

4.1.1 The Acid Oxidizing Region (AO)

In sulfide mineralized zones, an AO region normally signifies the corrosion of pyrite (FeS_2). In near surface environments (oxidizing), pyrite dissolves to produce ferrous sulphate and sulphuric acid, while consuming oxygen. The generally accepted reaction path is

$$FeS_2 + 1/2\ O_2(g) + H_2O = Fe^{2+} + 2SO_4^{2-} + 2H^+ \qquad (4.1)$$

The ferrous sulphate is further oxidized according to:

$$Fe^{2+} + 1/4\ O_2(g) + H_2O = 1/2\ Fe_2O_3(S) + 2H^+ \qquad (4.2)$$

This reaction is a simplification of a more complex process involving many reaction steps. The free energy for reactions (4.1) and (4.2) are -280 kcal/mole and -11 kcal/mole, respectively. The overall, spontaneous, corrosion of pyrite in oxygenated solutions can therefore be represented by:

$$FeS_2(S) + 15/4O_2(g) + 2H_2O = 1/2Fe_2O_3(S) + 2SO_4^{2-} + 2OH^- \qquad (4.3)$$

Note that four moles of H^+ are produced for each mole of FeS_2 that dissolves, consequently, the drop in pH.

Conversely, chalcocite (Cu_2S) dissolves in oxygenated solutions according to,

$$Cu_2S(S) + 5/2O_2(g) + 2H_2O = 2Cu^{2+} + SO_4^{2-} + 2OH^- \qquad (4.4)$$

with an attendent rise in pH. Equation (4.4) shows Cu_2S corroding directly to Cu^{2+}. In practice, covellite (CuS) and perhaps dignite (Cu_9S_5) exist as intermediate solids (Sato, 1960).

Solutions in the AO region are capable of large concentrations of Cu^{2+} (and Cu^{+}) whereas iron ions precipate out as Fe_2O_3. These ideas are shown in the Pourbaix diagrams for Cu-S-H_2O (Figure 4.2), Fe-S-H_2O (Figure 4.3) and Cu-Fe-S-H_2O (Figure 4.4).

4.1.2 The Neutral Oxidizing Region (NO)

In geochemical aquatic systems, the pH of the neutral region (pH ≈ 7 to 9) is normally controlled by the amount of carbonate present. The carbonate usually exists in the form of $CaCO_3$. If additionally, the Eh is such that the solution is oxidizing, then the region may be classified as NO. In this NO region, the potentials of pyrite, chalcocite, covellite etc. tend to be controlled by oxide and hydroxide reactions.

If there is an infinite supply of oxygen, pyrite dissolves, thereby driving the solution into the AO region, unless it is strongly buffered by some substance such as $CaCO_3$. The dominant copper and iron species in this region are the oxides (see Table 3.1) and the concentration of the associated ionic species is very low.

4.1.3 The Neutral Reducing Region (NR)

Environments at depth are deficient in $O_2(g)$ and the corresponding Eh values are comparatively low. Figure 4.5 shows an Eh-pH diagram for

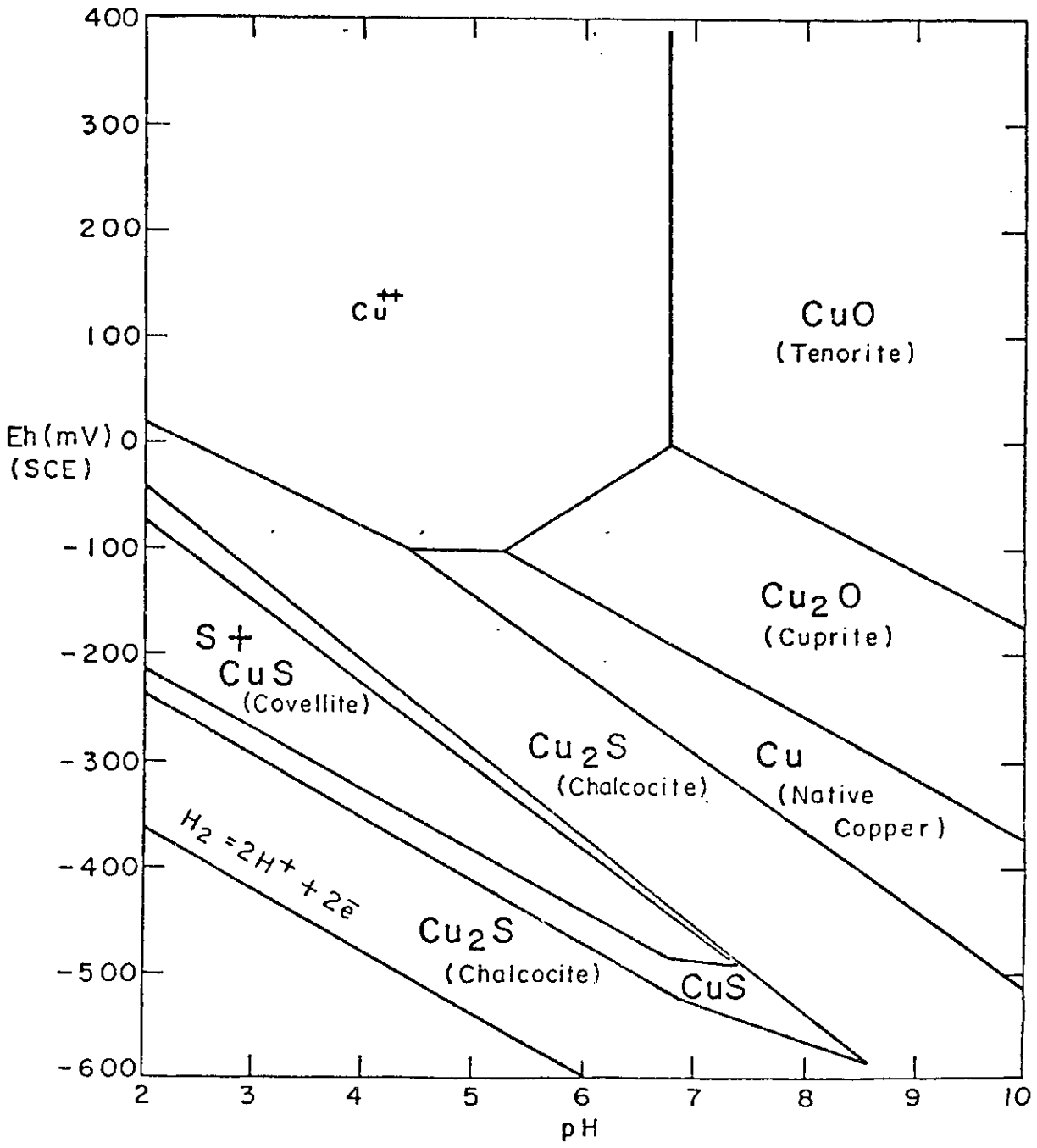


Figure 4.2 Eh-pH Diagram of Copper Sulfides (adapted from Garrels and Christ, 1965)

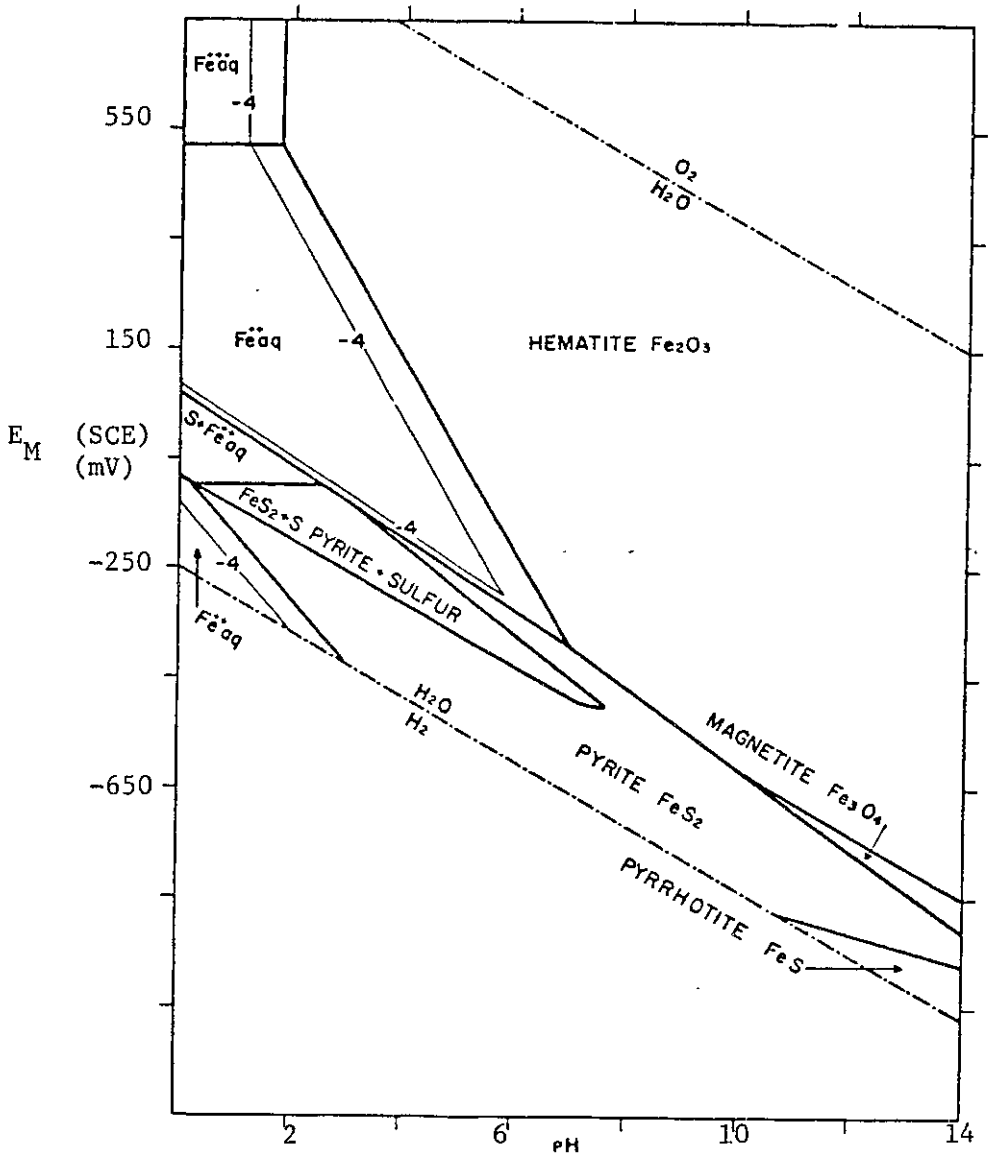


Figure 4.3: Pourbaix diagram for the system Fe-S-H_2O. Total sulfur=10^{-1} M. Adapted from Garrels and Christ (1965)

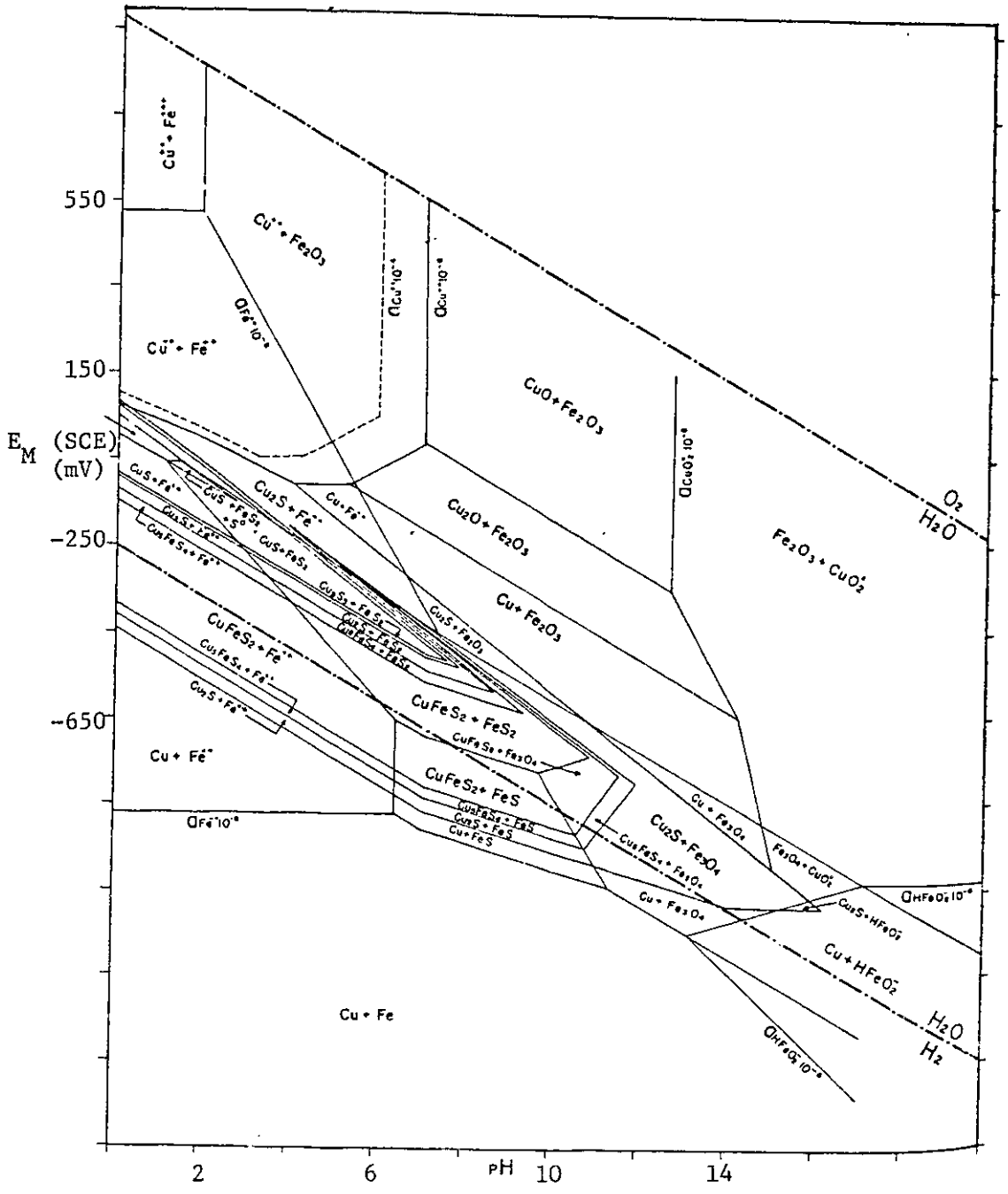


Figure 4.4: Pourbaix diagram for the system Fe-Cu-S-H_2O. Total sulfur = 10^{-4} M. Adapted from Garrels and Christ (1965).

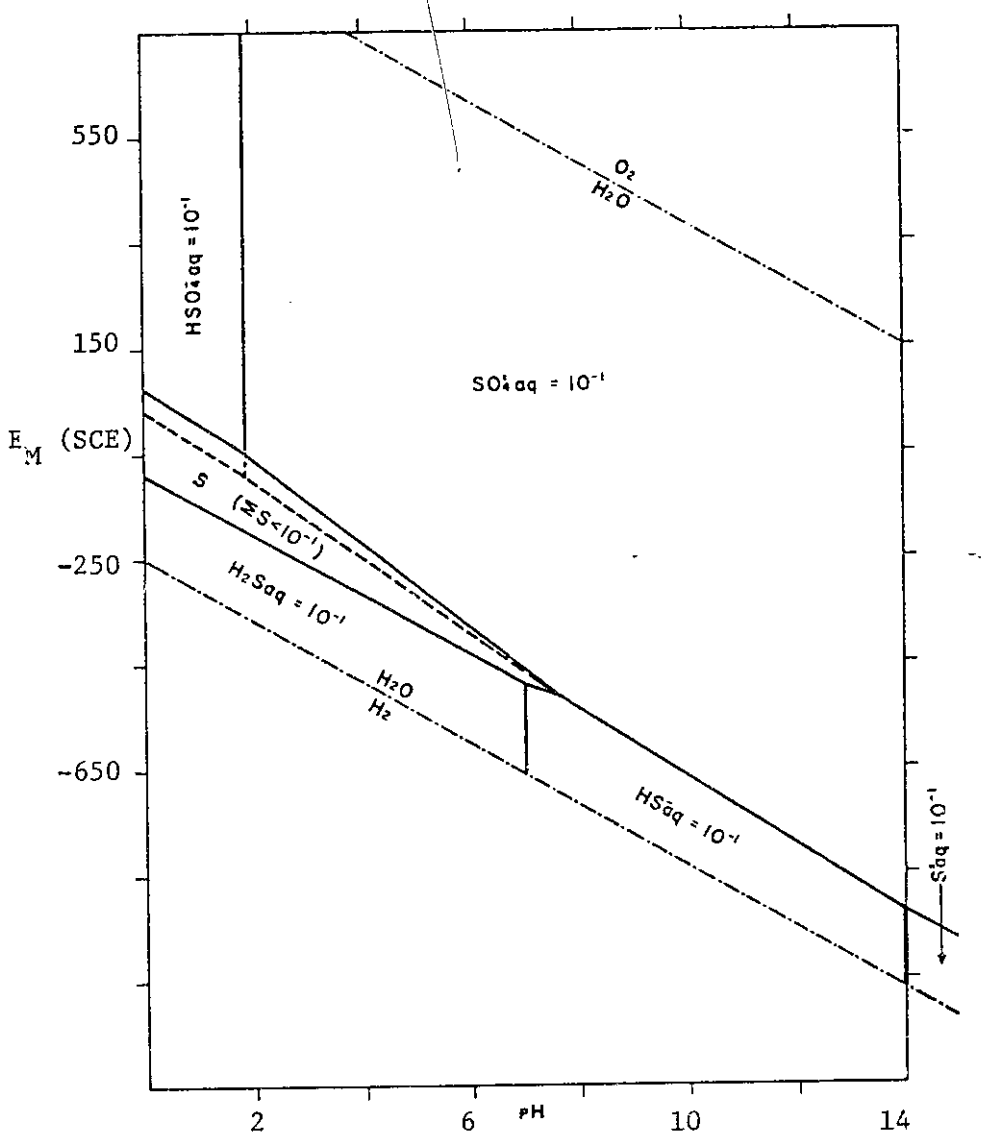


Figure 4.5: Pourbaix diagram for the system S-H_2O. Adapted from Garrels and Christ (1965)

the S-H_2O system. Note that for low Eh values the stable specie is no longer SO_4^{2-} but rather H_2S, HS^- or S^{2-}. In the NR region the dominant sulphur specie is HS^-. The predominant iron species are Fe_2O_3 (Hematite), Fe_3O_4 (Magnetite) and FeS_2. Correspondingly, for the copper system Cu, CuS or Cu_2S may be stable, depending on the Eh.

In the next section we give the results of various I.P. experiments conducted in the AO, NO and NR regions.

4.2 EXPERIMENTAL RESULTS

Recall that in Chapter III we emphasized that E_M should be used instead of Eh, for correlating the I.P. behavior of electrodes with their d.c. rest potentials. The data are organized into two divisions. In the first category, E_M-pH measurements are displayed for five sets of experiments. Pyrite and chalcocite were chosen as the minerals in these investigations. They were studied with copper, iron and sulfide species present in solution. The second set of results show corresponding I.P. impedance spectra.

4.2.1 Potentiometric (d.c.) Data

Figure 4.6 shows an E_M-pH plot for chalcocite. The solution was composed of 10^{-2}M K_2SO_4 + 10^{-3} $CuSO_4$ + KOH + H_2SO_4. In the AO region the potential agrees with the reaction,

$$Cu_2S = CuS + Cu^{2+} + 2e \qquad (4.5)$$

For this reaction, Sato (1960) gives,

$$E_M = 285 + 29.6 \log(Cu^{2+}) \qquad (4.6)$$

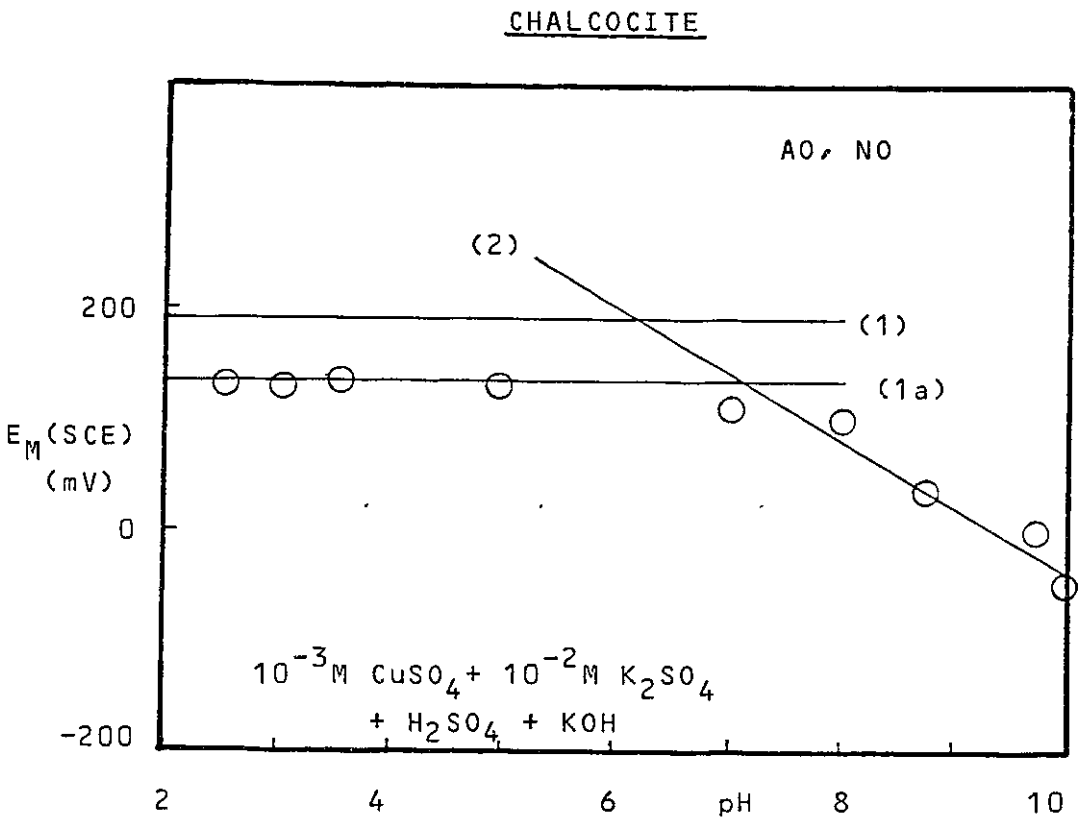


Figure 4.6: E_M-pH Behavior of Chalcocite in Acid-Oxidizing and Neutral-Oxidizing Environments

$$Cu_2S = CuS + Cu^{2+} + 2\ e$$
$$E_M = 285 + 29.6 \log(Cu^{2+}) \qquad (1)$$

$$E_M = 200 + 21.4 \log(Cu^{2+}) \qquad (1a)$$

$$Cu_2S + 2H_2O = CuS + Cu(OH)_2 + 2H^+ + 2e$$
$$E_M = 557 - 59.2\ pH \qquad (2)$$

we have also obtained empirically,

$$E_M = 200 + 21.4 \log(Cu^{2+}) \tag{4.7}$$

by taking an extensive set of E_M data for a number of known Cu^{2+} concentrations. This latter Nernst equation is in good agreement with the observed data. In the NO region, Sato (1960) reported,

$$Cu_2S + 2H_2O = CuS + Cu(OH)_2 + 2\ H^+ + 2\ e \tag{4.8}$$

as the controlling reaction, with the corresponding Nernst equation,

$$E_M = 557 - 59.2\ pH \tag{4.9}$$

This equation also agrees well with the measured values of E_M vs pH.

Figure 4.7 shows the response of pyrite under the same environmental conditions. There is reasonable agreement between the experimental points and,

$$E_M = 612 - 59.2\ pH \tag{4.10}$$

which is the Nernst equation for the reaction

$$FeS_2 + 3H_2O = Fe(OH)_3 + 2S\ (1\ atm) + 3H^+ + 3e \tag{4.11}$$

Two points should be noted here. Although we write equations such as (4.11) with S (1 atm), pure sulfur does not exist because a further reaction oxidizes it to SO_4^{2-}. The other feature of reactions such as (4.11) is that we conventionally write these reactions with H^+. In some cases these reactions are operative in basic solutions and the active ion is therefore OH^-. No generality is lost by adopting this convention.

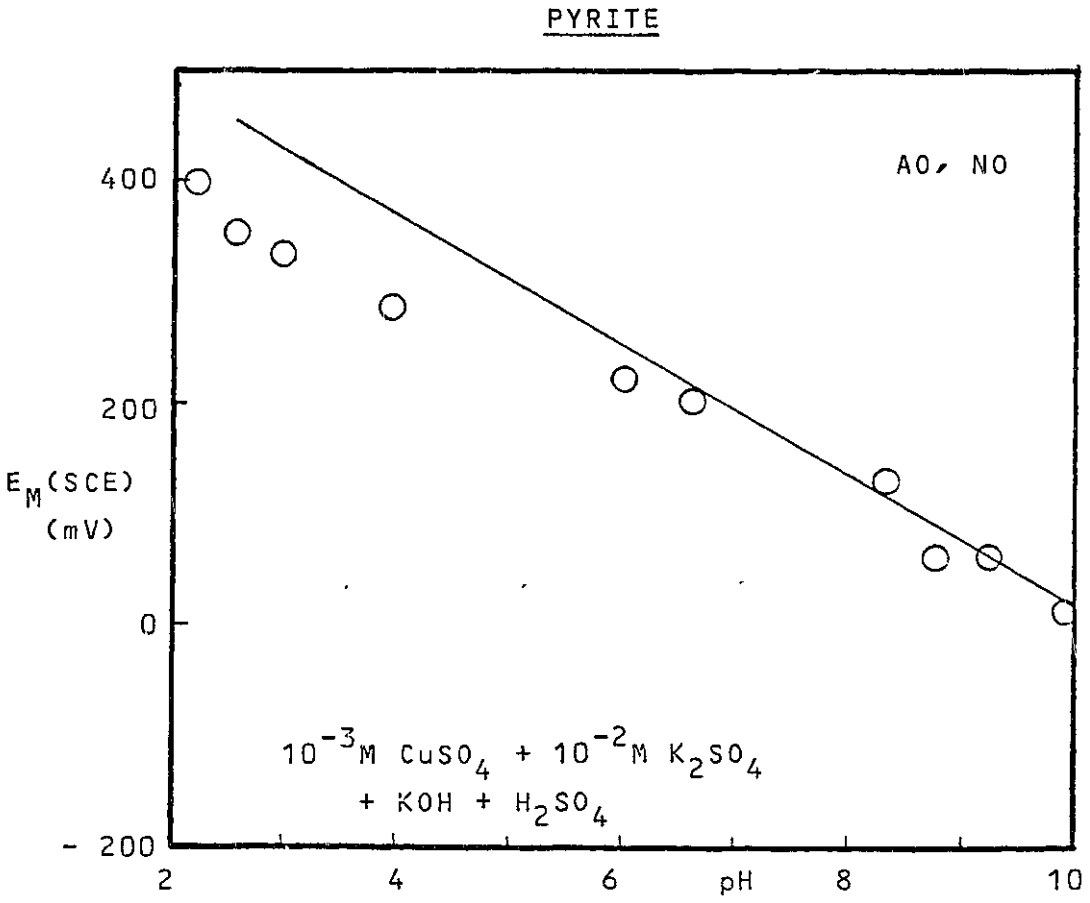


Figure 4.7: E_M-pH Behavior of Pyrite in Acid-Oxidizing and Neutral-Oxidizing Environments

$$FeS_2 + 3H_2O = Fe(OH)_3 + 2S\ (l\ atm) + 3H^+ + 3e \qquad (1)$$

$$E_M = 612 - 59.2\ pH$$

The general features of the data in Figure 4.8 are similar to those in Figure 4.6. The Cu^{2+} of approximately $10^{-3.7}$M in the AO region results from the rapid corrosion of the chalcocite electrode. Overall, the present of $FeSO_4$ in the aqueous environment did not seem to influence E_M to any marked degree.

With $FeSO_4$ present in the solution the pyrite electrode showed a narrow pH independent region, governed by, (Figure 4.9),

$$FeS_2 = Fe^{2+} + 2S \text{ (1 atm)} + 2e \qquad (4.12)$$

and

$$E_M = 512 + 29.6 \log(Fe^{2+}) \qquad (4.13)$$

The pH dependent portion behaves in a similar manner to that in Figure 4.7.

In the NR region a solution of 10^{-2}M NaCl + HCl + 10^{-2}M Na_2S was used. The corresponding Eh-pH behavior of pyrite and chalcocite are shown in Figure 4.10. For chalcocite, reasonable agreement with the data was obtained with the reaction,

$$Cu_2S + HS^- = 2CuS + H^+ + 2e \qquad (4.14)$$

for which

$$E_M = -371 - 29.6 \text{ pH} - 29.6 \log(HS^-) \qquad (4.15)$$

We also show the corresponding E_M-pH plot when H_2S is the dominant species. The pyrite potentials do not follow any known reaction mechanism. A similar conclusion was drawn by Sato (1960).

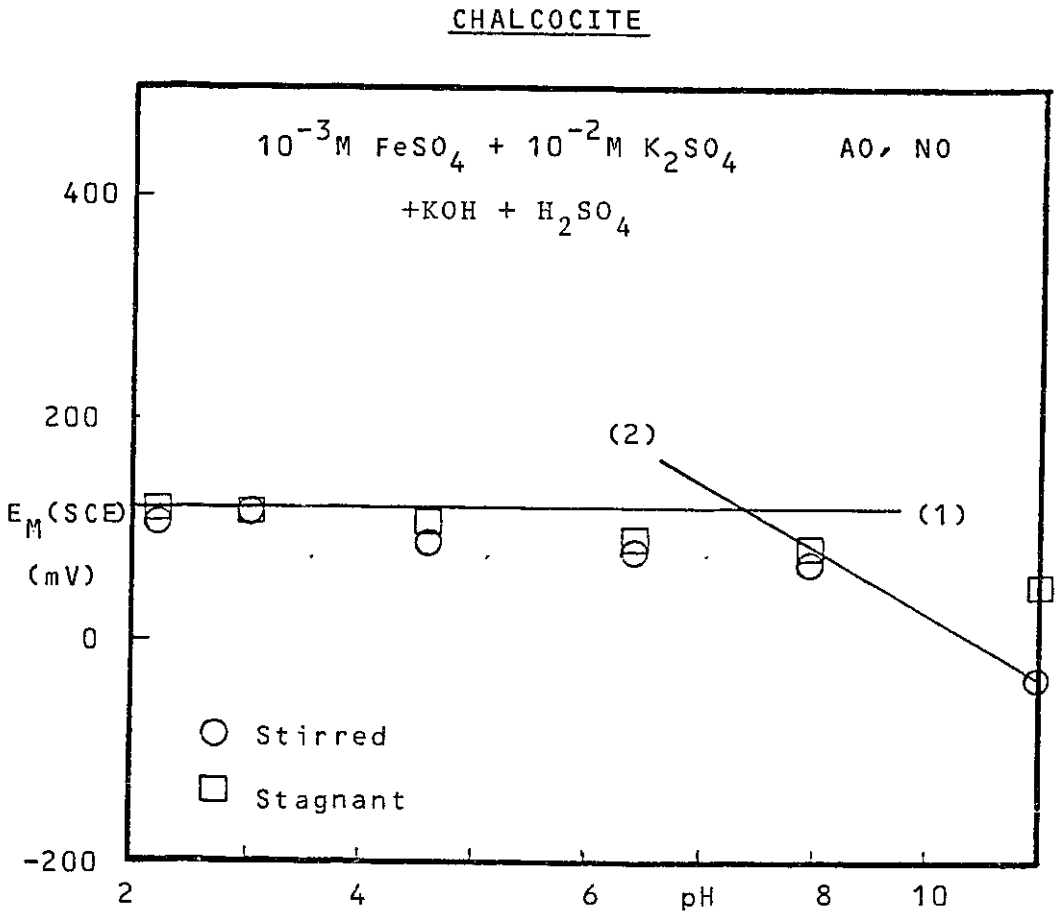


Figure 4.8: E_M-pH Behavior of Chalcocite in Acid-Oxidizing and Neutral Reducing Environments

$$Cu_2S = CuS + Cu^{2+} + 2e$$
$$E_M = 200 + 21.4 \log (Cu^{2+}) \qquad (1)$$

$$Cu_2S + 2H_2O = CuS + Cu(OH)_2 + 2H^+ + 2\,e$$
$$E_M = 557 - 59.6\ pH \qquad (2)$$

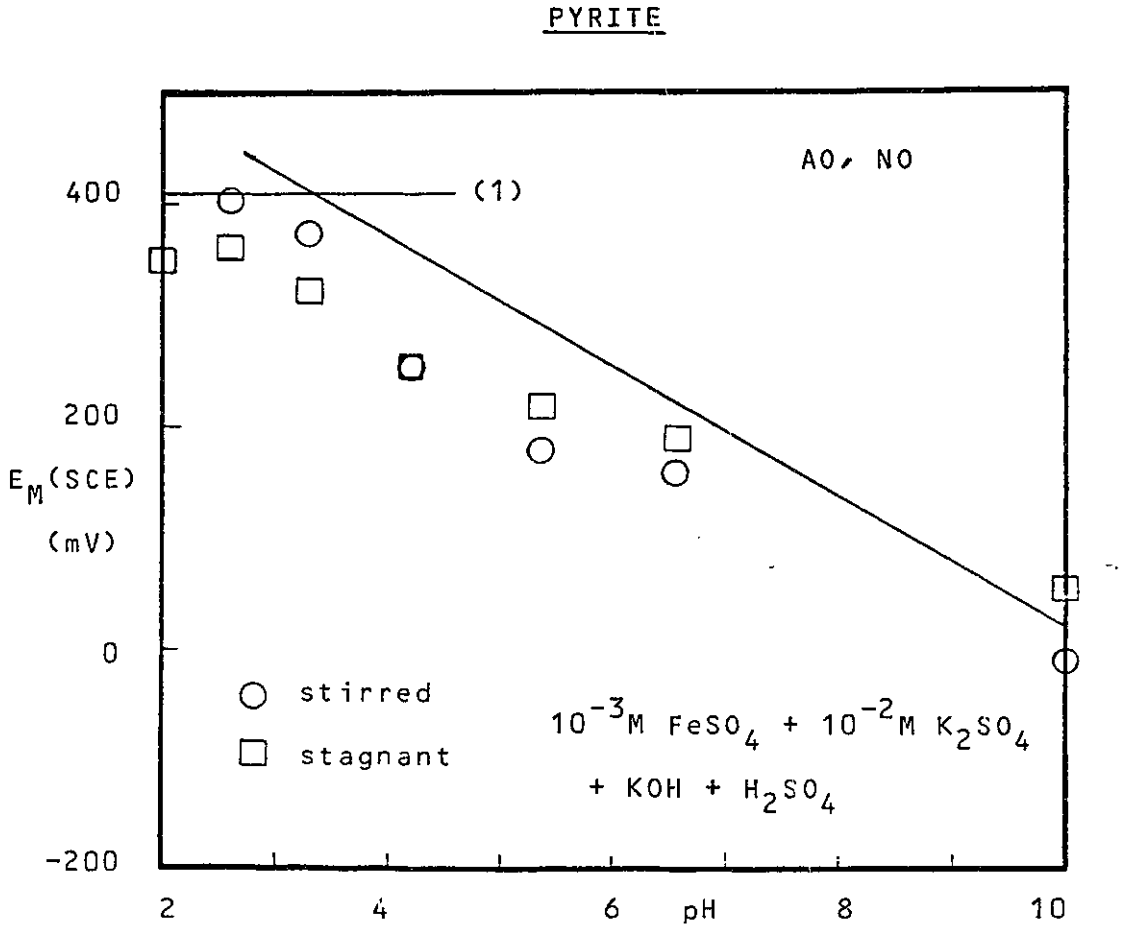


Figure 4.9: E_M-pH Behavior of Pyrite in Acid-Oxidizing and Neutral-Oxidizing Environments

$$FeS_2 = Fe^{2+} + 2S + 2\,e \qquad (1)$$

$$E_M = 512 + 29.6 \log(Fe^{2+})$$

$$FeS_2 + 3H_2O = Fe(OH)_3 + 3H^+ + 2S\ (1\ atm) + 3e \qquad (2)$$

$$E_M = 612 - 59.2\ pH$$

PYRITE AND CHALCOCITE

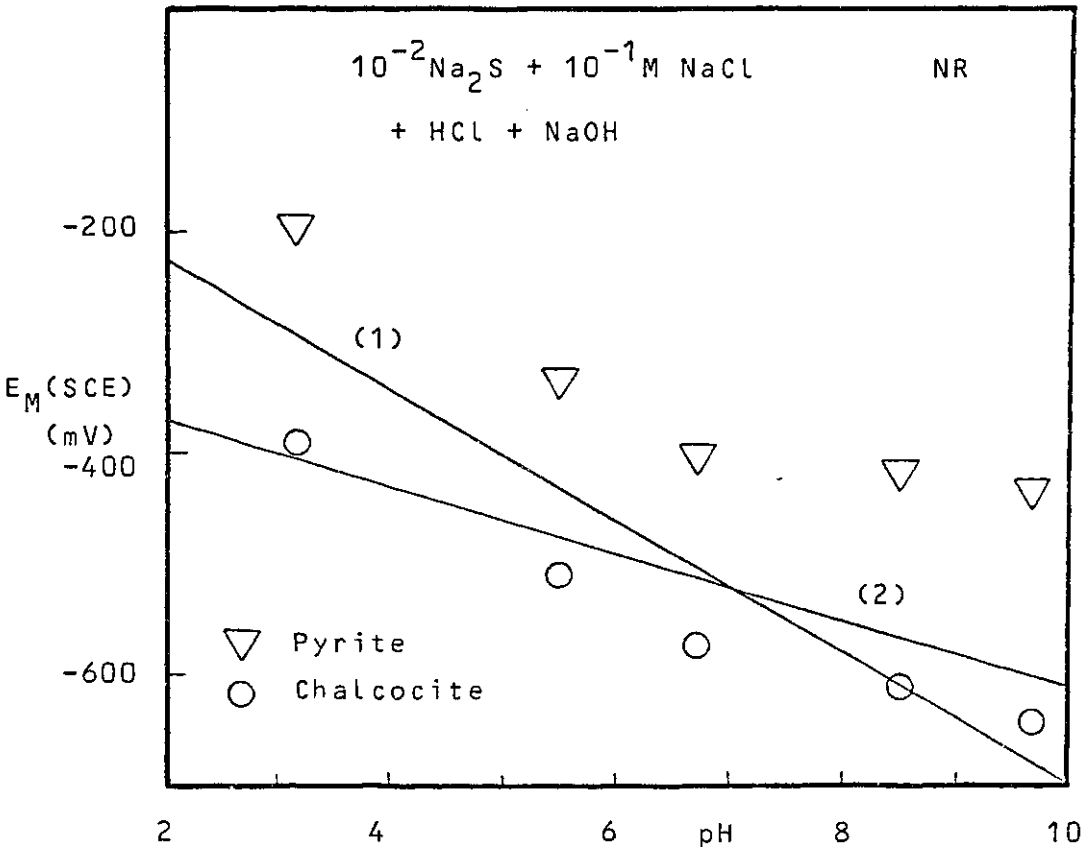


Figure 4.10: E_M-pH behavior of Chalcocite and Pyrite in a Neutral-Reducing environment

$$Cu_2S + H_2S = 2CuS + 2H^+ + 2\,e$$
$$E_M = -164 - 59.2\ pH - 29.6\ \log(H_2S) \qquad (1)$$

$$Cu_2S + HS^- = 2CuS + H^+ + 2e$$
$$E_M = -371 - 29.6\ pH - 29.6(HS^-) \qquad (2)$$

In general, it therefore seems as if the E_M-pH data can be reasonably explained by known redox reactions and their associated Nernst equations. Pyrite in sulfide reducing environments is an exception to this and the reaction mechanism associated with the E_M-pH behavior is still unknown.

4.2.2 I.P. Impedance Spectra

Impedance spectra were also recorded during the E_M-pH measurements of the last section. The data are shown in Tables 4.1 to 4.5.

4.3 INTERPRETATION OF I.P. RESPONSE

Past interpretations of I.P. data in this laboratory have relied heavily on the Randles equivalent circuit (Figure 2.1). As we mentioned before the most serious difficulty encountered was the apparent constancy of the Warburg impedance. Furthermore, the estimated values of C tended to be much larger than the values one would expect for typical triple layer capacitances. Generally, the RMS errors were in the vicinity of 6% which is somewhat higher than the experimental accuracy. These effects can be seen directly from the data. Consider for example experiment: pyrite #8 (Table 4.2). It is obvious that the impedance spectra do not change significantly even though the d.c. potential (E_M) varies with pH. The large phase angles at low frequencies give rise to the unusually high values of C. Any new equivalent circuit model we adopt should therefore attempt to account for these drawbacks in the Randles equivalent circuit.

Recall that our general equivalent circuit consists of three parallel paths in series with the solution resistance R_S. The three parallel paths are the non-faradaic, faradaic and adsorption branches considered in Chapter II. An equivalent circuit consisting of R_S, C, W_a and C_a, that is,

	5a		b		c	
f(HZ)	Z_o	$\emptyset_o$	Z_o	$\emptyset_o$	Z_o	$\emptyset_o$
.1	1731	59.9	257	41.3	203	40.5
1	278	58.2	86.1	35.5	74.0	32.7
10	66.1	35.5	38.3	21.1	36.1	18.7
100	35.7	16.9	27.8	7.5	27.0	6.6
1000	26.1	9.2	25.2	4.6	24.4	3.8
	pH=$10^{\pm}$.1 E_M=$50^{\pm}$10		pH=7.5 E_M=$100^{\pm}$3		pH=7 E_M=$105^{\pm}$3	

	d		e		f	
f(HZ)	Z_o	$\emptyset_o$	Z_o	$\emptyset_o$	Z_o	$\emptyset_o$
.1	42.6	30.0	47.0	29.7	47.9	30.0
1	24.2	17.5	25.2	17.5	25.7	17.5
10	17.0	8.1	17.4	8.0	17.4	8.3
100	15.7	3.4	15.7	3.2	15.7	3.4
1000	15.1	2.3	14.8	1.7	14.8	2.3
	pH=2.6 E_M=$129^{\pm}$1		pH=3.1 E_M=$126^{\pm}$1		pH=4.9 E_M=$126^{\pm}$1	

	g		h		i	
f(HZ)	Z_o	$\emptyset_o$	Z_o	$\emptyset_o$	Z_o	$\emptyset_o$
.1	1740	53.1	361	34.1	1349	58.8
1	413	56.6	166	31.0	282	57.7
10	111	43.6	70.5	41.0	77.4	42.8
100	38.3	26.1	26.1	31.9	30.0	29.3
1000	19.1	16.3	17.4	11.5	17.4	13.9
	pH=9.7 E_M=$0^{\pm}$10		pH=11.5 E_M=$-122^{\pm}$1		pH=8.75 E_M=$30^{\pm}$7	

Table 4.1: I.P. response of CHALCOCITE, Exp. # 5
Solution 10^{-2}M K_2SO_4 + $10^{-3}CuSO_4$ + KOH + H_2SO_4
Temperature: ≈ 22°C
Comments: Electrode not cleaned after experiment #5a.
All E_M values in mV, Z_o in Ω/cm^2 and $\emptyset_o$ in degrees.

	8a		b		c	
f(HZ)	Z_o	$\emptyset_o$	Z_o	$\emptyset_o$	Z_o	$\emptyset_o$
.1	5467	64.2	2671	64.2	2610	66.9
1	824	61.2	481	53.1	454	51.3
10	239	28.7	203	17.5	203	16.4
100	179	5.5	177	3.4	177	3.6
1000	172	1.1	171	1.3	174	1.3
	pH=8.7 $E_M=60\pm10$		pH=6.6 $E_M=203\pm2$		pH=6.1 $E_M=222\pm2$	

	d		e		f	
f(HZ)	Z_o	$\emptyset_o$	Z_o	$\emptyset_o$	Z_o	$\emptyset_o$
.1	3003	69.9	3465	69.9	4120	67.8
1	511	61.2	705	62.3	720	64.7
10	213	20.7	231	29.0	231	29.0
100	176	4.5	172	5.7	173	5.7
1000	174	1.3	169	1.0	171	1.3
	pH=4.0 $E_M=276\pm2$		pH=3.0 $E_M=332\pm2$		pH=9.9 $E_M=10\pm1$	

	g	
f(HZ)	Z_o	$\emptyset_o$
.1	4120	71.1
1	670	65.9
10	226	41.8
100	176	5.7
1000	170	1.6
	pH=8.3 $E_M=130\pm10$	

Table 4.2: I.P. response of Pyrite, Exp. #8
Solution: 10^{-2}M K_2SO_4 + 10^{-3}M $CuSO_4$ + KOH + H_2SO_4
Temperature: $\approx 22^oC$
Comments: Electrode not cleaned after experiment #8a. All E_M values in mV, Z_o in Ω/cm^2 and $\emptyset_o$ in degrees.

	6a		b		c	
f(HZ)	Z_o	$\emptyset_o$	Z_o	$\emptyset_o$	Z_o	$\emptyset_o$
.1	120.9	40.2	127.9	39.1	308	44.4
1	47.9	31.3	52.2	28.7	104	39.8
10	25.2	20.5	28.3	17.5	41.8	31.0
100	17.4	9.2	20.9	7.8	22.6	14.2
1000	15.8	3.4	19.1	3.4	19.1	3.7
	pH=2.2 $E_M=120\pm1$		pH=3.0 $E_M=120\pm1$		pH=4.6 $E_M=106\pm1$	

	d		e		f	
f(HZ)	Z_o	$\emptyset_o$	Z_o	$\emptyset_o$	Z_o	$\emptyset_o$
.1	809	51.3	896	52.2	2149	64.2
1	220	50.4	227	51.3	408	62.9
10	60.0	46.1	61.3	46.1	85.3	54.6
100	23.1	20.5	23.9	21.1	28.7	26.1
1000	19.1	5.2	19.1	5.7	20.0	5.0
	pH=6.4 $E_M=120\pm1$		pH=8.1 $E_M=88\pm3$		pH=10.0 $E_M=50\pm15$	

	f_s (stirred)	
f(HZ)	Z_o	$\emptyset_o$
.1	974	46.1
1	303	43.6
10	107	43.6
100	33.9	34.8
1000	20.0	8.0
	pH=10.0 $E_M=-32\pm1$	

Table 4.3: I.P. response of Chalcocite, Exp. #6
Solution: 10^{-2}M K_2SO_4 + 10^{-3}M $FeSO_4$ + KOH + H_2SO_4
Temperature: ≈ 22°C
Comments: Electrode not cleaned after experiment #6a. All E_M values in mV, Z_o in Ω/cm^2 and $\emptyset_o$ in degrees.

	9a		b		c	
f(HZ)	Z_o	$\emptyset_o$	Z_o	$\emptyset_o$	Z_o	$\emptyset_o$
.1	2726	51.3	1713	44.4	4543	59.3
1	685	53.1	562	41.3	855	64.2
10	219	27.4	226	23.6	222	29.7
100	169	4.0	173	4.6	173	4.6
1000	167	1.1	168	1.1	171	1.1
	pH=2.0 $E_M=345\pm1$		pH=2.6 $E_M=360\pm1$		pH=3.3 $E_M=320\pm1$	

	d		e		f	
f(HZ)	Z_o	$\emptyset_o$	Z_o	$\emptyset_o$	Z_o	$\emptyset_o$
.1	6237	70.9	6237	70.1	6545	75.9
1	884	71.8	875	70.1	862	73.7
10	216	31.0	212	30.7	212	30.0
100	171	4.1	172	4.6	170	4.3
1000	170	0.9	170	0.9	169	0.9
	pH=4.2 $E_M=251\pm2$		pH=5.4 $E_M=219\pm3$		pH=6.5 $E_M=182\pm6$	

	g		g_S (stirred)	
f(HZ)	Z_o	$\emptyset_o$	Z_o	$\emptyset_o$
.1	5467	75.9	2556	34.1
1	708	70.9	593	59.3
10	204	25.8	267	20.5
100	170	3.4	170	2.9
1000	169	0.6	169	0.0
	pH=10.0 $E_M=50\pm15$		pH=10.0 $E_M=-17\pm1$	

Table 4.4: I.P. response of Pyrite, Exp. #9

Solution: 10^{-2}M K_2SO_4 + 10^{-3}M $FeSO_4$ + KOH + H_2SO_4

Temperature: $\approx 22^{\circ}C$

Comments: Electrode not cleaned after experiment #9a. All E_M values in mV, Z_o in Ω/cm^2 and $\emptyset_o$ in degrees.

Chalcocite #7

	7a		7b	
f(HZ)	$Z_o(\Omega/cm^2)$	$\emptyset_o$(deg)	Z_o	$\emptyset_o$
.1	1131	32.7	195	6.3
1	363	46.9	142	26.2
10	112	32.7	71.3	19.4
100	74.0	8.0	49.6	8.3
1000	69.6	2.0	47.0	1.9
	pH 7.0 $E_M = -25 \pm 2$ mV		pH=8.0 $E_M = -565 \pm 5$ mV	

Pyrite #10

	10a		10b	
f(HZ)	$Z_o(\Omega/cm^2)$	$\emptyset_o$(deg)	Z_o	$\emptyset_o$
.1	6391	64.2	2195	42.1
1	1078	57.1	547	42.8
10	427	16.3	300	10.4
100	365	2.3	285	1.7
1000	365	0.0	285	0.0
	pH=7 $E_M = 110 \pm 10$ mV		pH=8.1 $E_M = -425 \pm 5$ mV	

Table 4.5: I.P. response of chalcocite, exp. #7 and pyrite exp. #10.
Solution 7a, 10a: 10^{-2}M NaCl
Solution 7b, 10b: 10^{-2}M NaCl + 10^{-2}M Na_2S + HCl
Temperature: ≈17°C
Comments: Solution deoxygenated and saturated with H_2(g)

R_S and the non-faradaic and adsorption branches forms a model that fits the data reasonably well (~5%). The most important aspect of this model, is the fact that the high capacitance of C is transferred into the adsorption capacitance C_a. We believe that we are dealing with the adsorption of the supporting electrolyte, since it is the only species with high enough concentrations. As a four parameter equivalent circuit (R_S, C, C_a, W_a) model it is superior to the Randles (R_S, C, W, R_1) model for explaining most of our data.

The fits between the data and model can be improved if the third, faradaic branch is included. Generally, the RMS error is reduced to 1 to 2%, but the inversions are not sensitive to the type of element(s) placed in the faradaic branch. We do need a faradaic path to explain the d.c. potential (E_M). Additionally, such a low phase ($\leq|45°|$) path is needed because we often see a phase decrease as the frequency is lowered, which cannot be explained by the finite diffusion layer argument given in Chapter II. Consider as an example experiment: pyrite #8C. We tried a variety of equivalent circuit models (Figure 4.11) on the impedance spectra. The results are given in Table 4.6. Every model includes R_S and the non-faradaic path represented by C. The type I model is the Randles circuit and incorporates a faradaic path given by W and R_1. Note the large value of C (340μF) which cannot be explained as a triple layer capacitance. Model III uses a more involved faradaic path. Model II is the basic adsorption controlled equivalent circuit. Note that C is reduced although the value is still somewhat large. In many cases the reduction in C is more drastic than this. Models IV to VII represent

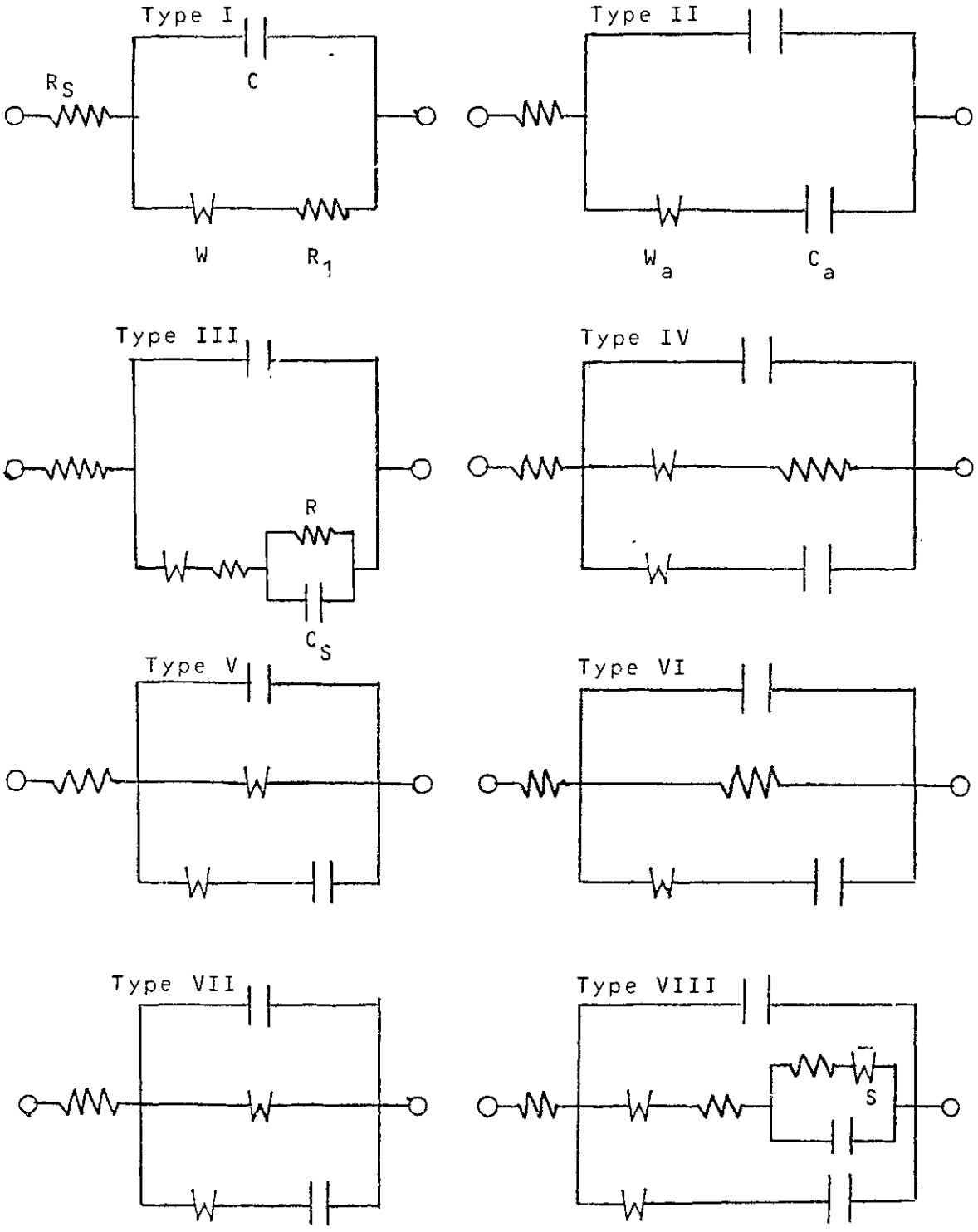


Figure 4.11: Some Possible Equivalent Circuit Models

Type	RMS(%)	R_S	C	R_1	W	C_S	R	W_a	C_a	W_{S_1}	W_{S_2}
I	7.7	182 (1.0)	340 (1.0)	(0.0)	3662 (1.0)						
II	5.2	177 (1.0)	244 (1.0)					1905 (0.9)	970 (0.9)		
III	1.5	175 (1.0)	151 (1.0)	(0.0)	791 (1.0)	599 (1.0)	7820 (1.0)				
IV	1.1	172 (1.0)	48 (0.6)	(0.0)	5052 (1.0)			370 (1.0)	431 (1.0)		
V	1.1	172 (1.0)	52 (0.7)		5063 (1.0)			409 (1.0)	403 (1.0)		
VI	1.3	174 (1.0)	126 (1.0)	13K (1.0)				713 (1.0)	587 (1.0)		
VII	1.0	173 (1.0)	78 (0.9)					510 (1.0)	419 (1.0)	9 (0.7)	17K (1.0)

Table 4.6: Parameter estimates using different circuit models (see figure 4.11). Pyrite #8c. Entries are for 1 cm^2 of electrode area. Value in bracket is the diagonal element of the resolution matrix for the given parameter. Resistances in Ω/cm^2, capacitance in $\mu F/cm^2$ and Warburg impedances in Ω-cm^2.

different attempts at modelling the third, faradaic path. Note that the RMS errors are not very different and also that R_S, W_a and C_a are approximately constant. Two conclusions may be drawn from the results:

1. The faradaic path can be well resolved.
2. The actual circuit element(s) involved in the faradaic path cannot be uniquely determined.

This behavior holds in general. Note that model VIII is not shown in Table 4.6 because there are so many parameters involved that the parameter estimation methods would fail.

In view of the above results, we will adopt a new equivalent circuit (type IV of Figure 4.11) consisting of R_S, a non-faradaic path (C), an adsorption path (W_a, C_a) and a faradaic path (W, R_1). We choose this model because it reduces to the Randles circuit when adsorption is absent or negligible, a situation that does occur in practice.

Using the type IV model we interpreted all of our data. We had hoped that with this new equivalent circuit model, the faradaic path would indeed show pH dependence in accord with the E_M-pH behavior. Unfortunately, the faradaic path still showed the approximate pH independence. The results of experiment: pyrite #9 are shown in Table 4.7 as an example. We feel that this problem is still somewhat unresolved, but we offer below a possible explanation.

Consider as an example the pyrite reaction(4.11). Although this represents the overall electrochemical reaction, the actual mechanism certainly involves intermediate steps. For example, we might have

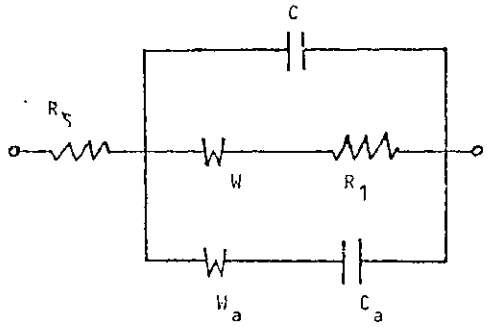
$$FeS_2 = Fe^2_{ads} + 2S\ (1\ atm) + 2e \qquad (4.16)$$

$$Fe^{2+}_{ads} = Fe^{3+}_{ads} + e \qquad (4.17)$$

PYRITE #9

Experiment #	pH	R_S (Ω)	C(μF)	W_a (Ω)	C_a (μF)	W(Ω)	R_1 (Ω)	RMS(%)
9a	2.0	165 (1.0)	- (0.0)	161 (0.7)	132 (1.0)	2518 (1.0)	- (0.0)	2
b	2.6	167 (1.0)	16 (0.1)	185 (0.7)	118 (0.9)	1356 (1.0)	102 (0.7)	1
c	3.3	168 (1.0)	- (0.0)	262 (0.9)	163 (1.0)	5192 (1.0)	1133 (0.7)	2
d	4.2	167 (1.0)	34 (0.2)	276 (0.7)	140 (1.0)	11,929 (1.0)	- (0.0)	3
e	5.4	169 (1.0)	102 (0.9)	1214 (0.4)	75 (0.9)	11,692 (1.0)	- (0.0)	2
f	6.5	166 (1.0)	30 (0.2)	270 (0.8)	158 (1.0)	17,566 (1.0)	- (0.0)	3
g	10.0	166 (1.0)	26 (0.1)	225 (9)	207 (1.0)	15,704 (1.0)	- (0.0)	3

Table 4.7: Parameter estimates of experiment: Pyrite #8. Type IV equivalent circuit used.



Equivalent Circuit
Type IV Model

$$Fe^{3+}_{ads} + 3OH^{-}_{ads} = Fe(OH)_3(S) \qquad (4.18)$$

These reaction steps occur in series with an overall reaction given by a mechanism similar to (4.11), but with one important difference. We have replaced OH^- with an adsorbed species OH^-_{ads} such that (4.11) now reads

$$FeS_2 + 3OH^-_{ads} = Fe(OH)_3(S) + 2S\ (1\ atm) + 3\ e \qquad (4.19)$$

In this scheme, the two electrochemical reactions (4.16) and (4.17) are pH independent and they may control the impedance of the faradaic path either through a reaction resistance on a surface impedance. The third step (4.18) is a chemical reaction and since we have insisted that the surface possesses enough OH^- to supply the reaction we need not consider diffusional processes in solution.

Virtually all reactions in which we observe pH independence in the faradaic path, while E_M shows pH dependence, involves oxides and hydroxides. Accordingly, it is always possible, and likely, that multistep reactions occur similar to reactions (4.16) to (4.18). As another example we break reaction (4.8) into three steps according to:

$$Cu_2S = CuS + Cu^+_{ads} + e \qquad (4.19)$$

$$C^+_{ads} = Cu^{2+}_{ads} + e \qquad (4.20)$$

$$Cu_{ads} + 2OH^-_{ads} = Cu(OH)_2(S) \qquad (4.21)$$

The arguments are similar to those given above for pyrite. In summary, we therefore adopt the type IV model (Figure 4.11), where we interpret the adsorption path to be due to the supporting electrolyte and the

faradaic path to surface phenomena between adsorbed intermediate species.

The ideas and circuit models considered in this section will now be used in discussing the I.P. response of some sulfide minerals.

4.4 INDUCED POLARIZATION RESPONSE OF CHALCOCITE

4.4.1 Chalcocite in the AO Region

Typical of the experiments in this region are: chalcocite #5e and chalcocite #6b. Parameter estimates using the type I equivalent circuit are shown in Table 4.8. The estimated Warburg impedances of 28 and 91Ω-cm^2 correspond to concentrations of approximately $10^{-2.7}$M and $10^{-3.3}$M respectively. These values are in good agreement with those obtained from the potentiometric data. The values obtained for C, namely 39 and 86μF/cm^2 respectively are not unreasonably large. We therefore conclude that in the AO region reaction (4.5) is operative, implying that Cu^{2+} is active at the electrodes. Accordingly, the chalcocite electrode impedance is comparatively small in the AO region.

4.4.2 Chalcocite in the NO Region

As chalcocite is moved from the AO into the NO region there is a general tendency for the impedance spectra to increase (see Tables 4.1 and 4.3). This increase in impedance is caused by the drop in the concentration of Cu^{2+} which is produced by the formation of hydroxides and oxides such as $Cu(OH)_2$ and CuO. The total electrode impedance is therefore to a large extent still controlled by mechanism (4.5), although adsorption becomes increasingly important at higher pH values. As examples we present the parameter estimates for experiments, chalcocite #5b and 6e,(Table 4.9).

Table 4.8: Results of experiments: chalcocite #5e and #6b.
Type I model used.

#5e

f(HZ)	Z_o (Ω/cm^2)	$\emptyset_o$ (deg)	Z_M	$\emptyset_M$	Parameters/cm^2
1000	15	2	15	2	R_S = 14Ω
100	16	3	16	3	C = 39μF
10	17	8	18	8	R_1 = 1Ω
1	25	18	24	19	W = 27Ω
.1	47	30	47	32	

RMS = 3.6%

#6b

f(HZ)	Z_o (Ω/cm^2)	$\emptyset_o$ (deg)	Z_M	$\emptyset_M$	Parameters/cm^2
1000	19	3	19	39	R_S = 18Ω
100	21	8	21	30	C = 85μF
10	28	18	28	17	R_1 = 1Ω
1	52	29	51	7	W = 91Ω
.1	128	39	129	3	

RMS = 1.7%

Resolution Matrices

#5e

	R_S	C	R_1	W
R_S	1.0	0	0	0
C		.1	.2	0
R_1			.5	0
W				1.0

#6b

	R_S	C	R_1	W
R_S	1.0	0	0	0
C		.5	0	0
R_1			.9	0
W				1.0

#5b

f(HZ)	$Z_o(\Omega/cm^2)$	ϕ_o(deg)	Z_M	ϕ_M	Parameters/cm^2
1000	25	5	25	3	R_S = 24Ω
100	28	8	28	8	C = 17μF
10	38	21	39	22	W_a = 344Ω
1	86	36	86	37	C_a = 358μF
.1	257	41	252	43	W = 193Ω

RMS = 3.2%

#6e

f(HZ)	$Z_o(\Omega/cm^2)$	ϕ_o(deg)	Z_M	ϕ_M	Parameters/cm^2
1000	19	6	19	4	R_S = 19Ω
100	24	21	24	22	C = 108μF
10	61	46	62	45	W_a = 1270Ω
1	227	51	226	52	C_a = 479μF
.1	876	52	878	52	W = 873Ω

RMS = 2.3%

Resolution Matrices

#5b

#	R_S	C	W_a	C_a	W
R_S	1.0	0.0	0.0	0.0	0.0
C		0.0	0.1	0.0	0.0
W_a			0.7	0.0	0.1
C_a				0.8	0.0
W					1.0

#6e

	R_S	C	W_a	C_a	W
R_S	1.0	0.0	0.0	0.0	0.0
C		1.0	0.0	0.0	0.0
W_a			1.0	0.0	0.0
C_a				0.8	0.0
W					1.0

Table 4.9: Results of experiments: chalcocite #5b and 6e. Type V equivalent circuit

4.4.3 Chalcocite in the NR Region

Table 4.10 displays the parameter estimates using the data of experiment, chalcocite #7b. Table 4.11 shows the impedance parameter before an Na_2S was added. Clearly HS^- is active at the electrode as evidenced by the low solution Warburg ($W \simeq 4\ \Omega\text{-cm}^2$). Even though the resolution of this parameter is low the value of $4\Omega\text{-cm}^2$ is very close to the Warburg expected for a 10^{-2}M concentration. One feature of Table 4.10 needs some explanation. The Warburg impedance estimated in experiment: chalcocite #7a is $296\Omega\text{-cm}^2$. This corresponds to a concentration of approximately 10^{-4}M. We believe this is due to some corrosion of the chalcocite or the pyrite electrodes. The species involved is most likely HS^- since this is stable in this reducing environment.

4.5 INDUCED POLARIZATION RESPONSE OF PYRITE

4.5.1 Pyrite in the AO and NO Regions

A glance at Tables 4.2 and 4.4 shows that the impedance spectra of pyrite are not very different in the AO and NO region. Pyrite does not seem to be sensitive to Cu^{2+} in solution (experiment #8). In experiment #9, $FeSO_4$ was added to the solution but the impedance of the pyrite electrode did not change significantly. This is easy to explain since the Fe^{2+} readily combines to produce solid Fe_2O_3 or $Fe(OH_3)$. The faradaic path is also approximately pH independent. It is therefore likely that the rate controlling reaction involves pH independent adsorbed species, as was the case with chalcocite. Table 4.12 shows two typical results. Note that W is larger in #9f than in #8b, this difference holds for most of experiments #9 and #8,

Chalcocite #7b

f(HZ)	$Z_o(\Omega/cm^2)$	ϕ_o(deg)	Z_M	ϕ_M	Parameters/cm^2
1000	47	2	46	2	R_S = 45Ω
100	50	8	51	7	C = 13μF
10	71	19	69	20	W_a = 214Ω
1	142	26	142	23	R_1 = 156Ω
.1	195	6	200	6	C_a = 1458μF
					W = 3.6Ω

RMS = 3.8%

Pyrite = 10b

f(HZ)	$Z_o(\Omega/cm^2)$	ϕ_o(deg)	Z_M	ϕ_M	Parameters/cm^2
1000	285	0	282	0	R_S = 281Ω
100	235	2	286	2	C = 12μF
10	300	10	303	10	W_a = 202Ω
1	547	43	547	43	R_1 = 1862Ω
.1	2195	42	2190	42	C_a = 429μF
					W = 1011Ω

RMS = 5.0%

Resolution Matrices

#7b

	R_S	C	W_a	R_1	C_a	W
R_S	1.0	0.0	0.0	0.0	0.0	0.0
C		0.0	0.0	0.0	0.0	0.0
W_a			1.0	0.0	0.0	0.0
R_1				1.0	0.0	0.0
C_a					1.0	0.0
W						0.1

#10b

	R_S	C	W_a	R_1	C_a	W
R_S	1.0	0.0	0.0	0.0	0.0	0.0
C		0.0	0.1	0.0	0.0	0.0
W_a			1.0	0.0	0.0	0.0
R_1				1.0	0.0	0.0
C_a					1.0	0.0
W						0.0

Table 4.10: Results of experiments: chalcocite #7b and pyrite #10b. Type IV equivalent circuit

Chalcocite #7a

f(HZ)	$Z_o(\Omega/cm^2)$	$\emptyset_o$(deg)	Z_M	$\emptyset_M$	Parameters/cm^2
1000	70	2	70	1	R_S = 70Ω
100	74	8	73	8	C = 119μF
10	112	33	113	32	W_a = 819Ω
1	365	47	366	47	R_1 = 1152Ω
.1	1131	33	1131	33	C_a = 751μF
					W = 296Ω

RMS = 1.4%

Pyrite #10a

f(HZ)	$Z_o(\Omega/cm^2)$	$\emptyset_o$(deg)	Z_M	$\emptyset_M$	Parameters/cm^2
1000	365	0	366	1	R_S = 364Ω
100	365	2	373	3	C = 16μF
10	427	16	418	17	W_a = 447/Ω
1	1078	57	1084	57	R_1 = 917Ω
.1	6391	64	6344	65	C_a = 114μF
					W = 9645Ω

RMS = 2.1%

Resolution Matrices

#7a

	R_S	C	W_a	R_1	C_a	W
R_S	1.0	0.0	0.0	0.0	0.0	0.0
C		1.0	0.0	0.0	0.0	0.0
W_a			1.0	0.0	0.0	0.0
R_1				1.0	0.0	0.0
C_a					1.0	0.0
W						1.0

#10a

	R_S	C	W_a	R_1	C_a	W
R_S	1.0	0.0	0.0	0.0	0.0	0.0
C		0.1	0.2	0.0	0.1	0.0
W_a			0.9	0.0	0.0	0.0
R_1				0.0	0.1	0.0
C_a					1.0	0.0
W						1.0

Table 4.11: Results of experiments: chalcocite #72a and pyrite #10a. Type IV equivalent circuit.

Pyrite #8b

f(HZ)	$Z_o(\Omega/cm^2)$	$\emptyset_o$(deg)	Z_M	$\emptyset_M$	Parameters/cm^2
1000	171	1	171	1	$R_S = 169\,\Omega$
100	177	3	176	4	$C = 8\mu F$
10	203	18	203	17	$W_a = 284\,\Omega$
1	481	53	483	53	$R_1 = 443\,\Omega$
.1	2672	64	2666	64	$C_a = 394\mu F$
					$W = 4200\,\Omega$

RMS = 1%

Pyrite # 9f

f(HZ)	$Z_o(\Omega/cm^2)$	$\emptyset_o$(deg)	Z_M	$\emptyset_M$	Parameters/cm^2
1000	169	1	167	1	$R_S = 166\,\Omega$
100	170	4	171	5	$C = 30\,\mu F$
10	212	30	209	28	$W_a = 270\,\Omega$
1	862	74	866	71	$R_1 = 463\,\Omega$
.1	6545	76	6682	76	$C_a = 158\mu F$
					$W = 17600\,\Omega$

RMS = 3%

Resolution Matrices

#8b

	R_S	C	W_a	R_1	C_a	W
R_S	1.0	0.0	0.0	0.0	0.0	0.0
C		0.0	0.1	0.0	0.0	0.0
W_a			1.0	0.0	0.0	0.0
R_1				0.0	0.1	0.0
C_a					1.0	0.0
W						1.0

#9f

	R_S	C	W_a	R_1	C_a	W
R_S	1.0	0.0	0.0	0.0	0.0	0.0
C		0.2	0.3	0.0	0.3	0.0
W_a			0.8	0.0	0.0	0.0
R_1				0.0	0.0	0.0
C_a					1.0	0.0
W						1.0

Table 4.12: Parameter estimates of Pyrite in A0 and N0 regions. Experiments #8b and 9f.

although generally the ratio is more on the order of two.

4.5.2 Pyrite in NR Regions

The results in Table 4.11 when compared with Table 4.10, show a small decrease in the impedance, when Na_2S is added. It is very difficult to measure the significance of this drop in impedance. This is one region in which much experimental work is needed. Recall that we don't even have a good explanation for the E_M-pH behavior in the NR region.

4.6 INDUCED POLARIZATION RESPONSE OF COPPER

Copper can exist in its pure state in nature. Figure 4.2 shows that it is stable under NR conditions. Native copper usually forms in reducing environments when there is a deficiency in sulfur. The results of two experiments on copper in a NR environment are shown in Table 4.13. The adsorption seems to be somewhat reduced when compared to the results of pyrite and chalcocite. This reduced adsorption may be due to the difference in electrode type or to the lower concentration of supporting electrolyte used in the present experiments. Generally, E_M-pH plots for this system follow the reaction.

$$2Cu + H_2O = Cu_2O + 2H^+ + 2e \qquad (4.20)$$

with the corresponding Nernst equation,

$$E_M = 230 - 59.2\ pH \qquad (4.21)$$

However, the impedance still shows an insensitivity to pH variations which may again be explained in terms of adsorbed surface intermediates.

Copper #50b

f(HZ)	$Z_o(\Omega/cm^2)$	$\emptyset_o$	Z_M	$\emptyset_M$	Parameters/cm^2
1000	78	10	82	14	R_S = 73Ω
100	166	37	153	38	C = 4μF
10	563	66	577	61	W_a = 2987Ω
1	3343	70	3409	70	R_1 = 775Ω
.1	20625	64	20487	65	C_a = 39μF
	pH = $8.5\pm.1$	E_M = -250 ± 10 mV			W = 29139Ω

RMS = 7%

Copper #50c

f(HZ)	$Z_o(\Omega/cm^2)$	$\emptyset_o$	Z_M	$\emptyset_M$	Parameters/cm^2
1000	81	10	81	10	R_S = 72 Ω
100	125	30	124	30	C = 4μF
10	394	55	386	54	W_a = 1743Ω
1	1950	64	1868	59	R_1 = 199Ω
.1	7500	57	8033	53	C_a = 45μF
	pH = $6.5\pm.1$	E_M = -150 ± 10 mV			W = 7641Ω

RMS = 7%

Resolution Matrices

#50b

	R_S	C	W_a	R_1	C_a	W
R_S	1.0	0.0	0.0	0.0	0.0	0.0
C		0.6	0.2	0.0	0.0	0.0
W_a			0.9	0.0	0.0	0.0
R_1				0.0	0.0	0.0
C_a					1.0	0.0
W						1.0

#50c

	R_S	C	W_a	R_1	C_a	W
R_S	1.0	0.0	0.0	0.0	0.0	0.0
C		0.1	0.2	0.0	0.0	0.0
W_a			0.9	0.1	0.0	0.0
R_1				0.0	0.0	0.0
C_a					1.0	0.0
W						1.0

Table 4.13: Results of experiments. Copper #50b and c.
Solution: 10^{-3} K_2SO_4 + H_2SO_4 + KOH
Temperature: ≈22°C
Comments: Solution deoxygenated with $N_2(g)$, then saturated with $H_2(g)$

4.7 INDUCED POLARIZATION RESPONSE OF OTHER COPPER AND IRON SULFIDES

For the sake of completeness we thought it advisable to comment on the I.P. behavior of some other common sulfide minerals.

Covellite (CuS) behaves in much the same manner as chalcocite. Chalcopyrite ($CuFeS_2$) exhibits behavior ranging from that of pyrite to that of chalcocite. Of ten samples measured four behaved somewhat like pyrite, although the impedance levels are generally higher. Four other samples behaved like chalcocite. The remaining two samples showed responses intermediate between that of pyrite and chalcocite. Visual examination of the samples indicate that there might be a correlation between the impedance of chalcopyrite and the quantity of Cu present. Such a correlation might exhist because chalcopyrite may actually occur as $Cu_x Fe_{1-x} S_2$, where a solid mixture of Cu and Fe is allowed. This problem seems quite interesting and certainly worthwhile of further examination.

SUMMARY

In this chapter we presented much I.P. data on pyrite and chalcocite. The data were interpreted using many different types of equivalent circuits. Unfortunately, the equivalent circuits are not unique in their ability to fit the data. Accordingly, we had to rely on physical and chemical arguments to justify the choice of one model over another. We propose the general use of an equivalent circuit incorporating an adsorption path in parallel with the faradaic and non-faradaic paths.

A discussion of the differences in the I.P. response of the minerals and the possibility of mineral discrimination, will be treated in the next chapter.

V

SPECTRAL I.P.

INTRODUCTION

In the early days of field I.P. measurements it was standard practice to measure the impedance at two frequencies and then to compare their magnitudes. This method is still used for reconnaissance and small surveys. Recently, electronic instrumentation has become sophisticated enough to allow impedance measurements to be taken over a wide range of frequencies. Field measurements are recorded with frequencies as low as 10^{-3} Hz. These low frequency spectral I.P. studies are made with the hope of being able to discriminate between different minerals. In this regard, low-frequency phase measurements seem to be promising.

We will briefly discuss in this chapter how our laboratory experiments are related to such field applications.

5.1 CONTRIBUTION OF ELECTRODICS TO SPECTRAL I.P.

The final goal of I.P. research in this laboratory has always been to better understand the I.P. response of mineralized rocks in the field. Recently, the important question of the possibility of mineral discrimination has received much attention (Hallof, 1979, Halverson, 1979). These studies are based principally on low frequency field measurements of phase, commonly referred to as "Spectral I.P.".

Mineralized rocks and hence field I.P. data show reduced sensitivity to frequency variations. In fact, the total impedance change is hardly ever more than a factor of two and the maximum phase difference about

200 milliradians (Bertin and Loeb, 1979, Sumner, 1979). This dilution of the I.P. effect is caused mainly by the large resistivity of the rock and by geometric modifications of the normal I.P. model. If we model the rock resistance as acting in series with the basic I.P. phenomena and that resistance is comparatively large, then the overall spectra will show small changes in Z and $\emptyset$. There is another reason for reduced I.P. effect in mineralized rocks. Madden (1959) showed that for I.P. occurring parallel to the current direction, the diffusion impedance varies as $f^{-1/4}$ instead of $f^{-1/2}$ and also that the magnitude of the phase is reduced from 45° to 22 1/2°. Such geometries occur when the mineral faces form one of the side walls of a crack rather than forming an end wall. We studied I.P. occurring between plan parallel electrodes. A rock consists of some mixture of the above effects. This is a complex problem needing further work. Nevertheless, it is important to see if discrimination between mineral types exist from our results, because such effects, though reduced by the complex rock geometry, should still maintain some of its relative characteristics. We discuss each major electrochemical region separately.

5.1.1 Mineral Discrimination in the AO Region

Figure 5.1 shows impedance data for pyrite and chalcocite. We show regions of possible impedance magnitudes and phases based on all of the data we possess. The higher pyrite impedance at high frequencies is due to the intrinsic resistivity of the pyrite. Removal of this high frequency resistance would not affect appreciably the low frequency data in which we are primarily interested. Clearly, mineral discrimination is possible

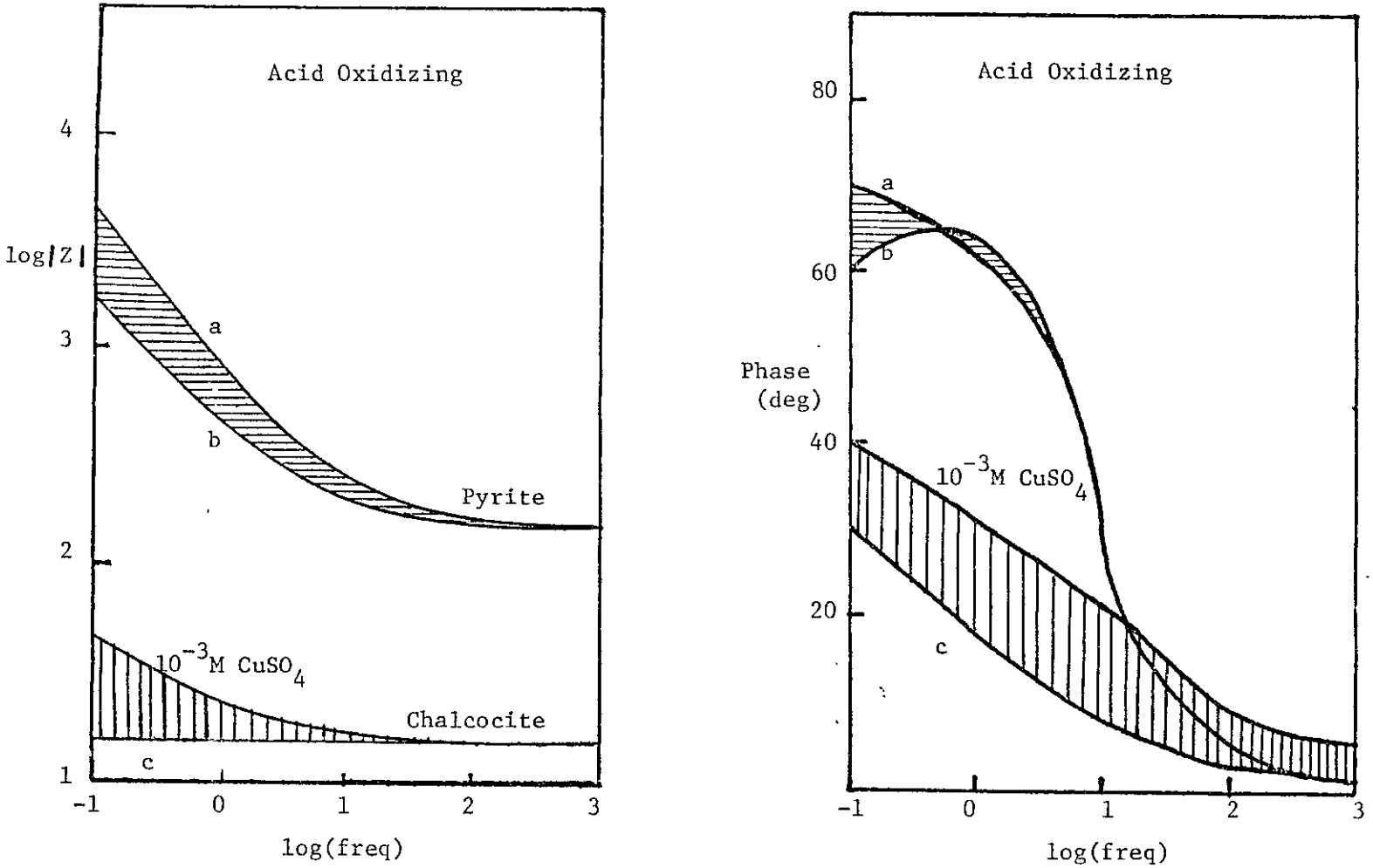


Figure 5.1: Range of Magnitude and Phase Data for Acid-Oxidizing conditions.

a. Solution doped with 10^{-3}M $CuSO_4$.

b. Solution doped with 10^{-3}M $FeSO_4$.

c. solution doped with 10^{-1}M $CuSO_4$.

in this region. Note that the upper limit of the cahlcocite impedance is given for 10^{-3}M Cu^{2+} present. In the AO region much more copper can be present rendering the discrimination even more effective.

5.1.2 Mineral Discrimination in the NO Region

In the neutral oxidizing region differences in I.P. response do exist between pyrite and chalcocite (Figure 5.2.). The discrimination is less well defined in comparison with the AO region especially for the phase data which is the more important measurement for spectral I.P.

5.1.3 Mineral Discrimination in the NR Region

We possess only limited data in this region. When no sulfur species is present (Figure 5.3) we still observe the general discriminatory trend in which the magnitude of the impedance and phase of pyrite are larger than those of chalcocite. In the neutral reducing region H_2S and HS^- may exist as stable species. Figure 5.3 shows the results of an experiment with 10^{-2}M HS^- present in solution. The differences are clear and pronounced at lower frequencies.

SUMMARY

With the limited data we presented in Figure 5.1 to 5.3 it seems rather convincing that discrimination between pyrite and chalcocite are indeed possible. The general trends are that the pyrite shows greater magnitudes and phases in its spectra than chalcocite. Note that the discrimination becomes more pronounced at lower frequencies. In some cases the phase angles are so large for pyrite (70° to 75°) that the impedance actually approaches a capacitive behavior. We explained this as being due to adsorption effects of the supporting electrolyte.

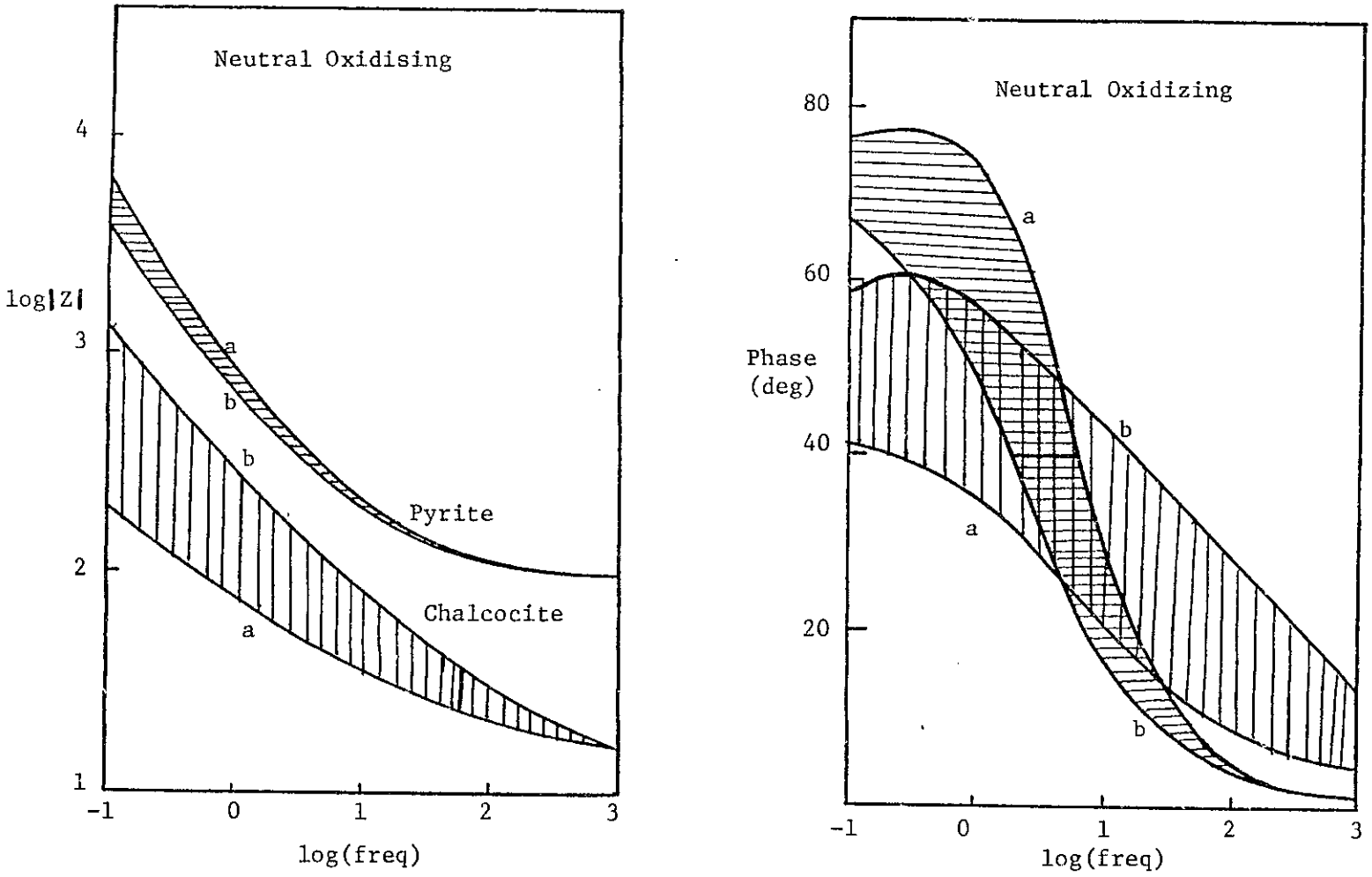


Figure 5.2: Range of Magnitude and Phase Data for Neutral-Oxidizing conditions.

a. Solution doped with 10^{-3}M $CuSO_4$.

b. Solution doped with 10^{-3}M $FeSO_4$.

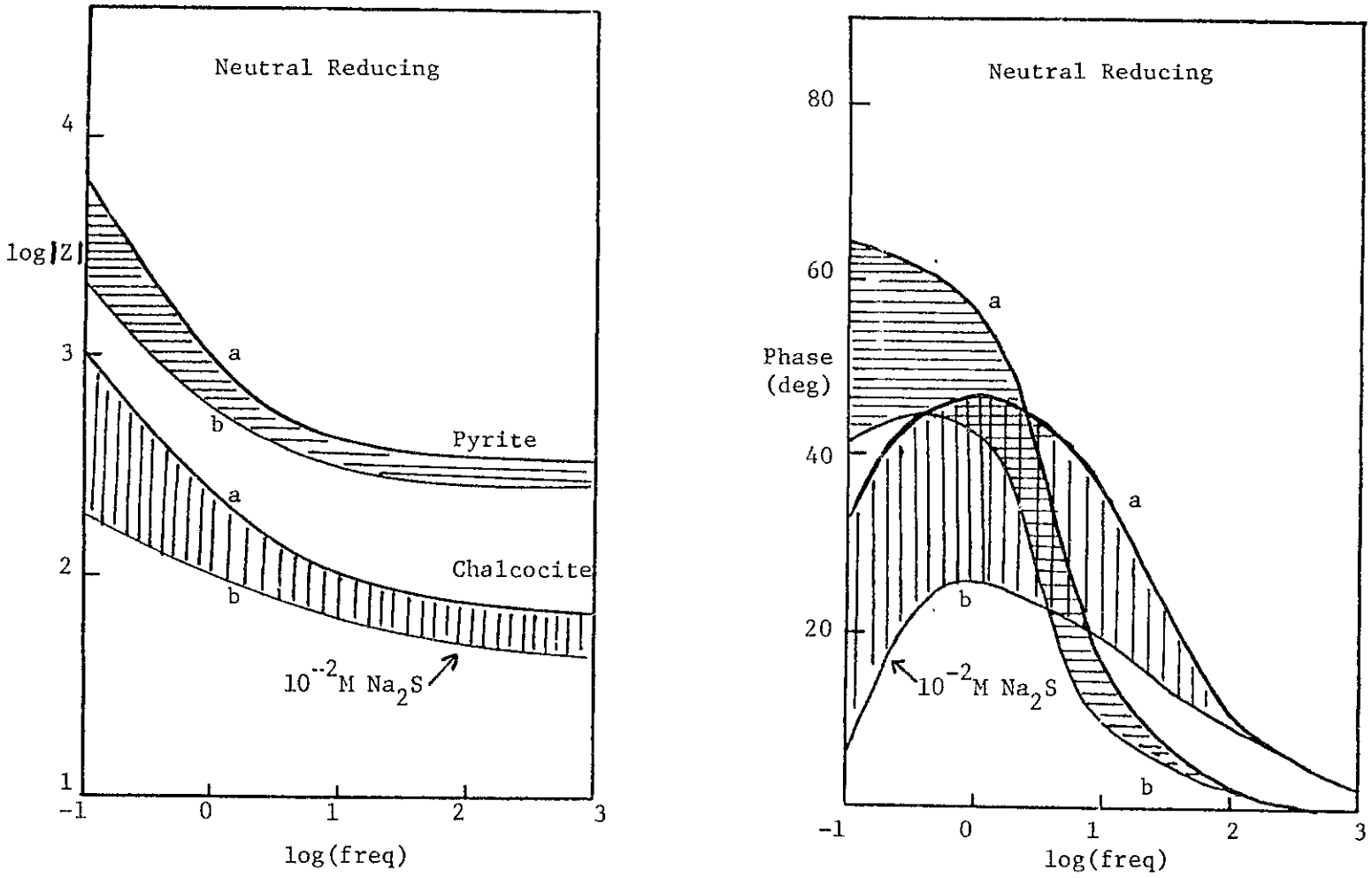


Figure 5.3: Range of Magnitude and Phase Data for Neutral-Reducing conditions, with and without Na_2S in solution.

a. No Na_2S present

b. 10^{-2}M Na_2SO_4.

One surprising result is that pyrite is not reactive to HS^-. This must be due to the different crystallographic structure of pyrite (FeS_2) as compared to chalcocite (Cu_2S). Pyrite normally possesses a cubic structure, whereas chalcocite and covellite (CuS) are normally found with hexagonal symmetires. The sulfur is bonded in pyrite quite differently when compared with Cu_2S or CuS. The two sulfur atoms form a covalent bound to produce S_2^{2-}, which then combines with Fe^{2+}. Conversely, both Cu_2S and CuS possess sulfur in the form S^{2-}. These differences are intriguing and should be investigated further. One particularly interesting experiment would be to see if HS^- is active on troilite (FeS) since this mineral has the hexagonal structure and it contains sulfur as S^{2-}.

The two recent studies of mineral discrimination in the field, base their explanations on different grain size among the disseminated sulfide ores (Hallof, et al., 1979 and Halverson et al., 1979). We predict one could have distinct impedance spectra based on differences in electrochemical behavior. The relative contributions of electrochemical properties and grain size effects to the total I.P. spectra remain an open question, requiring further investigation.

VI

SUMMARY

INTRODUCTION

In this final chapter we propose a number of related problems that we feel warrant further research. Suggestions for future studies are considered in two categories. In the first part, we discuss possible extensions of the present study into the fundamental aspects of I.P. Secondly, future studies of a more general nature are considered. In the concluding remarks we review the thesis. In so doing we comment on progress we have made in accomplishing the objectives outlined in Chapter 1.

6.1 SUGGESTIONS FOR FURTHER RESEARCH - Electrochemical Studies

We itemize below some problems we consider worthwhile of further investigations.

1. The details and relative contribution of surface processes and adsorption to the electrode impedance certainly need further investigation. For example, experiments with different supporting electrolytes and surface roughness would produce useful results.
2. Extend the present study to other metallic minerals.
3. Investigate the non-linear response when adsorption and surface phenomena are included. We have observed that the adsorption impedance is much more linear than the faradaic impedance.

6.2 SUGGESTIONS FOR FURTHER RESEARCH - General Studies

Since the ultimate goal of I.P. studies is to understand field data, the following problems should be considered, perhaps concurrently

with those described in Section 5.2.

1. Measure the I.P. response of metallic mineralized rocks. Such I.P. responses should be correlated with volume percent of minerals, pore-width distributions, pore solution chemistry, etc.
2. Model the I.P. response of rocks as a random network (Madden, 1975). In order to do this we need plausible electrical circuit models for I.P. in rocks. This poses some interesting problems such as understanding I.P. response when the electrodes are very close together (interacting diffusion layers) or when the current direction is parallel to the metallic mineral grains.

6.3 CONCLUSIONS

The study reported here was a modest attempt at furthering our knowledge of the basic electrochemical phenomena which produce the I.P. effect. The methods employed measurements of impedance spectra between plane parallel electrodes. Interpretation of the I.P. spectra were based on electrical circuit models. In Chapter I, two main objectives were stated. For convenience, we repeat them here:

Objectives of Study

1. Investigate the properties of the impedance spectra in an attempt to understand why it is approximately constant in many different environments. In attempting this we seek correlations between the impedance data and the associated Eh-pH environmental conditions.
2. Look for systematic differences in the impedance spectra among various mineral types, in an attempt to discriminate between minerals using I.P.

In attempting to meet these objectives, we considered a number of extensions of the classical Randles equivalent circuit. These extensions were discussed in Chapter II.

In Chapter III, the experimental methods were presented. We emphasized that the potential of the electrode under study (E_M), should be used instead of Eh, the potential measured with a Pt electrode wherever Pourbaix diagrams are discussed. Two illustrative experiments were given that demonstrated the applicability and accuracy of the methods, both experimental and interpretational.

Chapter IV presented much experimental data on pyrite and chalcocite. It was argued there that the most appropriate model consisted of the solution resistance R_S in series with three parallel paths. One path consisted of the non-faradaic impedance represented by the triple layer capacitance C. The second path (W_a-C_a) was due to adsorption effects. The faradaic processes constituted the third branch. This third branch was modelled as a Warburg impedance in series with a reaction resistance (W-R_1). The large phase angles observed could be accounted for by the adsorption path. In order to explain the observed behavior of the faradaic path we relied on the concept of adsorbed intermediates.

The question of mineral discrimination was addressed in Chapter V. It was demonstrated there that on the basis of our measurements discrimination between pyrite and chalcocite is indeed feasible. The magnitude of the impedance and the phase angles produced with pyrite electrodes are generally larger than those measured with chalcocite electrodes. The spectral I.P. techniques used in the field should therefore result in larger phase angles for pyrite .

We began this thesis by stating two major objectives. We will end in a similar way by remarking on how well we have resolved these problems. The contribution of this study may therefore be summarized as follows:

Conclusions of Study

1. The large phase angles often measured can be related to adsorption effects associated with the supporting electrolyte. In order to explain the insensitivity of the impedance spectra to solution chemistry, we suggested the importance of pH independent adsorbed intermediates.

2. On the basis of the results presented the discrimination among mineral types is certainly possible.

APPENDIX A

PARAMETER ESTIMATION

This study relies heavily on our ability to estimate the parameters of electrical equivalent circuit models accurately and uniquely. Electrochemists usually estimate circuit parameters by using graphical methods incorporating real/imaginary data plots. This method was popularized by Sluyters-Rehbach and Sluyters (1970). It is inherently inaccurate and parameters whose influence on the impedance spectra are mixed and spread over a wide frequency range cannot be well determined. Conversely, estimation using least squares is more accurate and reliable. In geophysics, parameter estimation is normally called "inversion". These inverse methods have been developed to a high degree of sophistication. We will not treat the subject in any great detail, but the reader may refer to Aki (1980), Bard (1974), Beck and Arnold (1977) and, Madden and Aki (class notes: Inverse Problems in Geophysics) for further details.

We commence by expanding the impedance Z in a Taylor series,

$$Z(f_j) = Z_o(f_j) + \left(\frac{\partial Z(f_j)}{\partial x_i}\right) \Delta x + \ldots \qquad (A.1)$$

where i = 1 to M, the number of parameters and j = 1 to N, the number of data points. Using only the first order expansion we obtain the lineralized array,

$$\Delta x_i = \left(\frac{\partial Z(f_j)}{\partial x_i}\right) (Z(f_j) - Z_o(f_j)) \qquad (A.2)$$

In matrix notation this becomes

$$A\Delta x = \Delta b \qquad (A.3)$$

An initial guess x_o of the parameters is made. We then use x_o to compute $Z_o(f)$ and the sensitivity matrix A. The overdetermined system (A.3) is then solved using damped least squares with logarithmetic weighting to give,

$$\Delta x = (A^T A + \varepsilon^2 I)^{-1} A^T \Delta b \equiv A_g \Delta b \qquad (A.4)$$

The new estimate of the parameters is now given by: $x = x_o\{\exp(\Delta x)\}$. The process is continued. The error of misfit between the data and the model is computed according to,

$$\sigma^2_{RMS} \simeq \sigma^2_d = \left(\frac{\Delta b^T \Delta b}{N-M}\right) \qquad (A.5)$$

The iteration is continued until σ_{RMS} changes by less than 0.1% from one iteration to the next.

Equation (A.5) for σ_d represents the best least squares estimate of the data variance. σ_{RMS} is normally computed with N-M replaced by N in the denominator of (A.5). We prefer to use σ_{RMS} as defined in (A.5) because it allows the misfit to be somewhat weighed by the number of degrees of freedom, N-M.

The resolution matrix R, is an estimate of how accurately we could, in principle, obtain the estimated parameters. It is therefore a

measure of the sensitivity of the inversion to the various parameters. R is given by,

$$R = A_g A \tag{A.6}$$

A one on the diagonal element of the resolution matrix means that that parameter is highly resolved. Smaller values on the diagonal imply reduced sensitivity or resolution. The resolution may also be reduced or distributed if strong correlation exists among parameters. Correlation effects show up as non-zero values in the off-diagonal elements of R.

Whenever possible an attempt should be made to estimate, quantitatively the errors in the parameters. For linear uncorrelated problems, errors computed from a parameter covariance matrix are usually reliable. Unfortunately, this type of point estimation (i.e. using only the diagonal term of the covariance matrix) is grossly inadequate when the inverse is non-linear and the parameters strongly correlated. Resolving this problem is an active area of research in statistics. We will not go into the details of the techniques here but rather point out two general approaches. One method involves estimating the error bounds between two or more parameters. This results in confidence regions in two or more dimensions. Another technique gaining popularity is known as "jacknifing". It involves estimating the parameters using N-1 data points at a time, from which errors are then computed. Both of these approaches are laborious and time consuming and not very practical in our situation where we perform hundreds of inversions.

Our approach to parameter accuracy is therefore a qualitative one. If a parameter shows high resolution we assume it has been accurately determined. With lower resolution we have less confidence in the accuracy of the estimated parameter, although our convergence criterion is stringent enough to estimate approximately many parameters with low resolution. Another way of stating this is that highly resolved parameters approach their estimates rapidly, within a few iteration steps, whereas, less resolved parameters, because of their reduced sensitivity, change more slowly from one iteration to the next. Strongly correlated parameters should not be interpreted as being reliable estimates. As we pointed out above correlation between parameters can be observed from the resolution matrix R. A far more sensitive approach to observing correlation is to use a correlation matrix L, defined by,

$$L(I,J) = \frac{C(I,J)}{\sqrt{\{C(I,I)(J,J)\}}} \tag{A.7}$$

where C is a covariance matrix given by

$$C = \sigma_d^2 \, A_g \, A_g^T. \tag{A.8}$$

We also compute the relevance or information density matrix D. This is an NxN matrix defined by:

$$D = A \, A_g \tag{A.9}$$

D is particularly useful in the initial stages of experimental design since it allows us to assess the importance of each data point to the parameter estimation.

One major difficulty with using damped least squares, as defined by (A.4), is in making the optimum choice of ε^2. There have been many attempts at obtaining suitable algorithms which would choose ε^2 at each step of the iteration. The two methods most widely employed are Marquardt's algorithm (Marquardt, 1963) and ridge regression (Hoerl, 1962, 1964, Hoerl and Kennard, 1970; Marquardt, 1970). We wish ε^2 to be large at the commencement of the iterative process when we are far away from convergence. We then reduce ε^2 to obtain a greater convergence rate. If ε^2 is reduced too quickly divergence may result. Moreover some minimum ε^2 must always be decided upon. The latter is important because we do not wish the inversion to be so sensitive that it tries to fit the model to the noise in the data. We have implemented an algorithm that is fast and in accord with the above requirements.

Initially, ε^2 is held fixed, at 0.1 in our case. When $\sigma^2_{RMS} \leq \varepsilon^2 = 0.1$, we then set $\varepsilon^2 = \beta\sigma^2_{RMS}$. This turnover corresponds to a percentage error ($100\sigma_{RMS}$) of approximately 30%. As the iteration proceeds towards convergence σ_{RMS} decreases, hence also ε^2. The minimum value of ε^2 is also automatically set. A better fit, which implies a lower σ_{RMS}, also implies a lower ε^2 and this is reasonable since the data noise is probably reduced in this case. The constant β must be obtained empirically, by running a number of inversions with different β's and choosing the most appropriate, with respect to convergence/divergence, data accuracy, etc. We normally take $\beta = 1$, although in some cases we reduced it to 1/2 to improve the convergence sensitivity. At present we are investigating the basic properties of this algorithm.

APPENDIX B

ELECTRONIC INSTRUMENTATION

B.1 CONSTANT CURRENT SOURCE and AMPLIFIER with D.C. OFFSET

The circuit diagrams for the constant current source (bilateral voltage-to-current converter) and the amplifier with the Self Potential buck are shown in figures B.1 and B.2.

B.2 RECENT IMPROVEMENTS IN DATA ACQUISATION

In chapter III there were two obvious areas in which improvements could be made to the data acquisation system.

B.2.1 Compensation of the Solution Resistance, R_S

A very simple circuit capable of reducing the contribution of R_S is given in figure B.3. The solution resistance is bucked out at the highest frequency (10^3HZ) by adjustement of the external resistance R. The usual impedance measurements are then taken. A similar circuit may be used to cancel the resistance during studies of the I.P. behavior of rocks. The method is certainly more useful in this latter case.

B.2.2 Digital Data Acquisation

The method of recording the impedance spectra using the storage oscilloscope is slow and tedious, moreover, the impedance often changes during the course of obtaining a data set. We have recently implemented a digital data acquisation system (Figure B.4). A special crystal controlled oscillator was construced. This oscillator produces frequences between

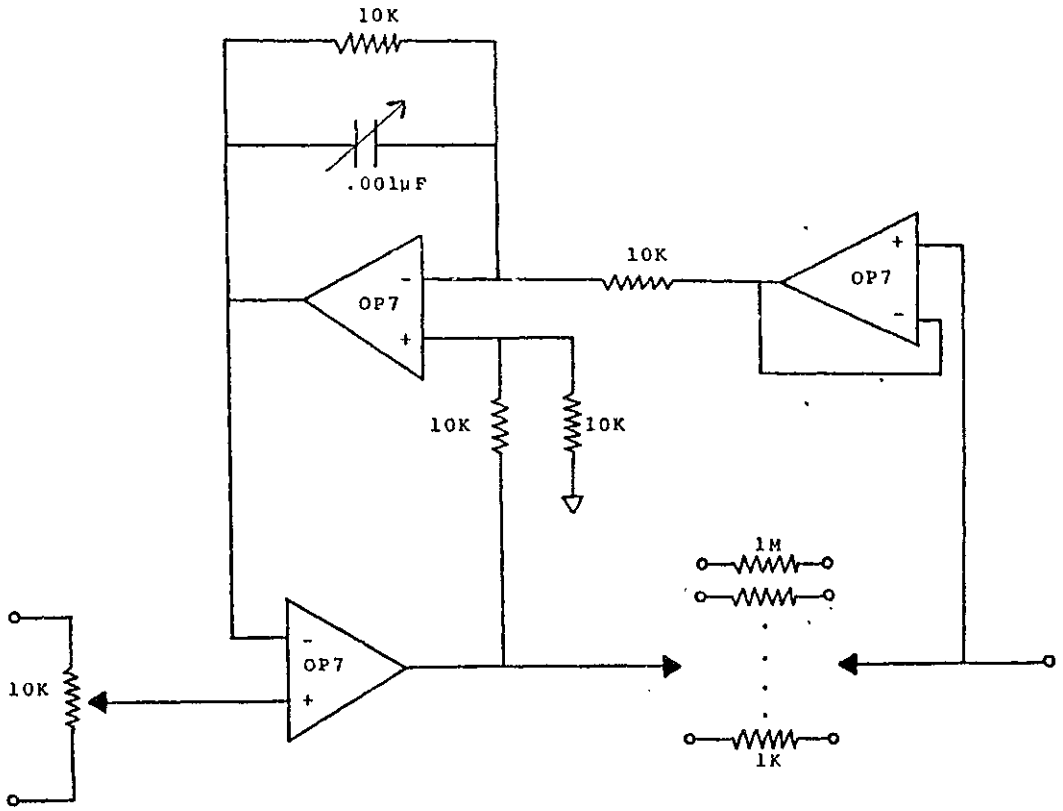


Figure B.1: A.C. Constant Current Source
(Voltage-to-Current Converter)

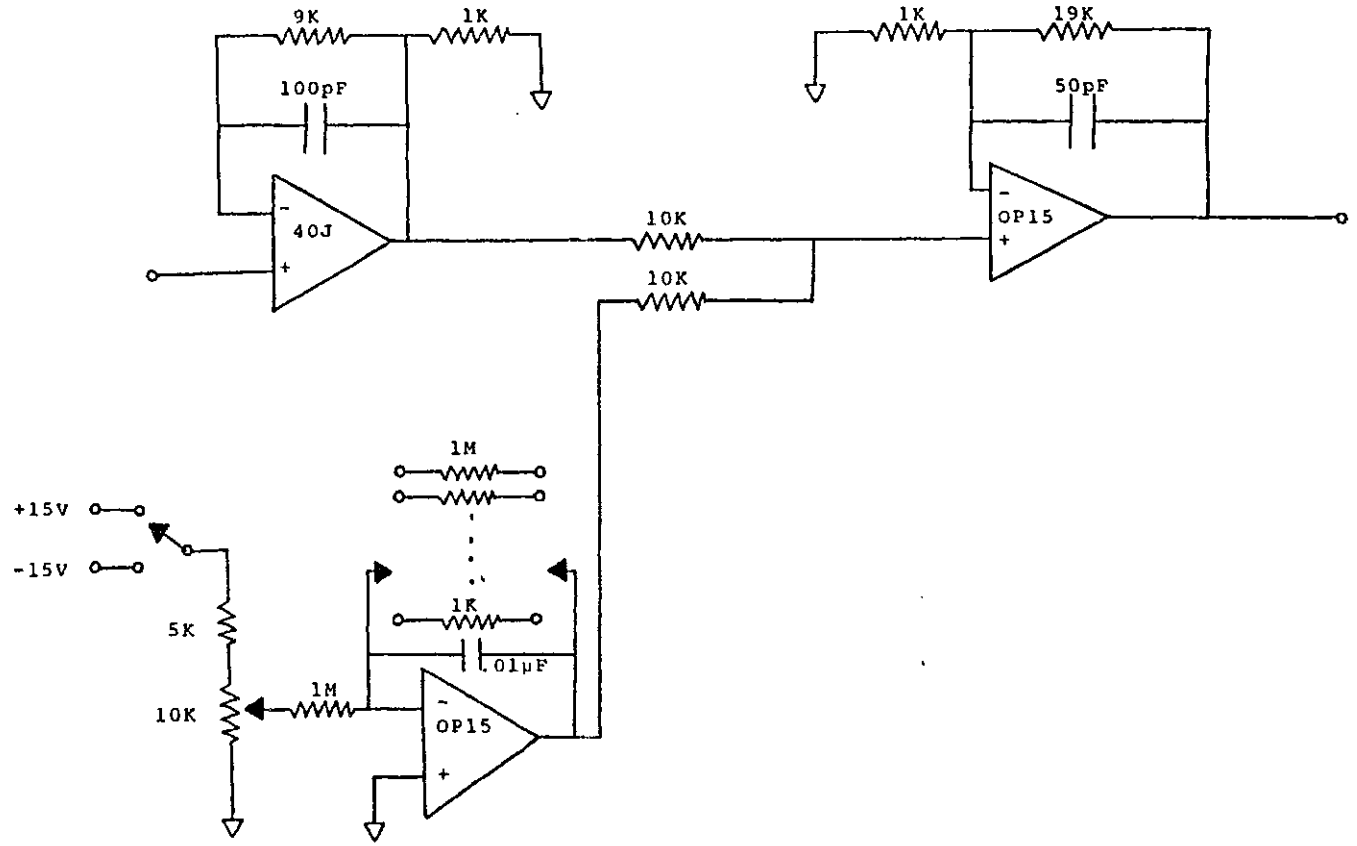


Figure B.2: A.C. Amplifier with D.C. Offset

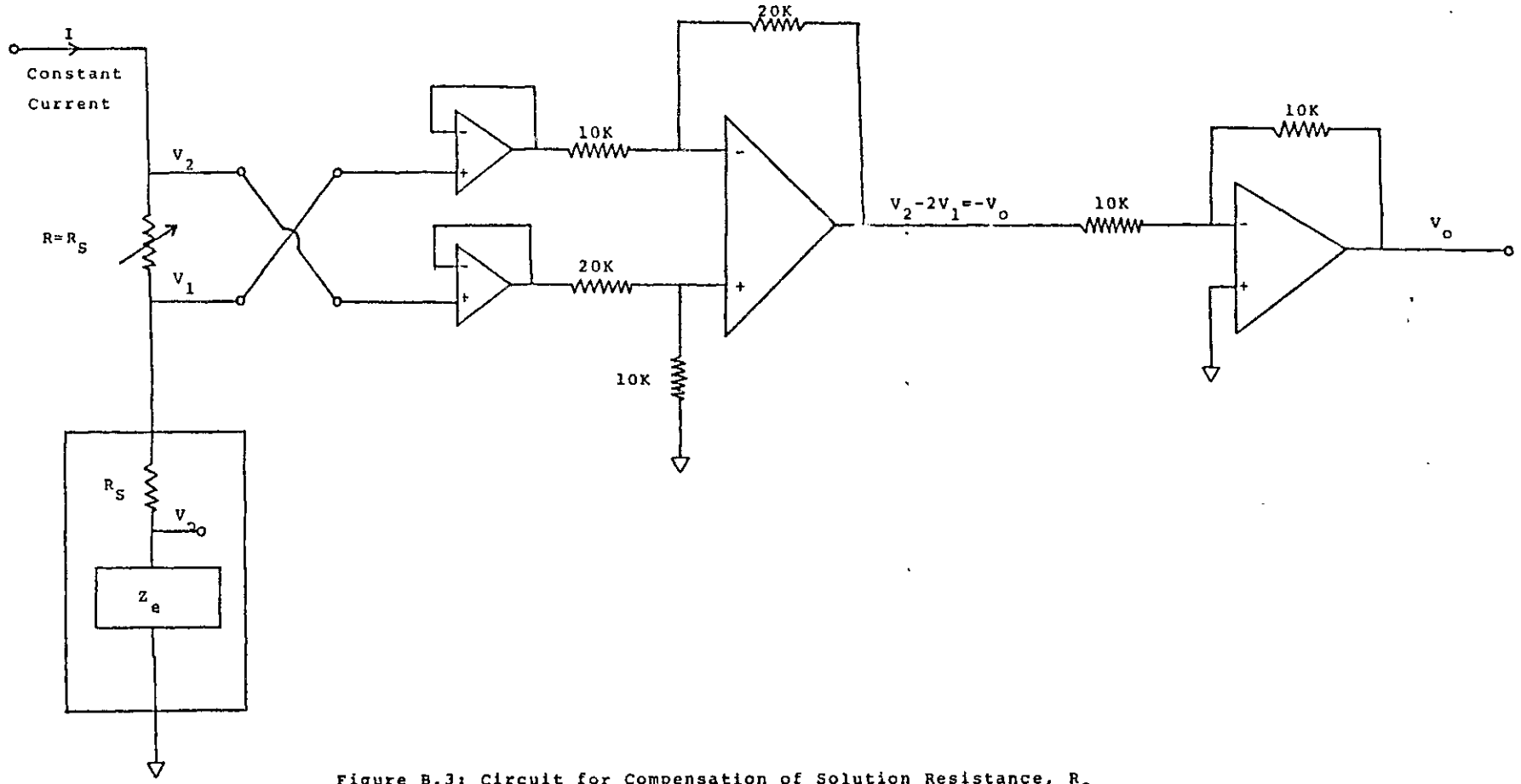


Figure B.3: Circuit for Compensation of Solution Resistance, R_S

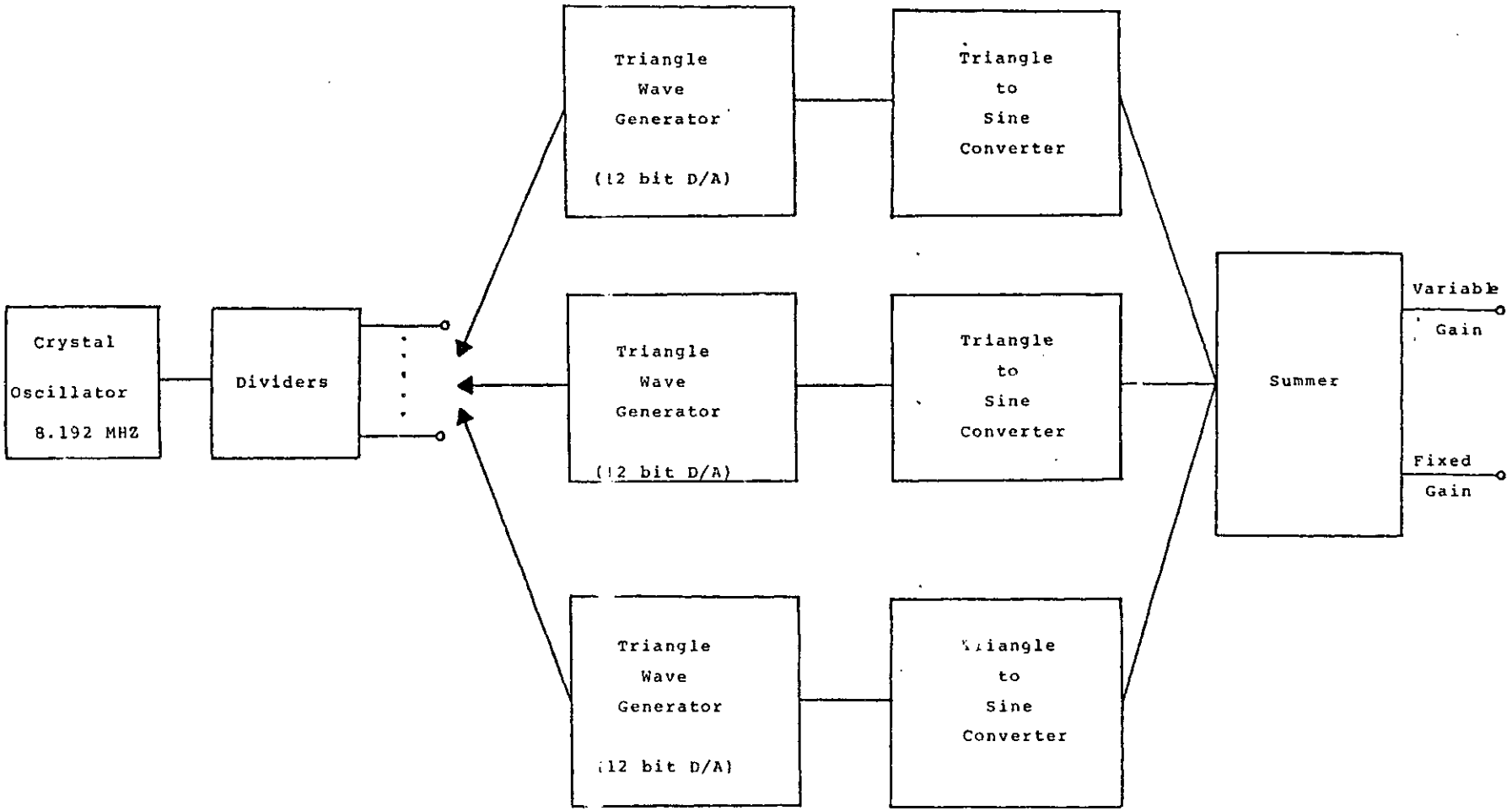


Figure B.4: Block Diagram of Multi-frequency Generator

10^{-3} and 10^{3}HZ. Three frequencies, each seperated by a decade, are summed and used as the input signal. The crystal oscillator frequency can also be divided by 2,4 or 8. This allows us to obtain intermediate data points. The output is recorded on a Nicolet digital oscilloscope. The data can then be transferred to the 9825B Hewlett-Packard computer for analysis. The analysis is capable of removing drifts in the d.c. potential of the electrodes which occur over the span of the experiment. Two such recordings allow us to span 10^{-2} to 10^{3}HZ. We are also now able to obtain reliable data at 10^{-3}HZ. as expected the overall accuracy and reproducibility of the system is quite good. From tests performed on R-C networks, errors in Z are usually less than 1% and in ϕ less than 1^{o}. This new method of data acquisation should prove very useful in future studies. Detailed circuit diagrams of the oscillator are shown in figures B.5 to B.8.

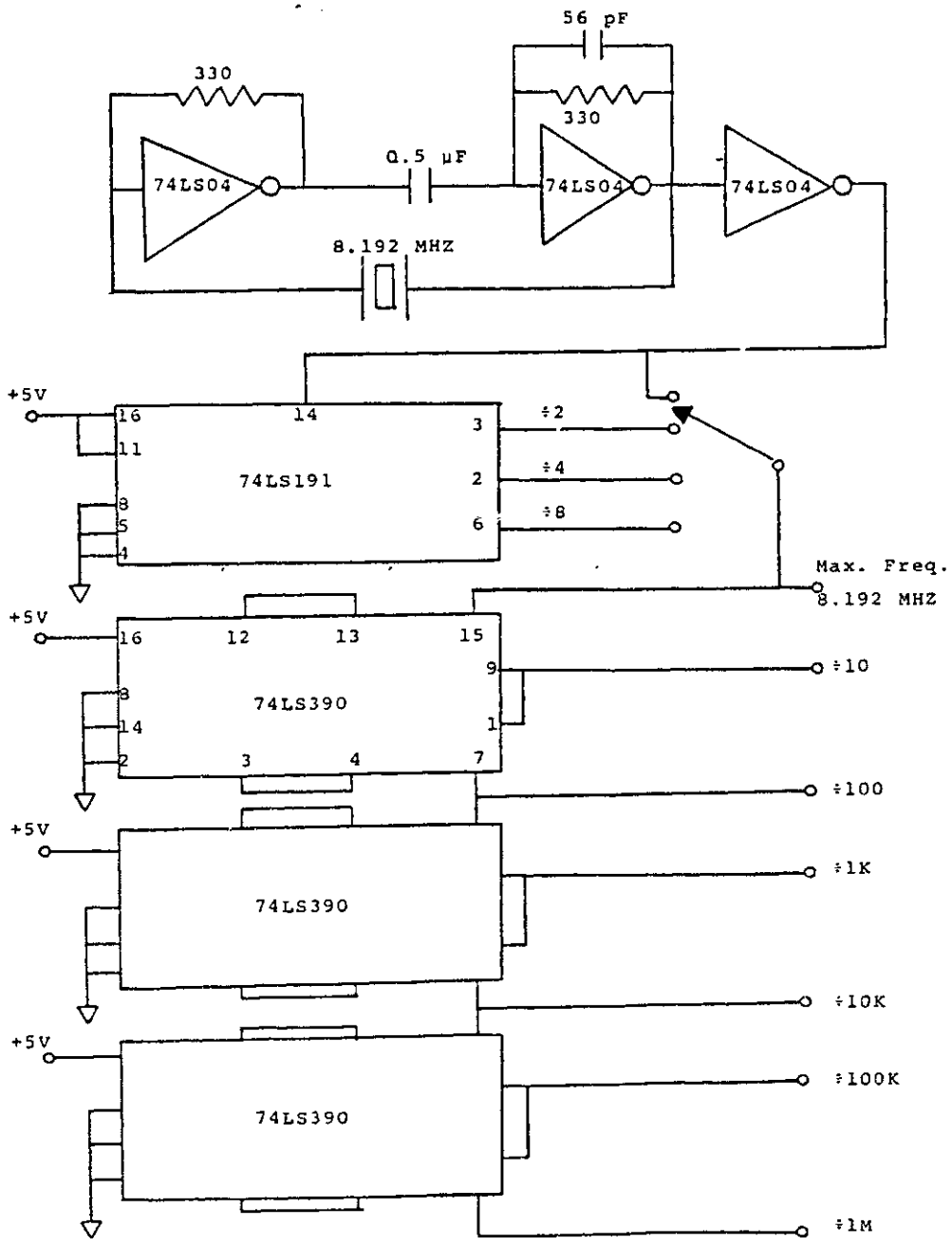


Figure B.5: Crystal Oscillator and Dividers

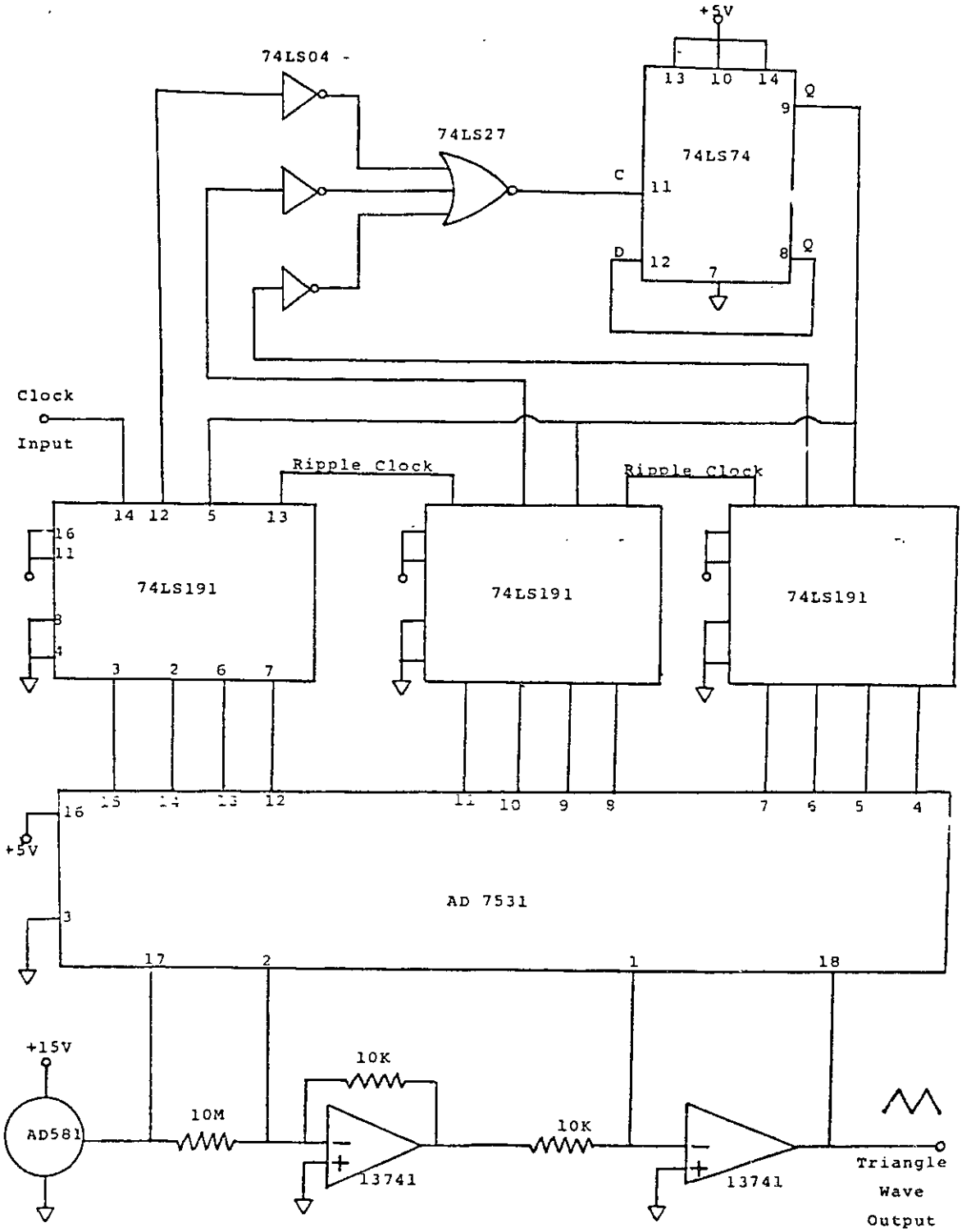


Figure B.6: Triangle Wave Generator

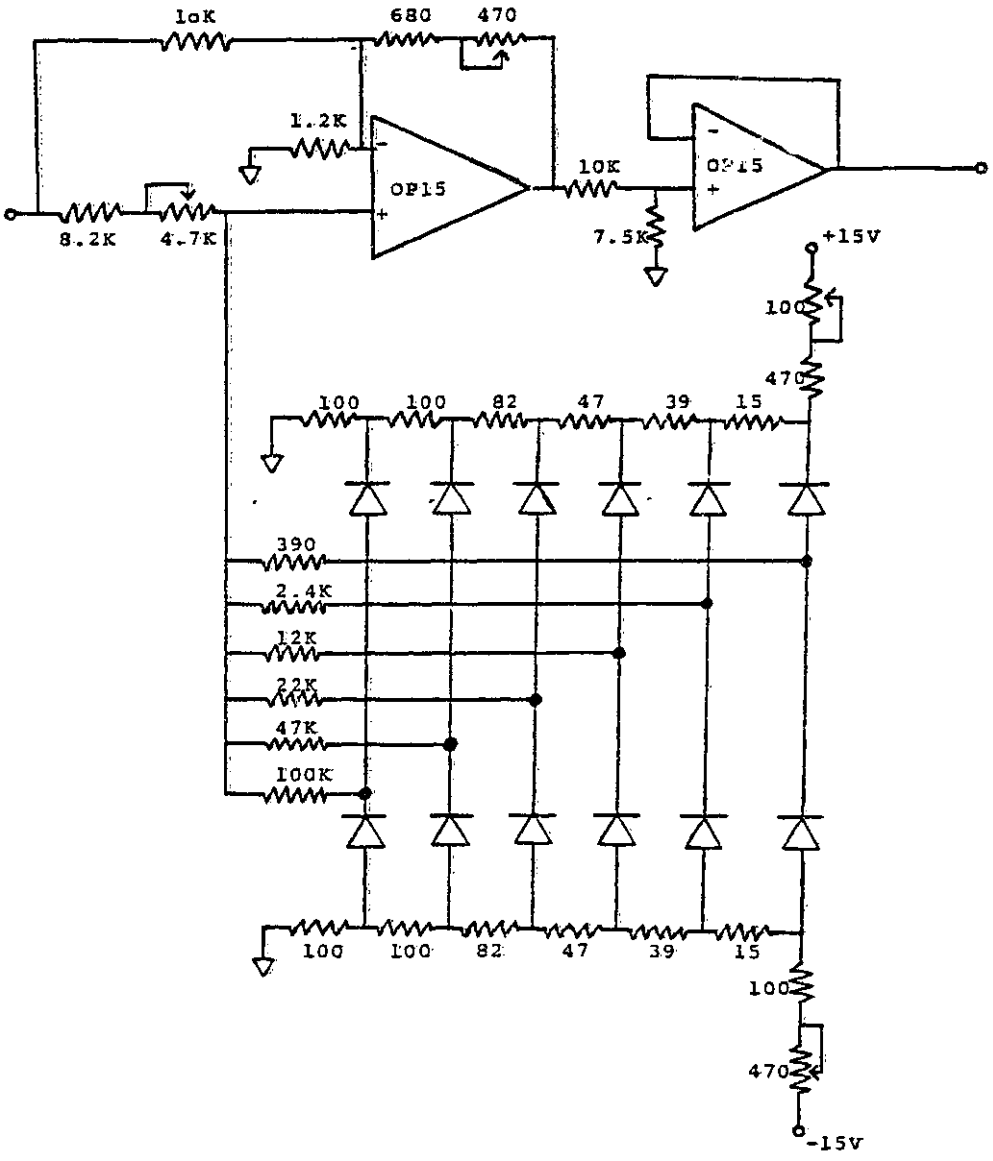


Figure B.7: Triangle-to-Sine Wave Converter.
(from: Sabah N.H., Wireless World 84, 34, Aug 1978)

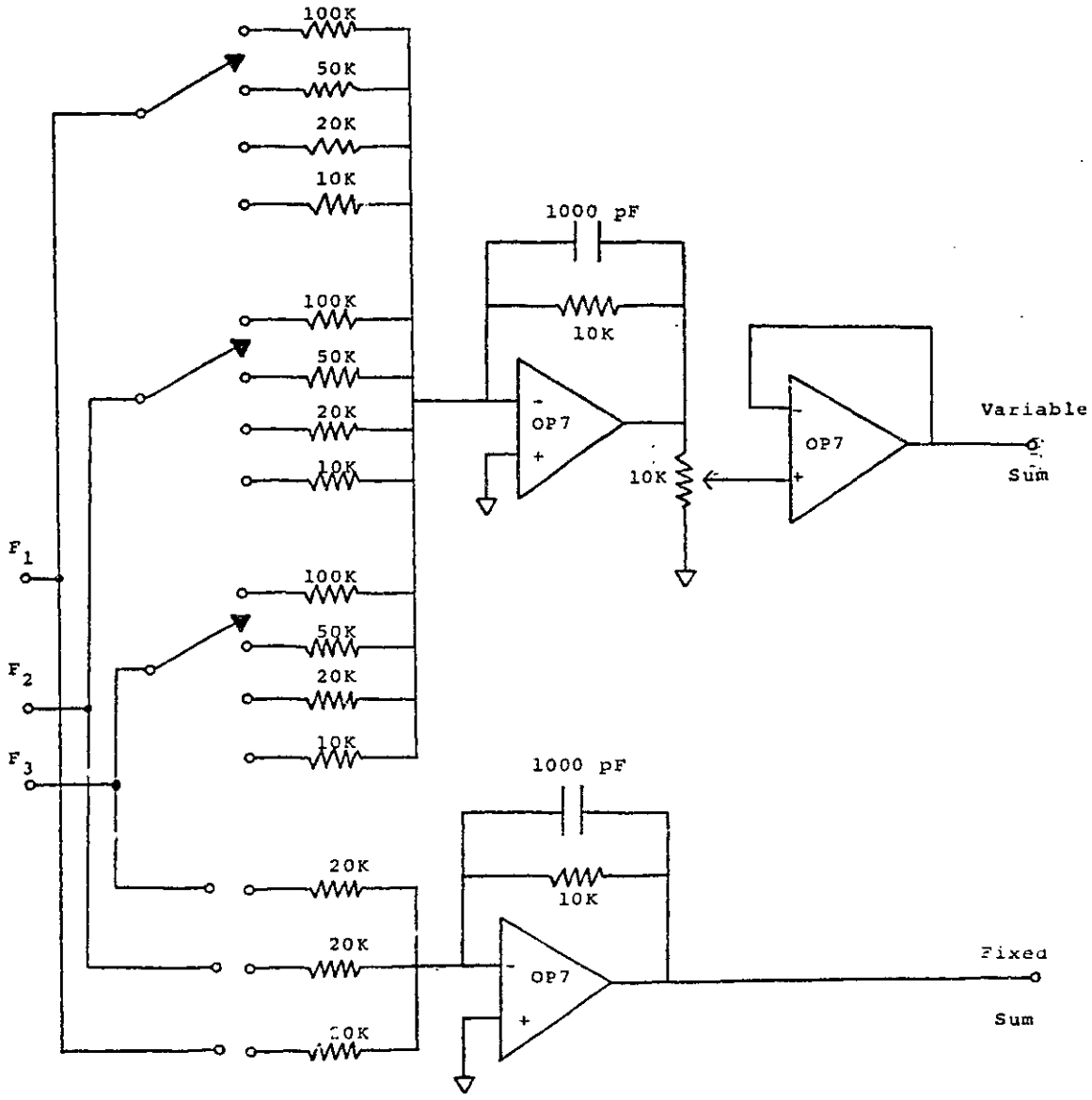


Figure B.8: Summers and Attenuator

REFERENCES

Aki, K. and Richards, P., "Quantative Seismology: Theory and Methods", Vol. II, Freeman and Company, San Francisco.

Angoran, Y. E., 1975, Ph. D. Thesis, M.I.T.

Barada, Y and Treemplev, G., (1954), Helv. Chim. Acta, 37, 583.

Bard, Y., 1974, Nonlinear Parameter Estimation", Academic Press, New York.

Bass Becking, L. C. M., Kaplan, I. R. and Moore, D., (1960), Jour. Geol. 68, 243.

Bauer, H. H., Herman, P. J. and Elving, P. J., 1973, "Critical Observations on Measurement of Adsorption at Electrodes." "Modern Aspects of Electrochemistry", J. O'M. Bochnes and Conway, B. D. (eds).

Beck, J. V. and Arnold, K. J., 1977, "Parameter Estimation in Engineering and Science", John Wiley and Sons, New York.

Bleil, D. F., 1953, Geophysics 18, 636-661.

Bockris, J. O'M. and Enyo, M., 1962, "Mechanism of Electrodeposition and Dissolution Processes of Copper in Aqueous Solutions." Trans. Faraday Soc. 58, 1187-1202.

Bockris, J. O'M. and Reddy, A. K. N., 1970, "Modern Electrochemistry", Vol. II. Plenum Press, New York.

Burrows, I. R., Harrison, J. A. and Thompson, J., 1975, Electroanaly. Chem. and Interfac. Electrochemistry, 58, 241-249.

Dawson, J. L., and John, D. G., 1980, J. Electroanalyz. Chem., 110, 37-47.

Delahay, P., 1954, "New Instrumental Methods in Electrochemistry", Interscience, New York.

Delahay, P., 1965, "Double Layer and Electrode Kinetics", Interscience Pub.

Delahay, P, 1966, J. Phys. Chem. 70, 2373.

Dermedts, G. and Van Peteghem, 1978, Corrosian Science, 18, 1041-1052.

Fleichmann, M. Rangarajan, S. K., Thirsk, H. R., 1967, Trans. Farad. Soc., 63, 1240-1260.

Garrels, R. M. and Christ, C. L., 1965, "Solutions, Minerals and Equilibrium", Harper and Row, New York.

Gilaedi, E. ed., 1967, "Electrosorption", Plenum Press, New York.

Grahame, D. C., 1952, J. of Electrochem. Soc. 99, 370C.

Halloff, P. G., 1957, Ph.D. thesis, M.I.T.

Halloff, P. G., Cartwright, P. A. and Pelton, W. H., 1979, "The Use of the Phoenix IPV-2 Phase IP Receiver for Discrimination between Sulfides and Graphite", Paper presented at the 49th annual meeting of the Society of Exploration Geophysicists, New Orleans.

Halverson, M. O., Zinn, W. G., McAlister, E. O., Ellis, R. B. and Yates, W. C., 1979. "Some Results of a Series of Geologically Controlled Field Tests of Broadband Spectral Induced Polarization." Paper presented at the 49th annual meeting of the Society of Exploration Geophysicists, New Orleans.

Hoerl, A. E., 1962, Chem. Eng. Progr 55, 54-59.

Hoerl, A. E., 1964, Chem, Eng. Progr. Symposium Series 60, 66-77.

Hoerl, A. E. and Kennand, R. W., 1970, Technometrics 12, 55-82.

Klein, J. D. and Shuey, 1978, Geophysics 43, Part I: Pyrite, Part II: Galena, Chalcopyrite and Graphite.

Kolthoff, I. M. and Lingane, J. J., 1946, "Polargraphy", Interscience, New York.

Laitenen, H. A., and Randles, J. E. B., 1955, Trans. Faraday. Soc. 51, 54.

Levich, V. G., 1962, "Physiochemical Hydrodynamics", Prentice-Hall, New Jersey.

Llopis, J. Fernandes-Biange and Fernandes Perez M., 1959, Electrochemica Acta 1, 130-145.

Llopis, J. and Colon, F., 1956, " Proc. of the Eight Meeting of the CITCE", Butterworths, London, 1958.

Madden, T. R., 1959, "Induced Polarization: A study of its causes and magnitudes in geologic materials". Report to U. S. Atomic Energy Commission, Division of Raw Materials, Contract AT (05-1)-718.

Madden, T. R., 1961, Ph.D. Thesis, M.I.T.

Madden, T. R. 1975, Geophys. 41 1104-1125.

Marquardt, D. W., 1963, SIAM J. 11, 401-411.

Marquardt, D. W., 1970, Technometrics, 12, 591-612.

Marshall, D. J., 1959, Ph.D. Thesis, M.I.T.

Overbeek, J. Th. G., 1952, in "Colloid Science", H. R. Kruyt, (ed.), Elsevier Publishing Co., Amsterdam.

Parsons, R., 1970, "Faradaic and Non-Faradaic Processes", 7, Adv. in Electrochem. and Electrochemical Eng., Interscience Pub. New York

Pelton, W. H., Ward, S. H., Hallof, P. G., Sill, W. R., and Nelson, P.H. (1978), Geophysics, 43, 588-610.

Peters, D. G., and Crusen, S. A., 1965, J. Electroanaly. Chem. 9, 27-40.

Pourbaix, M. 1949, "Thermodynamics of Dilute Aqueous Solutions, with Applications to Electrochemistry and Corrosion", Thesis, Delft (1945). Translated by J. N. Agar, Arnold, London.

Pourbaix, J., 1966, "Atlas of Electrochemical Equilibrium in Aqueous Solutions", Pergamon Press, New York.

Pourbaix, M., 1973, "Lectures on Electrochemical Corrosion", Plenum Press, New York.

Sato, M., 1960, Economic Geology, 55, I, "Geochemical Environments in Terms of Eh and pH", 928-961. II, "Oscidation Mechanisms of Sulfide Minerals at 25°C", 1202-1231.

Senda, M., and Delahay. P., 1961, J. Phys. Chem, 65, 1580-1588.

Sluyters-Rehbach, M. and Sluyters, J. H., 1967. Z. Phys. Chem. 52, 89.

Sluyters-Rehbach, M. and Sluyters, J. H., 1969, J. Electroanalyz. Chem., 23, 547.

Sluyters-Rehbach, M. and Sluyters, J. H., 1970, Electroanalytical Chemistry, Vol. 4, A. J. Bard (ed.).

Timmer, B., Sluyters-Rehbach, M. and Sluyters, J. H., 1967., J. Electroanaly. Chem., 15, 343.

Timmer, B., (1968), Ph.D. Thesis, State University of Utrecht, The Netherlands.

Timmer, B. Sluyters-Rehbach, M., and Sluyters, J. H., 1968, J. Electroanal. Chem., 18, 93.

Vacquer, V., Holmes, C. R., Kitzinger, P., and Lavergne, M., 1957, Geophysics 22, 660.

Vetter, K. J., 1967, "Electrochemical Kinetics", Academic Press, New York.

Wait, J. R., ed., 1959, "Overvoltage Research and Geophysical Applications", Pergamon Press, New York.

Warburg, E., 1899, Ann Physik, 67, 493.

Wong, J., 1979, Geophysics, 44, 1245-1266.

Wynn, J. C., and Zonge, K. L., 1975, Geophysics 40, 831-851.

BIOGRAPHICAL NOTE

The author Frank D. Morgan is a West Indian, born in Guyana, but is now a Trinidadian citizen. He attended high school at St. Stanislaus' College Guyana, St. Joseph's College and the Polytechnic Institute in Trinidad. He graduated from the University of the West Indies, Trinidad and Tobago in 1970 with the B.Sc in Mathematics and Physics, and in 1972 with the M.Sc in theoretical solid state physics. He was a lecturer in the Physics Department, University of the West Indies, Trinidad and Tobago from 1971 to 1975. He came to M.I.T. on a joint O.A.S./Trinidad Government Scholarship. His interests are in Applied Geophysics, particularly, Geoelectricity and Seismology.